D-33192
Version 2.0

Earth Observing System (EOS)
Tropospheric Emission Spectrometer (TES)

Data Validation Report
(Version F03_03 data)

Editor:

Gregory Osterman

Contributors:

Kevin Bowman, Karen Cady-Pereira, Tony Clough, Annmarie Eldering, Brendan Fisher, Robert Herman, Daniel Jacob, Line Jourdain, Susan Kulawik, Michael Lampel, Qinbin Li, Jennifer Logan, Ming Luo, Inna Megretskaia, Ray Nassar, Gregory Osterman, Susan Paradise, Vivienne Payne, Hank Revercomb, Nigel Richards, Mark Shephard, Dave Tobin, Solene Turquety, Felicia Vilnrotter, Helen Worden, John Worden, Lin Zhang

January 4, 2007

JPL
Jet Propulsion Laboratory
California Institute of Technology
Pasadena, California

Distributed by the Atmospheric Science Data Center
http://eosweb.larc.nasa.gov

Earth Observing System (EOS)
Tropospheric Emission Spectrometer (TES)

Data Validation Report
(Version F03_03 data)

Approved by:

_____	_____
Reinhard Beer	Rob Toaz
TES Principal Investigator	TES Ground Data Systems Manager
Jet Propulsion Laboratory	Jet Propulsion Laboratory

Distributed by the Atmospheric Science Data Center
http://eosweb.larc.nasa.gov

Revision History:

Version	Date	Description/Comments
1.0	8/15/2005	Initial Version of Validation Report for time frame "launch + 1 year"
2.0	1/4/2007	Validation Report for F03_03 data

Distributed by the Atmospheric Science Data Center
http://eosweb.larc.nasa.gov

TABLE OF CONTENTS

1. OVERVIEW OR TES L2 (LEVEL 2) PRODUCT VALIDATION 1

1.1 APPLICABLE DOCUMENTS 2

2. AN OVERVIEW OF THE TES INSTRUMENT AND DATA PRODUCTS 3

2.1 INSTRUMENT DESCRIPTION 3
2.2 TES OBSERVATION MODES 3
2.3 TES SCAN IDENTIFICATION NOMENCLATURE 4
2.4 WHERE TO OBTAIN TES DATA 4
2.5 L2 PRODUCT FILE FORMATS AND DATA VERSIONS 5
2.6 TES STANDARD L2 PRODUCTS 5
2.7 REFERENCES 6

3. EXECUTIVE SUMMARY 7

4. OVERVIEW OF TES L1B RADIANCE VALIDATION 9

4.1 TES COMPARISONS WITH SCANNING HIGH RESOLUTION INTERFEROMETER SOUNDER (SHIS) 9
4.2 TES COMPARISONS WITH ATMOSPHERIC INFRARED SOUNDER (AIRS) 10
4.3 REFERENCES 14

5. VALIDATION OF TES LEVEL 2 OZONE FOR V002 DATA 15

5.1 COMPARISON WITH OZONESONDES 15
5.1.1 Introduction 15
5.1.2 Comparison Methods 15
5.1.3 WOUDC and SHADOZ Comparisons 16
5.1.4 Case studies Over Specific Sonde Sites 20
5.1.5 ARM-SGP (36.6°N, 97.5°W) Oklahoma, USA: Identification of "Emission Layer Flag" 20
5.1.6 Sodankyla (67.4°N, 26.6°E) Finland 21
5.1.7 PNNL (46.2°N, 119.2°W) Richland, Washington, USA 24
5.1.8 Conclusions from TES-ozonesonde case studies: 26
5.1.9 References: 27
5.2 COMPARISON WITH LIDAR MEASUREMENTS 28
5.2.1 INTEX-B and DIAL Measurements 28
5.2.2 DIAL Comparisons with TES 31
5.2.3 Preliminary Conclusions 32
5.3 VALIDATION OF TES MEASUREMENTS OF THE TOTAL OZONE COLUMN 33
5.3.1 TES Total Ozone Column 33
5.3.2 TES Tropospheric and Stratospheric Column Values 33

6. VALIDATION OF TES RETRIEVALS OF CARBON MONOXIDE 36

6.1 INSTRUMENT PERFORMANCE BEFORE AND AFTER OPTICAL BENCH WARM-UP 36
6.2 GLOBAL DISTRIBUTIONS OF CO FROM TES MEASUREMENTS 38
6.3 CO VALIDATION: COMPARISONS TO *IN SITU* AIRCRAFT MEASUREMENT 39

Distributed by the Atmospheric Science Data Center
http://eosweb.larc.nasa.gov

6.3.1 Comparisons to Argus CO Data in October-November 2004 AVE Aircraft Campaign *39*
6.3.2 Comparisons to ALIAS CO Data in Jan-Feb 2006 CR-AVE Aircraft Campaign *45*
6.3.3 Comparisons to DACOM CO Data in March-May 2006 INTEX-B Aircraft Campaign *46*
6.4 CO VALIDATION: COMPARISONS TO MOZAIC DATA SET 50
6.5 CO VALIDATION: COMPARISONS TO MOPITT DATA 53
6.6 CO VALIDATION: COMPARISONS TO ACE AND MLS DATA 57
6.6.1 Comparisons to ACE *57*
6.6.2 Comparisons to MLS *58*
6.7 CO VALIDATION: SUMMARY AND FUTURE WORKS 59
6.8 REFERENCES 60

7. VALIDATION OF TES RETRIEVALS OF TEMPERATURE 61

7.1 COMPARISONS OF TES TEMPERATURE WITH AIRS, AIRCRAFT, AND SONDES 61
7.1.1 TES Temperature Comparisons with AIRS *61*
7.1.2 TES Temperature Comparisons with Aircraft in the Tropics *61*
7.1.3 TES Temperature Comparisons with Sondes *62*
7.1.4 Summary *62*
7.2 TES TEMPERATURES IN COMPARISON WITH NCEP SONDE TEMPERATURES 70

8. TES SEA SURFACE TEMPERATURE RETRIEVALS 73

8.1 INTRODUCTION 73
8.2 DATA 73
8.3 CLOUDS OPTICAL DEPTH AND DEGREES OF FREEDOM OF SIGNAL DISTRIBUTIONS 73
8.4 COMPARISON TO ROI DATA 76
8.5 DERIVED RMS SST ERROR FROM COMPARISON TO AMSR-E 78
8.6 REFERENCES 78

9. COMPARISON OF TES WATER VAPOR WITH AIRS, AIRCRAFT, AND SONDES 79

9.1 TES WATER VAPOR COMPARISONS WITH AIRS 79
9.2 TES WATER VAPOR COMPARISONS WITH *IN SITU* MEASUREMENTS FROM SONDE 80
9.3 TES WATER VAPOR COMPARISONS WITH *IN SITU* MEASUREMENTS FROM AIRCRAFT 80

10. VALIDATION OF TES HDO/H2O 87

11. TES CLOUD PRODUCTS 88

11.1 BACKGROUND 88
11.2 CLOUD TOP PRESSURE 88
11.3 CLOUD EFFECTIVE OPTICAL DEPTH 89

APPENDICES 93

A. ACRONYMS 93

Distributed by the Atmospheric Science Data Center
http://eosweb.larc.nasa.gov

LIST OF FIGURES

Figure 4-1 Plotted is the TES nadir-scan that consists of sixteen 0.5 x 5km rectangular pixels. Overplotted are nine SHIS scans for this underflight, which are ~2 km circles. 9

Figure 4-2 Comparison of TES - SHIS radiances for the 2B1, 1B2, and 2A1 filters. 10

Figure 4-3 Plot of the radiance ratio (TES/AIRS) vs. radiance and color coded for frequency ranges. Panel (A) shows the spread in values over the homogenous cases for the baseline calibration in V001. Panel (B) shows this for the improved V002 L1B calibration. 11

Figure 4-4 TES/AIRS radiance comparison in the 2B1 filter. 12

Figure 4-5 TES/AIRS radiance comparison in the 1B2 filter. 13

Figure 4-6 TES/AIRS radiance comparison in the 2A1 filter. 14

Figure 5-1 Examples of TES Nadir Ozone Averaging Kernels under (A) Clear and (B) Cloudy Conditions. Natal is at 6°S, 35°W and Kagoshima is at 32°N, 131°E. The colors indicate averaging kernel rows corresponding to the pressure levels as noted in the legend. DOFS (Degrees of Freedom for Signal) give the trace of the averaging kernel. 16

Figure 5-2 WOUDC and SHADOZ Sonde Sites with TES Measurement Coincidences for September 2004 to May 2006. 17

Figure 5-3 TES-Ozonesonde Differences for the Northern Mid-Latitudes, Tropics and Antarctic. Top panels show the difference in ppbv, the middle panels show the same profiles as the top panels in ppbv, but focused on the surface to 200 hPa. Bottom panels show the relative (%) difference for both troposphere and lower stratosphere. The thick red, green and blue lines indicate the zonal averages. 18

Figure 5-4 TES-Ozonesonde Differences for N. Mid-Latitudes, Tropics and Antarctic. Top panels show average differences for the upper troposphere (500 hPa to 200 hPa or the tropopause, whichever is larger). Bottom panels show average differences for the lower troposphere (surface to 500 hPa). For the Antarctic cases, the comparison in the lower troposphere gives no information due to the lack of TES sensitivity to ozone at those pressures for those latitudes. Bias and RMS values are also given for V001 data, for comparison. 19

Figure 5-5 Percent Differences in TES-Sonde (with TES Operator). The inner tropics were defined here as coincidences in the 10°S-10°N range and are shown in red. The subtropical (20-26°S/N) coincidences, shown in black are responsible for most of the negative bias between about 100-300 hPa. 20

Figure 5-6 Statistics for ARM-SGP TES-Sonde Comparisons. Maximum altitude is determined by the lowest sonde height in the ensemble. Panel A shows the average TES-Sonde (with TES operator) difference and RMS for night observations, screened only by the general quality flag. Note the large values for both average difference and RMS near the surface. Panel B has night observations excluding TES scenes with an emission layer identified. Panel C shows day observations, which did not have any emission layer scenes detected. I.G. indicates initial guess. 21

Distributed by the Atmospheric Science Data Center
http://eosweb.larc.nasa.gov

Figure 5-7 Target Locations for TES Transect Observations near Sodankyla and an Example of Averaging Kernel Diagonals vs. Pressure and Latitude Along the Track. The tropopause pressure was around 290 hPa in these measurements. 22

Figure 5-8 Profile Comparison for Closest TES Measurement (12 km) on March 31, 2006 (left) and Curtain Plot of Sonde(w/TES operator) – TES Percent Difference Showing better Agreement Close to the Sonde Site. 22

Figure 5-9 72 Hour NOAA-HYSPLIT Backward Trajectories, March 31, 2006, for TES Measurement Locations (Left Panels) and Sodankyla (Right Panels). Pressures of trajectories at the sonde site are shown on the right and colors indicate pressure in hPa along the trajectory. 23

Figure 5-10 Statistics for TES Comparisons to Sodankyla Sondes from the March-April 2006 SAUNA Campaign with Coincidence Criteria as Shown. These plots show that the average fractional difference (avg. [TES-sonde]/sonde) only varies slightly for the different coincident criteria while the rms of fractional differences (red dashed line) decreases to where it is mostly explained by the estimated observational error from TES (black dotted line) for the tightest criteria (panel C: 100 km, 6 hr.). 24

Figure 5-11 TES Measurement Locations (Left) for Closest Run to the IONS NATIVE (PNNL) Sonde on April 21, 2006 and Averaging Kernel Diagonal Curtain Plot (Right) Corresponding to Ozone Profiles Along the Track Between the Green Bars. 25

Figure 5-12 Profile Comparison for Closest TES Measurement (108 km) with Sonde, Sonde with TES Operator and TES Initial Guess on April 21, 2006 (left) and Curtain Plot of Sonde(w/TES operator) – TES Percent Difference Showing Better Agreement within about 200 km of the Sonde Site. 25

Figure 5-13 72 Hour NOAA-HYSPLIT Backward Trajectories, April 21, 2006, for TES Measurement Locations (Left Panels) and PNNL (right panels). Pressures of trajectories at the sonde site are shown on the right and colors indicate pressure in hPa along the trajectory. 26

Figure 5-14 The TES step and stare tracks during the INTEX-B campaign. 29

Figure 5-15 The DC-8 flight tracks that provided the best coincidences with TES nadir measurements. 29

Figure 5-16 A DIAL ozone curtain for the DC-8 flight of April 23, 2006. 30

Figure 5-17 The DIAL standard error for the April 23, 2006 DC-8 flight. 30

Figure 5-18: The DIAL ozone curtain as measured with the DIAL vertical resolution (upper left). The DIAL ozone curtain with the scaled TES a priori used to extend the profile (lower left). The TES step and stare curtain (upper right) and the DIAL curtain after application of the TES averaging kernel (lower right). 31

Figure 5-19 Percentage difference between TES and individual (black) and averaged (red) DIAL profiles for different TES step and stare observations. The final plot is the percentage difference between the mean of all TES and DIAL coincident profiles for the Houston based flights of INTEX-B. 32

Figure 5-20 TES and OMI measurements of the total ozone column from April 4-5, 2006. 34

Distributed by the Atmospheric Science Data Center
http://eosweb.larc.nasa.gov

Figure 5-21 The mean value of TES and OMI measurements of the total ozone column in 10 degree bins, clearly showing TES biased high by 3-5% over mid-latitudes and tropics..... 35

Figure 6-1 Time series of measured normalized Integrated Spectral Magnitude (ISM) (top panel), beamsplitter temperature (middle panel), and average DOFS for 30°N-30°S latitude. The ISM is normalized to 1.0 at the beginning of the time series. 37

Figure 6-2 Latitudinal distributions of the degrees of freedom for signal (DOFS) of the TES CO retrievals for two global survey runs pre- and post optical bench warm up. 37

Figure 6-3 Latitudinal Distributions of the Total Errors and The Precisions for TES CO Retrievals in Two Global Survey Runs of Pre and Post Optical Bench Warm-up. 38

Figure 6-4 TES CO Global Distributions at 681.3 hPa for the Four Typical Months, Oct 2005, Jan, April, and July 2006. 39

Figure 6-5 One day (October 30, 2004) during the AVE-04 campaign, plots show the WB-57 flight track in red and a fraction of the TES step and stare observation geolocations in blue. The green cross marks the starting and end points of the TES measurements along the aircraft track. 41

Figure 6-6 The cross section of TES CO profiles along its orbit track from the equator to 63°N latitude, from a step and stare observation on October 31, 2004. The flight pressures of WB-57 as a function of latitude are overlaid in gray. 42

Figure 6-7 The Argus Measurements of CO VMR Plotted along the Flight Track in Comparison to that of TES in Figure 6-5 for October 31, 2004. Several TES profiles are chosen for comparisons as their latitudes marked by red or black bars on top. 42

Figure 6-8 CO profile comparisons between TES and Argus measurements made during takeoff and landing of the WB-57 on October 31, 2004. Shown in top left panel are the Argus CO profiles, the four TES CO profiles (blue or black) with error bars, and the TES *a priori* profile (green) used in the retrievals. The top right panel shows the rows of TES averaging kernels at three pressure levels. The bottom left panel shows TES and Argus profiles again and the vertically smoothed profiles for Argus CO measurements with TES averaging kernel and *a priori* profile applied described in detail in the text. The bottom right panel shows the percent differences between the four TES CO profiles and the two vertically smoothed Argus CO profiles. 43

Figure 6-9 Same as Figure 6-8, except that the Argus CO Profiles are from the profiling portion of the flight. For this case, before applying the averaging kernel to the Argus profiles, they are extended downward with the TES *a priori* profile. 44

Figure 6-10 Percent Differences between TES and Argus CO Profiles from all Five Days of Measurements during AVE-04 WB-57 Campaign listed in Table 6-1. The solid green is the mean of all comparisons. The other curves are plotted with respect to zero: the standard deviation (STD) of all percent difference (dashed green), the STD of all Argus measurements (red), the STD of all TES (solid blue), and the averaged percent error for the TES measurements (dashed blue). 44

Figure 6-11 The Averaged CO Profiles of TES and ALIAS (Left Panel) and the Averaged Difference between TES and ALIAS CO Profiles (Right Panel, Green). The standard

Distributed by the Atmospheric Science Data Center
http://eosweb.larc.nasa.gov

deviations for the TES and ALIAS CO profiles are also calculated, together with the averaged retrieval errors for the TES CO profiles (right panel). 46

Figure 6-12 The Correlation Plot for TES and DACOM CO Profiles. Data are taken during 1st phase of INTEX-B campaign near Houston, March 2006. Left panel: there are 9 profiles from DACOM *in situ* measurements and 1-4 TES profiles per DACOM profile. Right panel: for each DACOM profile, only the single TES profile is considered closest to the DACOM averaged location. The correlation coefficients are 0.81 and 0.89 for the two comparisons respectively. 49

Figure 6-13 Same Data Sets for Figure 5-12. The average profiles of TES and DACOM are overlaid and the averaged different between TES and DACOM CO profiles (green). The standard deviations for the TES and DACOM CO profiles are also calculated, together with the averaged retrieval errors for the TES CO profiles. 49

Figure 6-14 Airport Locations in the MOZAIC Program. The colored locations are those having TES coincidences. 50

Figure 6-15 Correlation Plot of all TES and MOZAIC CO Comparison Profiles for Airport Munchen. The correlation coefficient is 0.82. 51

Figure 6-16 Same Data in Figure 5-15. Left panel shows the averages of the TES and MOZAIC CO profiles, and the right panel shows the difference, the standard deviations derived from the two data sets and the average for the TES retrieval errors. 51

Figure 6-17 Same Data in Figure 5-15. The Time Trends of the TES and MOZAIC CO Data at Three Pressure Levels, 681.3, 510.9, and 215.4 hPa. 52

Figure 6-18 Total Column of TES CO shown as enlarged nadir footprints for TES Run ID 2147 (September 20-21, 2004). Elevated CO over and near the coasts of S. America and Africa are observed due to extensive biomass burnings in both regions. Larger CO values also showed up in expected pollution regions in E. Asia. 54

Figure 6-19 TES CO Column from Figure 6-18 mapped to uniform grids in latitude and longitude, using Delaunay triangulations and the 2-D linear interpolation method. White marks are TES geolocations. The features in CO global distributions are more clearly displayed. 55

Figure 6-20 Degree of freedom for signal as a function of latitude for TES nadir CO retrieval on Sept. 20-21, 2004. 55

Figure 6-21 Terra-MOPITT CO total column observed in TES global survey period of Run ID 2147, Sept.20-21, 2004. Black marks are TES geolocations. Orbits of Terra and Aura have equator ascending crossing times of about 9:30 am and 1:45 pm respectively. 56

Figure 6-22 The top panel shows the comparisons of TES and MOPITT total CO columns as functions of Latitude for TES Run ID 2147, Sept.20-21, 2004. Note that TES CO column is visibly lower than that of MOPITT in Southern high latitudes. The bottom panel is the percent errors in TES and MOPITT CO columns. The global average values of their percent errors are 8.7% for TES and 11.7% for MOPITT, respectively. 56

Figure 6-23 Time Trend of Latitude Coverage for ACE. 57

Distributed by the Atmospheric Science Data Center
http://eosweb.larc.nasa.gov

Figure 6-24 Examples of TES-ACE CO Profile Comparisons. Solid blue is TES retrieved profile and dotted blue is TES *a priori* profile. Solid magenta is ACE retrieved profile. ... 58

Figure 6-25 Time Trend of TES and ACE CO Comparisons at 316.2 hPa for Data in 30S-30N Latitude. ... 58

Figure 6-26 Comparison of TES and MLS Global Retrievals of CO at 215.4 hPa, September 20-21, 2004. ... 59

Figure 7-1 Comparison of TES v002 Global Surveys with AIRS v4.0 from matched Temperature Retrievals. The temperature bias (green) is TES minus AIRS. ... 63

Figure 7-2 (a) Comparison of TES v002 and AIRS v4.0 from matched Temperature Retrievals over all Latitudes, 90 S to 90 N. (b) Comparison of TES v002 and AIRS v4.0 from matched Temperature Retrievals from 60 S to 60 N. (c) Comparison of TES v002 and AIRS v4.0 from matched Temperature Retrievals in the Tropics, 30 S to 30 N. ... 64

Figure 7-3 Flight track of the WB-57F Aircraft (Black) and TES Global Survey Locations (Blue Dots) on 7 February 2006. ... 65

Figure 7-4 Flight Track of the WB-57F Aircraft (black) and TES Global Survey Locations (blue dots) on 9 February 2006. ... 65

Figure 7-5 Nearby Temperature Profiles from MTP (red) and TES (blue) on 7 February 2006. 66

Figure 7-6 Nearby Temperature Profiles from MTP (red) and TES (blue) on 9 February 2006. 66

Figure 7-7 (a-c) Comparisons of TES Temperature with Aircraft *in situ* Temperature from the WB-57F during CR-AVE ... 67

Figure 7-8 Comparison of TES Temperature Retrievals with ARM Site Radiosondes and GMAO GEOS-4. ... 68

Figure 7-9 (a-c) Comparisons of TES Temperature Retrievals with Sondes launched during Ticosonde in Costa Rica and Galapagos. ... 69

Figure 7-10 Comparison of Mean Difference between TES and NCEP Sonde Temperature Profiles for four Time Periods. The solid line is the mean temperature difference and the dashed line is the RMS of the differences. The dotted line shows zero for reference. ... 71

Figure 7-11 Comparison of Mean Difference between TES and NCEP Sonde Temperature Profiles for four Time Periods. The solid line is the mean temperature difference and the dashed line is the RMS of the differences. The dotted line shows zero for reference. ... 72

Figure 8-1 Histograms and Gaussian Fits to TES-ROI. (a) Black histogram is all Data - Fit by red Gaussian. Green Histogram is QA = 1 (good) fit by yellow Gaussian. (b) Histogram and Fit for DOFS > 0.8 (c) Histogram and Fit for Cloud OD < 0.05. ... 76

Figure 8-2 SST Differences vs. Latitude. Black shows all data, red shows data with QA = 1 (good). ... 77

Figure 9-1 TES Nadir Water Vapor Averaging Kernel from a good Tropical Retrieval (Runid 3277, Sequence 1, Scan 022) Demonstrates Excellent Sensitivity and Vertical Resolution throughout the Troposphere, up to 150 hPa. ... 81

Distributed by the Atmospheric Science Data Center
http://eosweb.larc.nasa.gov

Figure 9-2 Mean Water Vapor Profiles for matched Retrievals from AIRS v4.0 and nine TES v002 Global Surveys. Left: TES Water (red), AIRS Water (blue); Right: Percent Bias (green) calculated as (TES-AIRS)/TES, and Rms Differences (black). 81

Figure 9-3 (a) Water Comparisons for matched Retrievals from AIRS v4.0 and nine TES v002 Global Surveys: 90 S to 90 N. (b) Water Comparisons for matched Retrievals from AIRS v4.0 and nine TES v002 Global Surveys: 60 S to 60 N. (c) Water Comparisons for matched retrievals from AIRS v4.0 and nine TES v002 Global Surveys: 30 S to 30 N. 82

Figure 9-4 Left: Water Comparisons between TES and Sondes at all three ARM Sites, NSA, SGP, and TWP, calculated as (TES-sonde)/TES. Middle: water Comparisons between GMAO GEOS-4 and Sondes. Right: Water Comparisons between TES and GMAO GEOS-4..... 83

Figure 9-5 TES transect across the Galapagos Islands, RunID = 3277, 25 January 2006, shows Uniform Field of Water Vapor. 83

Figure 9-6 San Cristobal, Galapagos Water Vapor Profiles on 25 January 2006: TES and CFH. 84

Figure 9-7 Water Vapor Profiles over Costa Rica on 22 January 2006: TES and WB-57F Aircraft (average of several *in situ* instruments)..... 85

Figure 9-8 Water Vapor Profiles over Costa Rica on 7 February 2006: TES and WB-57F Aircraft (average of several *in situ* instruments)..... 86

Figure 10-1 A comparison of the HDO/H2O ratio as measured by TES and the JPL ALIAS instrument on a WB-57 flight from the Costa Rica Aura Validation Experiment..... 87

Figure 11-1 TES Retrieved Cloud Top Pressure (hPa) and Cloud Effective Optical Depth at 975 cm^{-1} with Error Estimates for Runid 3396. See tif scat_ctp_od_Run3396_R9.tif..... 89

Figure 11-2 As Figure 11-1, but for a Collection of Step and Stare Special Observation Runids. 90

Figure 11-3 Histogram of Cloud Top Pressure Differences between MODIS and TES in hPa.. 90

Figure 11-4 Histogram of TES-MODIS Cloud Top Pressure Differences. Left column is effective optical depth less than 3, right hand column greater than 3. Upper row is cloud top pressure less than 350 hPa, middle row is cloud top pressure between 350 and 700 hPa, and bottom row is cloud top pressure greater than 700 hPa. 91

Figure 11-5 Scatter plot of Average Effective Cloud Optical Depth and Effective Cloud Optical Depth at 975 cm^{-1} 92

Figure 11-6 Scatterplot of MODIS Visible Cloud Optical Depth and TES Effective Cloud Optical Depth at 975 cm^{-1}. 92

Distributed by the Atmospheric Science Data Center
http://eosweb.larc.nasa.gov

LIST OF TABLES

Table 1-1. Definitions of Data Maturity from the EOS-Terra MISR Team 1
Table 1-2. Current Validation Status of TES L2 Data Products 1
Table 2-1. Description of TES Special Observation Modes 4
Table 2-2. Description of the TES L2 Data Product Version Labels 5
Table 2-3 Description of the TES L2 Data Product Files Currently Available 5
Table 6-1 This table Includes Information Pertaining to TES – Aircraft Comparisons for the AVE 2004 Campaign near Houston, TX. 40
Table 6-2 ALIAS on WB-57 and TES Measurements during CR-AVE, Jan – Feb 2006. 45
Table 6-3 TES and DACOM Information for Flights near Houston, March 2006. 47
Table 6-4 TES and DACOM Information for Flights near Hawaii, April-May 2006 47
Table 6-5 TES and DACOM Information for Flights near Anchorage, May 2006. 48
Table 6-6 Summary for TES-MOZAIC CO Comparisons, Sept 2004 – May 2005 52
Table 6-7 Comparisons of Global Averages of TES and MOPITT Reported CO Volume Mixing Ratios at Three Pressure Levels and Total Column for Data taken in September 20-21, 2004 54
Table 6-8 A summary list for TES CO validation activities. Red marks the future works. 60
Table 7-1 Nine TES v002 Global Surveys Compared with AIRS Temperatures 61
Table 8-1 Table showing Retrievals within Cloud Optical Depth Bins 74
Table 8-2 Table showing Retrievals within 0.1 DOFS Bins 74
Table 8-3 Bias, Sigma and RMS Statistics 76
Table 9-1 Nine TES v002 Global Surveys Compared with AIRS v4.0 Nadir Retrievals 79

Distributed by the Atmospheric Science Data Center
http://eosweb.larc.nasa.gov

1. Overview or TES L2 (Level 2) Product Validation

This document is intended to provide our best determination of the quality of the TES data products based on detailed comparisons between TES L2 data products and other independent data sets.

Validation is defined, for purposes of this report, as comparison between quantities measured by TES and other data products that represent the state of the atmosphere. This definition will evolve as the validation effort matures. Data used in these figures come from processing at the TES Science Computing Facility and are all publicly available.

The TES L2 nadir products have undergone extensive quality control and validation testing. Table 1-1 shows the definitions of data maturity developed by the Terra-MISR (Multi-angle Imaging SpectroRadiometer) team and adopted by the TES team (http://eosweb.larc.nasa.gov/PRODOCS/misr/Quality_Summaries/maturity_def.html).

Using these definitions, the current validation status of the TES L2 data products are given in Table 1-2. Currently, the TES L2 products that are ready for scientific use are the nadir retrievals of ozone, carbon monoxide, temperature and water.

Table 1-1. Definitions of Data Maturity from the EOS-Terra MISR Team

Term	Definition
Beta	Early release products for users to gain familiarity with data formats and parameters.
Provisional	Limited comparisons with independent sources have been made and obvious artifacts fixed.
Validated Stage 1	Uncertainties are estimated from independent measurements at selected locations and times.
Validated Stage 2	Uncertainties are estimated from more widely distributed independent measurements.
Validated Stage 3	Uncertainties are estimated from independent measurements representing global conditions.

Table 1-2. Current Validation Status of TES L2 Data Products

Species	Validation Status
Nadir Ozone	Validated Stage 2
Nadir Carbon Monoxide	Validated Stage 2
Nadir Water (Lower/Middle Troposphere)	Validated Stage 2
Nadir Water (Upper Troposphere)	Validated Stage 1

Distributed by the Atmospheric Science Data Center
http://eosweb.larc.nasa.gov

Species	Validation Status
Nadir Temperature	Validated Stage 2
Sea Surface Temperature	Validated Stage 2
Land Surface Temperature/Emissivity	Beta (Provisional in 2007)
Nadir Methane	Beta (Provisional in 2007)
Nadir HDO	Validated Stage 1
Limb Nitric Acid	Beta (Provisional in 2007)
Limb Ozone	Beta (Provisional in 2007)
Limb Temperature	Beta (Provisional in 2007)

In order to compare TES profile data with other measurements, vertical smoothing and sensitivity must be accounted for by applying the appropriate averaging kernels (such as those supplied with the TES data products). The error estimates included in the L2 data products are meaningful based on the current validation analysis.

The details of validation of products described as "beta" validated in Table 1-2 will be described in the next version of this report.

1.1 Applicable Documents

[1] Osterman, G., (editor), K. Bowman, K. Cady-Pereira, T. Clough, A. Eldering, B. Fisher, R. Herman, D. Jacob, L. Jourdain, S. Kulawik, M. Lampel, Q. Li, J. Logan, M. Luo, I. Megretskaia, G. Osterman, S. Paradise, H. Revercomb., N. Richards, M. Shephard, D. Tobin, S. Turquety, H. Worden, J. Worden, and L. Zhang, Tropospheric Emission Spectrometer (TES) Validation Report, JPL Internal Report D-33192, Version 1.00, August 15, 2005.

[2] Osterman, G., (editor), K. Bowman, A. Eldering, B. Fisher, R. Herman, D. Jacob, L. Jourdain, S. Kulawik, M. Luo, R. Monarrez, G. Osterman, S. Paradise, N. Richards, D. Rider, D. Shepard, H. Worden, J. Worden, and H. Yun, Tropospheric Emission Spectrometer TES L2 Data User's Guide (up to & including version F03_03 data), Version 2.00, June 1, 2006.

[3] Lewicki, S., Science Data Processing Standard and Special Observation Data Products Specifications, Version 9.1 (Science Software Release 9.3) JPL Internal Report D-22993, May 24, 2006.

Distributed by the Atmospheric Science Data Center
http://eosweb.larc.nasa.gov

2. An Overview of the TES Instrument and Data Products

This section provides information about the TES instrument and the L2 data products. More detailed information on the TES data products is available in the TES L2 Data User's Guide and the TES Data Product Specification Document.

2.1 Instrument Description

The Tropospheric Emission Spectrometer (TES) on EOS-Aura was designed to measure the global, vertical distribution of tropospheric ozone and ozone precursors such as carbon monoxide (Beer, et al., 2001; Beer, 2006). TES is a nadir and limb viewing infrared Fourier transform spectrometer (FTS) (http://tes.jpl.nasa.gov/mission/instrument.cfm). The TES spectral range is from 650 to 3250 cm^{-1}. The apodized resolution for standard TES spectra is 0.10 cm-1, however, finer resolution (0.025 cm^{-1}) is available for special observations. The footprint of each nadir observation is 5 km by 8 km, averaged over detectors. Limb observations (each detector) have a projection around 2.3 km x 23 km (vertical x horizontal).

TES is on the EOS-Aura platform (http://aura.gsfc.nasa.gov/) in a near-polar, sun-synchronous, 705 km altitude orbit. The ascending node equator crossings are near 1:45 pm local solar time.

2.2 TES Observation Modes

TES makes routine observations in a mode referred to as the "global survey". A global survey is run every other day on a predefined schedule and collects 16 orbits (~26 hours) of continuous data. Each orbit consists of a series of repetitive units referred to as a sequence. A sequence is further broken down into scans. Global surveys are always started at the minimum latitude of an Aura orbit.

The at-launch version of the global survey consisted of 1152 sequences (72 per orbit). Each sequence was made up of 2 calibration scans, 2 nadir viewing scans and 3 limb scans. The two nadir scans for this version of the global survey were acquired at the same location on the spacecraft ground track and the radiances averaged, leading to a single TES L2 profile. The along-track distance between the successive nadir scan locations is ~544 km for this version of the global survey.

On May 25, 2005 the global survey was modified to conserve instrument life. The three limb scans were eliminated from the sequences and replaced by an additional nadir scan. In this version the three nadir scans are acquired at locations equally spaced along the spacecraft ground track. The spacecraft ground track distance between successive nadir observations is ~182 km. The radiances of individual scans are not averaged for data acquired with this version of the global survey. As with the original global survey there are 1152 sequences per global survey and with the additional nadir scans there is a maximum of 3456 profiles for these global surveys.

On January 10, 2006 the last sequence in each orbit was replaced with an instrument maintenance operation. All global surveys taken after 1/10/2006 include 1136 sequences per global survey (71 per orbit), meaning a maximum of 3408 L2 profiles. The along-track distance between successive nadir observations was unchanged.

Observations are sometimes scheduled on non-global survey days. In general these are measurements made for validation purposes or with highly focused science objectives. These

Distributed by the Atmospheric Science Data Center
http://eosweb.larc.nasa.gov

non-global survey measurements are referred to as "special observations". The primary special observation modes that have been used to date by TES are summarized in Table 2-1.

Table 2-1. Description of TES Special Observation Modes

Name	Pointing	Sequences	Scans per Sequence	Distance Between Scans	Comments
Step and Stare (prior to Jan 1, 2006)	Nadir	1	125	45 km	Continuous along-track nadir views, ~50 degrees of latitude.
Step and Stare (after Jan 1, 2006)	Nadir	6	25	40 km	Continuous along-track nadir views, ~45 degrees of latitude.
Transect	Near Nadir	1	40	12 km	Hi density along-track, near nadir views.
Stare	Near Nadir	1	32	0 km	All measurements at a single location.
Limb Only	Limb	1	62	45 km	Continuous along-track limb views, 25 degrees of latitude.
Limb HIRDLS	Limb	142	3	182 km	2 orbits of continuous limb measurements for HIRDLS comparison

2.3 TES Scan Identification Nomenclature

Each TES scan is uniquely identified by a set of three numbers called the run ID, the sequence ID and the scan ID. Each major unit of observation is assigned a unique run ID. Run IDs increase sequentially with time. The first on-orbit run ID is 2000. The seq ID is assigned to repetitive units of measurements within a run. They start at 1 and are automatically incremented serially by the TES flight software. The scan ID is also incremented by the flight software each time a scan is performed. Each time the sequence is set to 1, the scan ID is reset to 0.

Each time TES makes a set of measurements, that data set is assigned an identification number (referred to as a "run ID"). A calendar of the TES run IDs for global surveys and a list of all TES run IDs (including observation data, time and date) can be found at http://tes.jpl.nasa.gov/science/dataCalendar.cfm .

2.4 Where to Obtain TES Data

The primary location to obtain the TES data products is the Langley Atmospheric Science Data Center (ASDC) which can be found at http://eosweb.larc.nasa.gov/. The site contains all TES data as well as supporting documentation. All TES data products are in Hierarchical Data Format (HDF) 5 format and completely documented in the TES Data Product Specification documents referenced in Section 2.7.

Distributed by the Atmospheric Science Data Center
http://eosweb.larc.nasa.gov

2.5 L2 Product File Formats and Data Versions

Information about the TES data file content and format versioning can be found in the L2 product filenames. There are currently four different versions of TES L2 data products publicly available. It is currently planned that the entire TES L2 data product set shall be processed with the latest software release by approximately October 1, 2006. In the meantime it is important to understand the differences in the data versions and file formats.

Table 2-2 provides an explanation of the TES versions strings and more information about the different data versions is provided in the following sections. A change in the format number corresponds to changes in the fields available or minor bug fixes. A change in content number means a major change in the science content of certain fields in the data products. Version F03_03 is the first version to provide limb data results and is a minor upgrade to F03_02. Version F03_02 data was a significant upgrade to the science content in the data products compared to previous versions. The combination of F03_03 and F03_02 are referred to as V02 TES data.

Table 2-2. Description of the TES L2 Data Product Version Labels

TES Version String	Format Version	Science Content Version	Description
F01_01	1	1	The first publicly released L2 data
F02_01	2	1	Bug fixes and additional fields
F03_02	3	2	Some additional fields but major upgrade to scientific quality of data.
F03_03	3	3	Minor upgrade to F03_02. Limb data and some bug fixes. Most recent version.

2.6 TES Standard L2 Products

Currently the TES data products available for any given run ID are listed in Table 2-3. The products are separated by species with an ancillary file providing additional data fields applicable to all species. A description of the contents of the product files, information on the Earth Science Data Type names and file organization can be found in the TES DPS document (Lewicki, 2006). The TES methane products should not be used at this time.

Table 2-3 Description of the TES L2 Data Product Files Currently Available

TES L2 Standard Data Product	TES View Mode	Description
Ozone	Nadir and Limb	TES ozone profiles and some geolocation information

Distributed by the Atmospheric Science Data Center
http://eosweb.larc.nasa.gov

TES L2 Standard Data Product	TES View Mode	Description
Temperature	Nadir and Limb	TES atmospheric temperature profiles and some geolocation information.
Water	Nadir	TES nadir atmospheric temperature profiles and some geolocation information
Carbon Monoxide	Nadir	TES nadir carbon monoxide profiles and some geolocation information
HDO	Nadir	TES nadir HDO profiles and some geolocation information
Methane	Nadir	TES nadir methane profiles and some geolocation information
Nitric Acid	Limb	TES limb nitric acid profiles and some geolocation information
Ancillary	Nadir	Additional data fields necessary for using retrieved profiles.

TES retrieves surface temperature and it is reported in each species file, however the value in the atmospheric temperature file is the one that should be used for scientific analysis.

The TES L2 Data Products are provided in files separated out by the atmospherics species being measured. An example file name is:

TES-Aura_L2-O3-Nadir_r000002945_F03_03.he5

This particular file contains TES nadir measurements of ozone for run ID 2945 (000002945). The data version number is provided after the "F" in the filename. Additionally there are data files with additional (ancillary) data that are important for working with TES data. These ancillary files can be used with any species data file and contains the string "Anc" in the filename.

2.7 References

[1] Beer, R., T. A. Glavich, and D. M. Rider, Tropospheric emission spectrometer for the Earth Observing System's Aura satellite, *Applied. Optics, 40* (15), 2356-2367, 2001.

[2] Beer, R., TES on the Aura Mission: Scientific Objectives, Measurements and Analysis Overview, *IEEE Transactions on Geoscience and Remote Sensing, 44*, 1102-1105, May 2006.

[3] Lewicki, S., Science Data Processing Standard and Special Observation Data Products Specifications, Version 9.1 (Science Software Release 9.3) JPL Internal Report D-22993, May 24, 2006.

Distributed by the Atmospheric Science Data Center
http://eosweb.larc.nasa.gov

3. Executive Summary

Below is a summary of each data validation section.

- Section 4 – TES L1B Radiances: Version 2 TES data feature an improved L1B calibration that brings the TES into very good agreement with the aircraft instrument Scanning HIS and the AIRS instrument on the NASA Aqua satellite. TES radiances show agreement to within 0.5 K with both Scanning HIS and AIRS.

- Section 5 – Ozone: TES ozone profiles have been compared to ozonesonde and lidar measurements. Comparisons with these other ozone measurements show that TES generally sees higher ozone in the lower and middle troposphere than the sondes and lidar. The magnitude of this difference varies somewhat with different geographic regions. In the upper troposphere, TES sees lower values than the sondes and lidar. In addition, comparisons of TES total column ozone with OMI show similar global distributions, but TES measures 3-7% more ozone. The source of these biases is currently under investigation.

- Section 6 – Carbon Monoxide: Comparisons have been carried out between TES carbon monoxide retrievals and those from a variety of satellite and aircraft instruments. Global patterns of carbon monoxide as measured by TES are in good qualitative agreement with those seen by MOPITT on the NASA Terra satellite. Comparisons of profiles of CO between TES and MOPITT show good agreement when *a priori* information is accounted for correctly. TES carbon monoxide agrees to within the estimated uncertainty of the aircraft instruments, including both errors and the variability of CO itself.

- Section 7 – Atmospheric Temperature: TES temperature retrievals have been compared with both remote sensing and *in situ* measurements. In all cases, TES temperature has a cold bias in the upper troposphere of typically 0.5 to 2 K. A TES warm bias is sometimes observed in the stratosphere. Comparisons of TES temperature profiles with NCEP sondes show TES having a warm bias of 0.5-1.0 K in the 700-900 hPa pressure range, and a 1-2 K cold bias in the 100-400 hPa pressure range. In some periods TES shows a cold bias in the lower stratosphere (e.g. Jan. 2005), but this bias is not persistent and is generally < 0.5K. Version 3 of the TES level 2 data products will include temperature profiles with a reduced bias by addressing CO2 spectroscopy errors.

- Section 8 – Sea Surface Temperature: TES measurements of sea surface temperature have been compared with the Reynolds Optimally Interpolated product. The comparison shows TES agrees well with ROI product with an RMS error of 0.3 K on the TES SST value. The error of the TES estimate of SST varies with the sensitivity of the TES measurement and with the cloud optical depth. The difference between TES and ROI is fairly consistent for all latitudes.

- Section 9 – Water Vapor: Comparisons of TES water vapor retrievals to those from AIRS show that TES tends to be 10 to 25% wetter than AIRS (version 4.0 data) at 150-500 hPa in the upper troposphere and 15 to 20% drier than AIRS in the lower troposphere (500-1000 hPa). Comparisons with sondes show TES to be wetter than the sondes at

Distributed by the Atmospheric Science Data Center
http://eosweb.larc.nasa.gov

around 300 hPa. Conclusions from comparisons of TES water retrievals with sondes and aircraft data are difficult due to the atmospheric variability of water and still being studied.

- Section 10 – HDO/H2O: TES estimates of HDO have undergone preliminary validation by comparison with models and aircraft data. A bias of approximately 5% has been seen, but the distribution of HDO/H2O as measured by TES and the JPL instrument ALIAS shows good agreement.

Distributed by the Atmospheric Science Data Center
http://eosweb.larc.nasa.gov

4. Overview of TES L1B Radiance Validation

4.1 TES Comparisons with Scanning High Resolution Interferometer Sounder (SHIS)

Validation of TES level 1B (L1B) radiance measurements are vital since the radiances are the fundamental quantity used in the TES retrievals. Any errors (e.g. calibration) not addressed in the radiances get propagated as errors in the retrieved parameters. TES nadir spectral radiances have been validated against both AIRS and SHIS. Provided are examples of the radiance comparisons.

During the Aura Validation Experiment (AVE) based in Houston, TX there were several underflights of TES by the NASA WB-57 aircraft. One of the instruments on the WB-57 was the University of Wisconsin Scanning-HIS (SHIS) (Osterman (ed), Bowman et al., 2005). Presented in Figure 4-1 is a cloud free scan from a November 7 2004 flight where SHIS flew under the TES overpass at an altitude of 18 km.

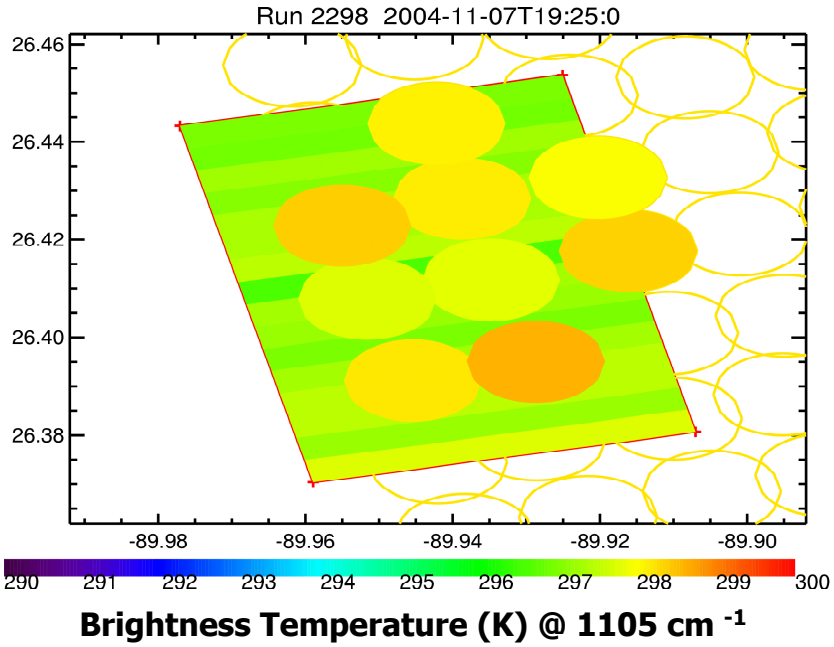

Figure 4-1 Plotted is the TES nadir-scan that consists of sixteen 0.5 x 5km rectangular pixels. Overplotted are nine SHIS scans for this underflight, which are ~2 km circles.

TES and SHIS have spectral resolutions of 0.06 cm^{-1} and 0.48 cm^{-1}, respectively. In order to put the two sensors on the same resolution for comparison purposes, TES was convolved with SHIS instrument line shape (ILS). In addition, the forward model calculations were utilized to account for the differences between altitude, viewing angles, etc. With this procedure, it is assumed that the modeled atmosphere between the aircraft altitude and the satellite is perfect. When the atmosphere above the nadir SHIS observation (18 km) does not represent the true atmospheric state then there will be additional residuals in the spectral regions where there is absorption above the aircraft (i.e. CO2 and O3 spectral regions). The comparison results in Figure 4-2 show that TES is within ~0.5K of the high radiometrically accurate SHIS instrument.

Distributed by the Atmospheric Science Data Center
http://eosweb.larc.nasa.gov

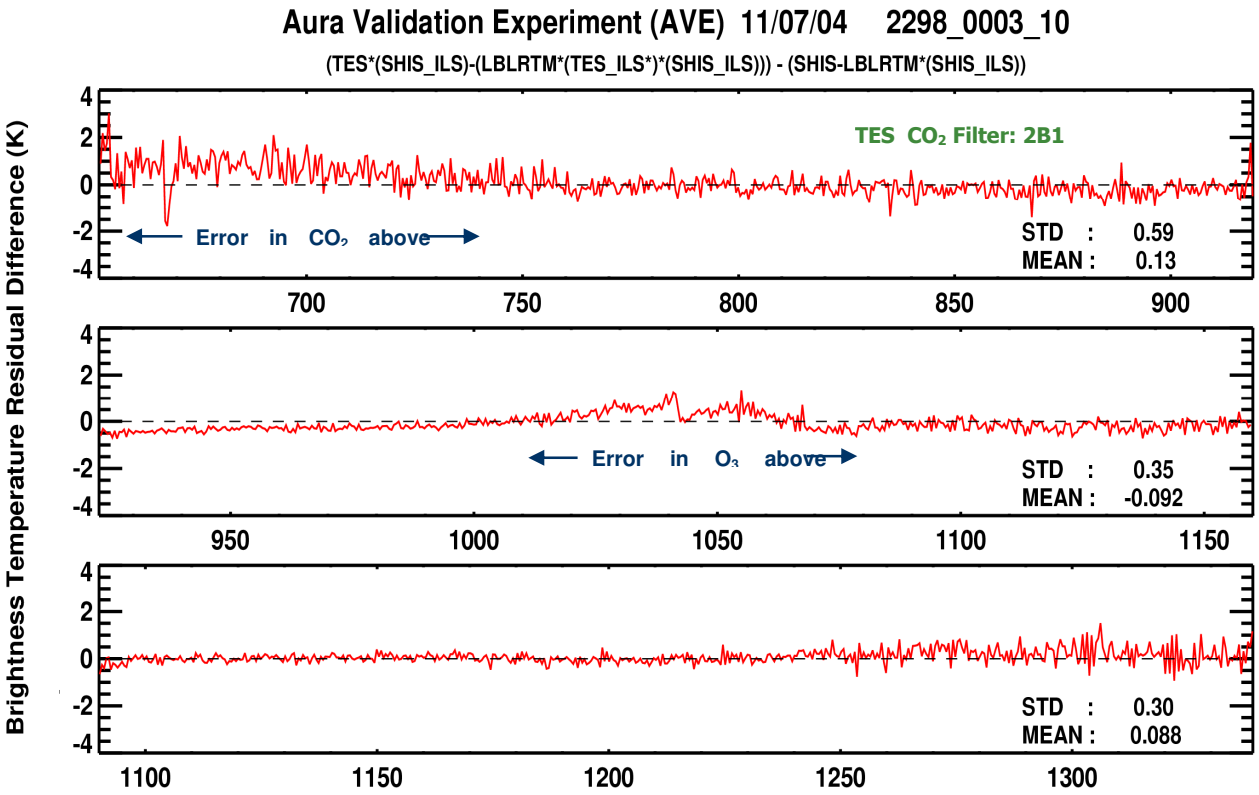

Figure 4-2 Comparison of TES - SHIS radiances for the 2B1, 1B2, and 2A1 filters.

4.2 TES Comparisons with Atmospheric InfraRed Sounder (AIRS)

The NASA JPL AIRS instrument on the Aqua satellite is 15 min ahead of TES (Aura satellite) in the same orbit as part of the A-Train. AIRS radiances have been well-validated and are a valuable source for TES radiance comparisons. For the TES/AIRS comparison, the TES spectrum was convolved directly with the lower resolution AIRS spectral response function (SRF). This direct application of the AIRS SRF to TES data is accurate to within 0.002 K (Sarkissian et al, 2005). After identifying 190 TES nadir targets (from a 16-orbit Global Survey) with 0.5 K homogeneity across a detector array, 50 of these were confirmed as homogenous for AIRS also. These homogenous nadir targets are the cases for TES L1B algorithm improvements used for TES V002. Figure 4-3 shows the improved comparison in the TES/AIRS ratio in the V002 (Panel B) calibration as compared with V001 (Panel A).

Distributed by the Atmospheric Science Data Center
http://eosweb.larc.nasa.gov

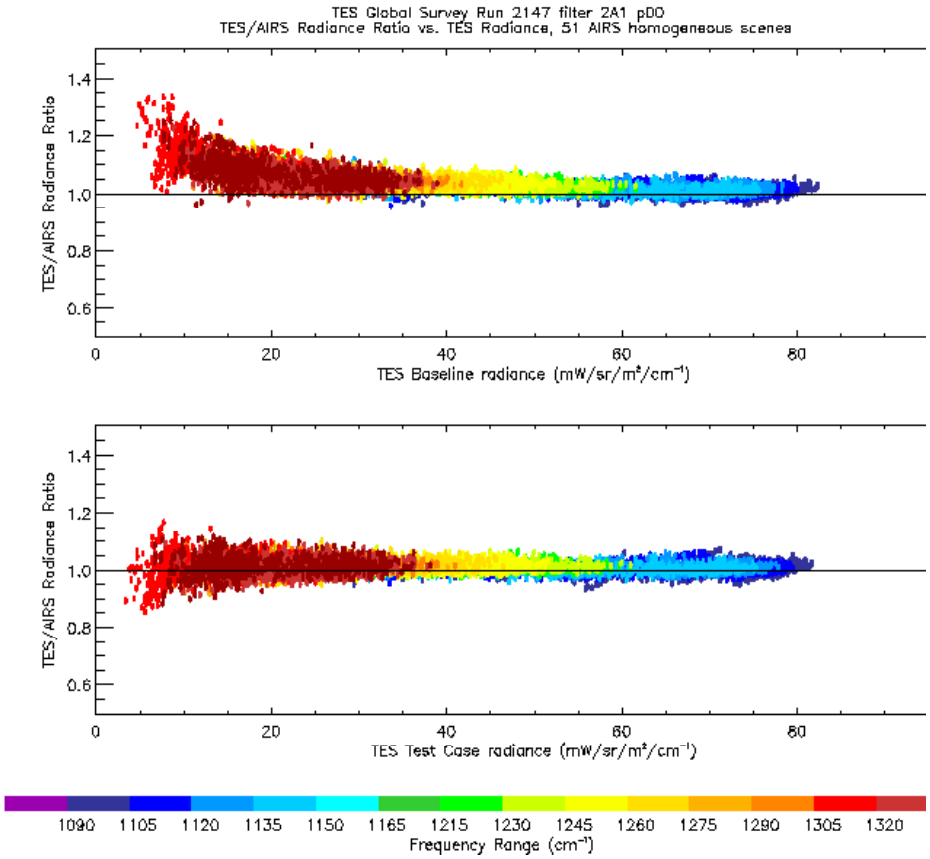

Figure 4-3 Plot of the radiance ratio (TES/AIRS) vs. radiance and color coded for frequency ranges. Panel (A) shows the spread in values over the homogenous cases for the baseline calibration in V001. Panel (B) shows this for the improved V002 L1B calibration.

Figure 4-4 - Figure 4-6 show the frequency and time dependence of AIRS-TES comparisons for TES 2B1, 1B2 and 2A1 filters. For each filter, the top panel shows the average over 50 nadir targets of the AIRS-TES brightness temperature difference as a function of frequency on the AIRS frequency grid. The bottom panels show averages over frequency as a function of target index or time - spanning about 26 hours. These plots demonstrate how the different V002 improvements affect our frequency ranges. In the 2B1 filter, the most significant improvement is from modeling the time dependence, while in 1B2 and 2A1, the time dependence is nearly flat in both the baseline and prototype runs, as expected from the spectral dependence of ice absorption. For 1B2, and especially 2A1, we see large improvements due primarily to the improved sampling phase alignment algorithm. These V002 L1B modifications have improved significantly the TES retrieval parameters.

Distributed by the Atmospheric Science Data Center
http://eosweb.larc.nasa.gov

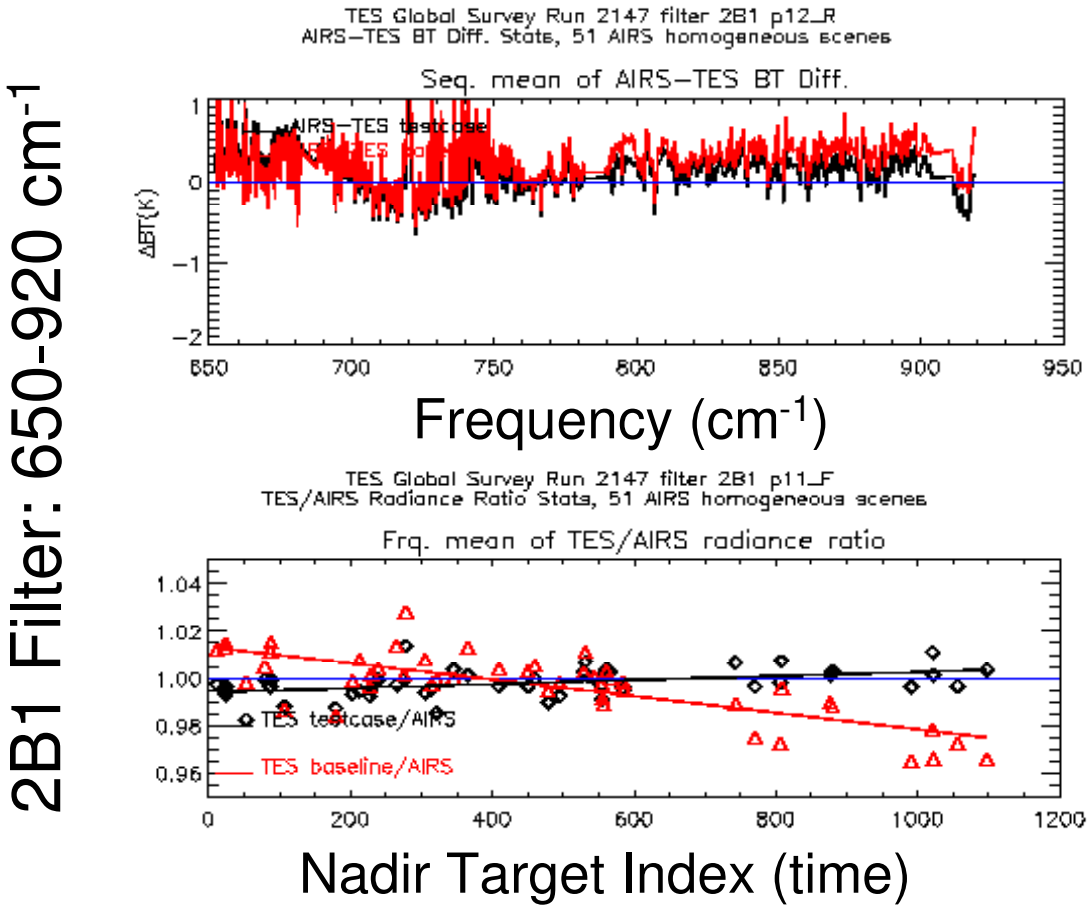

Figure 4-4 TES/AIRS radiance comparison in the 2B1 filter.

Distributed by the Atmospheric Science Data Center
http://eosweb.larc.nasa.gov

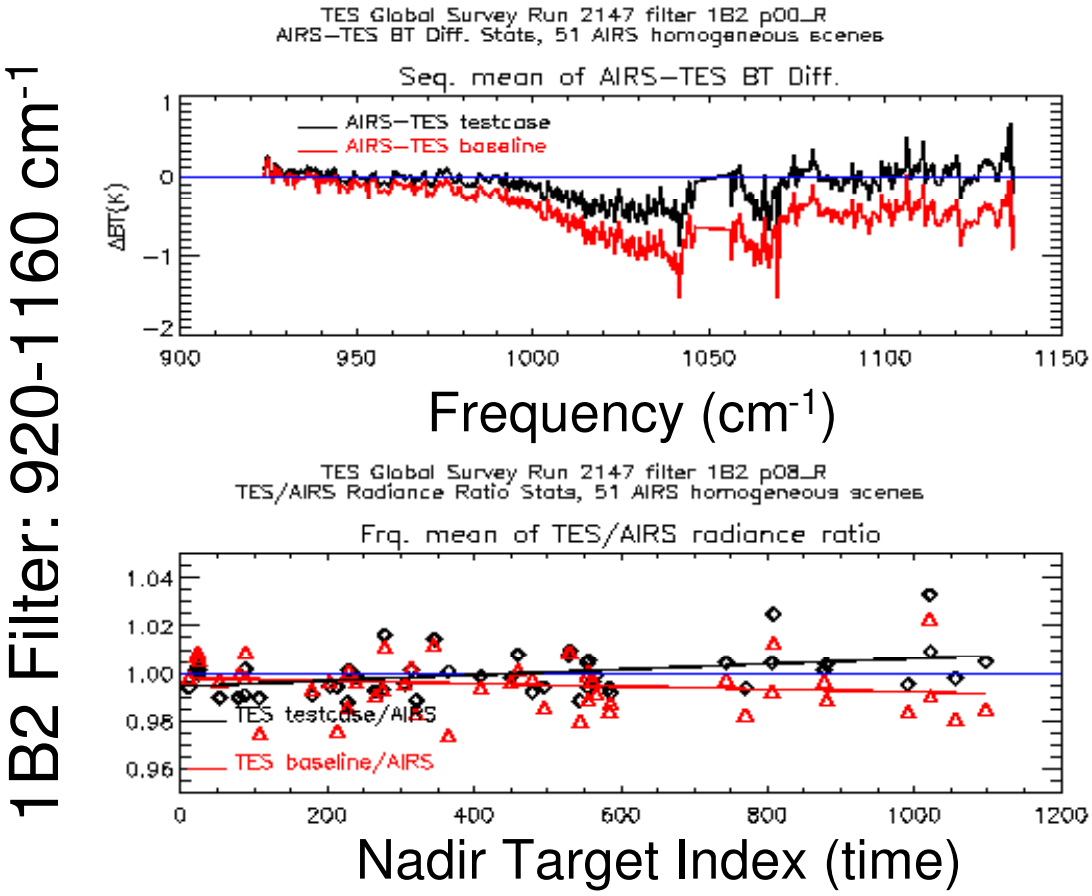

Figure 4-5 TES/AIRS radiance comparison in the 1B2 filter.

Distributed by the Atmospheric Science Data Center
http://eosweb.larc.nasa.gov

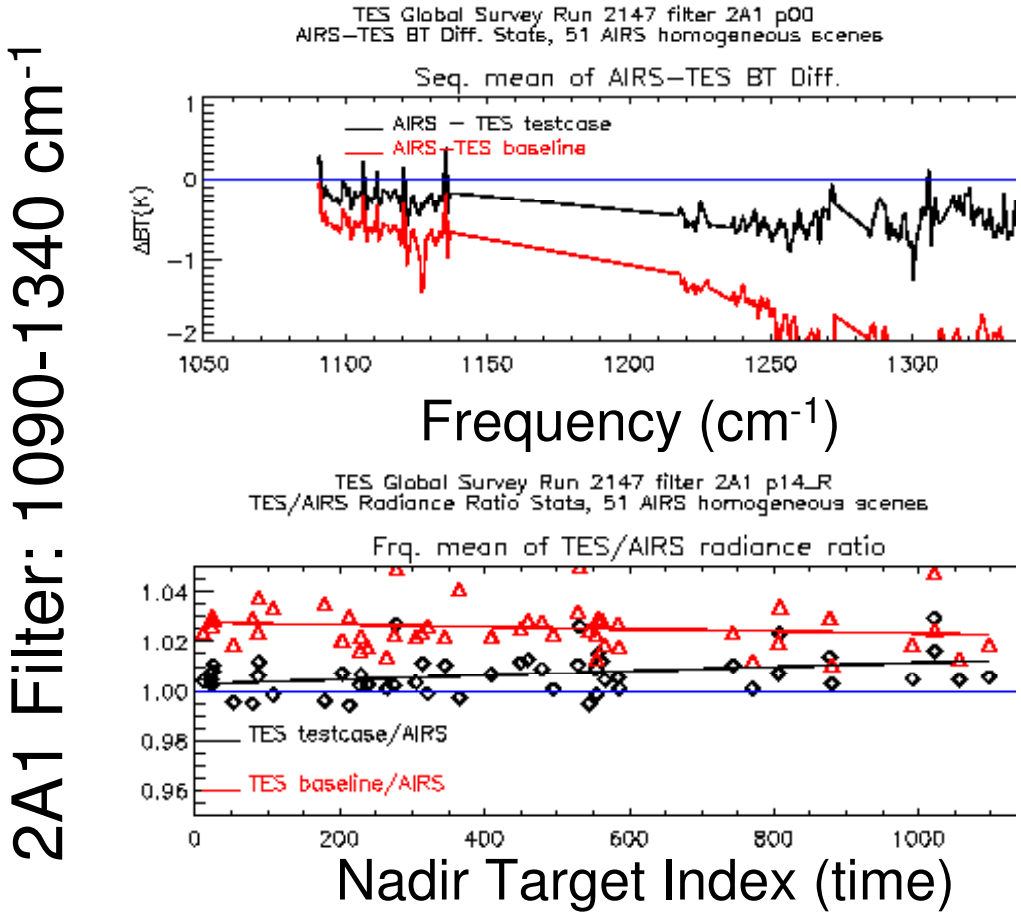

Figure 4-6 TES/AIRS radiance comparison in the 2A1 filter.

4.3 References

[1] Osterman, G., (editor), K. Bowman, K. Cady-Pereira, T. Clough, A. Eldering, B. Fisher, R. Herman, D. Jacob, L. Jourdain, S. Kulawik, M. Lampel, Q. Li, J. Logan, M. Luo, I. Megretskaia, G. Osterman, S. Paradise, Hank R., N. Richards, M. Shephard, D. Tobin, S. Turquety, H. Worden, J. Worden, and L. Zhang, Tropospheric Emission Spectrometer (TES) Validation Report, JPL Internal Report D-33192, Version 1.00, August 15, 2005.

[2] Sarkissian E., Worden H.M., Bowman K.W., Fisher B., Rider D, Aumann, H.H., Apoliniski M., Debaca R.C, Gluck S, Madatyan M., McDuffie J., Tremblay D., Shephard M.W., Cady-Pereria K., Tobin D., Revercomb H., "TES Radiometric Assessment", AGU Meeting, San Francisco, December 5-9, 2005 (available at the TES website http://tes.jpl.nasa.gov/docsLinks/presentations.cfm).

Distributed by the Atmospheric Science Data Center
http://eosweb.larc.nasa.gov

5. Validation of TES Level 2 Ozone for V002 data

5.1 Comparison with Ozonesondes

5.1.1 Introduction

O_3 profiles are retrieved from TES infrared radiances with roughly 6 km vertical resolution for nadir observations. The principal source of validation for TES O_3 measurements is ozonesondes. In some cases, we have sonde data from launches timed to the Aura overpass, such as those taken during the AVE, CR-AVE, SAUNA and IONS-06 campaigns. We also perform comparisons with the data available from the SHADOZ and WOUDC networks. We account for TES measurement sensitivity and vertical resolution by applying the TES averaging kernel and constraint to the ozonesonde data before differencing the profiles. This section gives an update to the comparisons using V001 data, which found a significant high bias for TES ozone compared to sondes in the upper troposphere, especially at mid-latitudes (H. Worden, *et al*, 2006.) We also describe some case studies for specific ozonesonde sites where we have enough statistics to examine coincidence criteria.

5.1.2 Comparison Methods

The procedure for comparing TES to sonde data by applying the averaging kernel and *a priori* constraint vector (hereafter referred to as the TES operator) to the sonde data is described in more detail in H. Worden, *et al*, 2006 and summarized briefly below. It is important to note that accounting for TES sensitivity by applying the TES operator to the sonde data yields a TES-sonde **difference** that is not biased by the TES *a priori.* We can then use the differences to assess systematic errors in the TES calibration and retrieval process, assuming we measure the same airmasses as the sondes.

We process sonde measurements as follows:

1. Map O_3 sonde profile to the TES 65 pressure level grid;

$$X_{sonde}^{pTES} = M_{pTES \Rightarrow Psonde}^{-1} X_{sonde}$$

(Equation 5-1)

2. Apply the TES operator (averaging kernel, A_{TES}, and *a priori* constraint):

$$X_{sonde}^{TES_{AK}} = X_{apriori} + A_{TES}[X_{sonde}^{pTES} - X_{apriori}]$$

(Equation 5-2)

3. Compare to TES profile using the measurement and cross-state error terms. This is denoted as the observational error in the TES data products and does not include the smoothing error term that is included in the total error estimate. Note that we account for smoothing error when we apply the averaging kernel to the sonde profile. Figure 5-1 shows examples of TES nadir ozone averaging kernels. (See C. Rodgers, 2000, J. Worden, *et al*., 2004 and K. Bowman *et al.,* 2006 for more details on error characterization and definitions.)

Distributed by the Atmospheric Science Data Center
http://eosweb.larc.nasa.gov

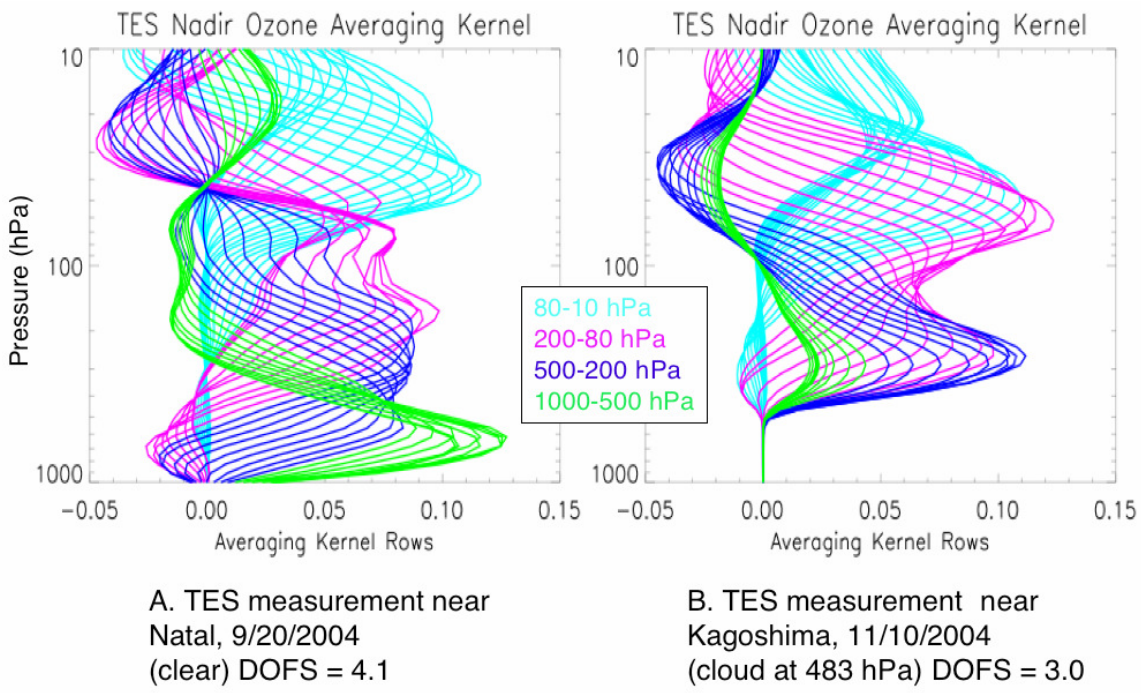

A. TES measurement near Natal, 9/20/2004 (clear) DOFS = 4.1

B. TES measurement near Kagoshima, 11/10/2004 (cloud at 483 hPa) DOFS = 3.0

Figure 5-1 Examples of TES Nadir Ozone Averaging Kernels under (A) Clear and (B) Cloudy Conditions. Natal is at 6°S, 35°W and Kagoshima is at 32°N, 131°E. The colors indicate averaging kernel rows corresponding to the pressure levels as noted in the legend. DOFS (Degrees of Freedom for Signal) give the trace of the averaging kernel.

5.1.3 WOUDC and SHADOZ Comparisons

Figure 5-2 shows the coincidence map for TES-sonde sites from the WOUDC (World Ozone and Ultraviolet Data Center) and SHADOZ (Southern Hemisphere Additional Ozonesonde) Archives. Sonde data were screened by the Harvard team and a total of 143 valid matches, with 200 km, 26 hour coincidence criteria, were found for data taken between September 2004 and May 2006. However, some of these were later rejected based on the TES data quality flags (41), the emission layer flag (3) which is explained later, or a temperature difference of greater than 5 K over multiple levels (14) indicating that TES and the sonde may have been measuring different air masses.

Figure 5-3 shows the TES-sonde differences, after applying the TES operator, for the data separated into northern mid-latitudes, tropics and Antarctic latitude ranges. Figure 5-4 gives the bias and Root-Mean-Square (RMS) values for upper and lower troposphere averages for TES vs. sonde (with TES operator) in the different latitude ranges. The apparent outliers in the northern mid-latitude upper troposphere correlations may result from the definition of the tropopause used which may have permitted some stratospheric ozone in the average. These will be investigated further at a later time. Another modification that will be addressed in a future publication is screening for low sensitivity due to either clouds or thermal conditions such as in the lower troposphere Antarctic cases.

To determine the origin of the anomalous low bias shown in the tropics in Figure 5-4, an additional analysis was performed to further separate this region into the inner tropics and subtropics as shown in Figure 5-5. This comparison indicated that the low bias originated almost

Distributed by the Atmospheric Science Data Center
http://eosweb.larc.nasa.gov

entirely from subtropical coincidences; however, the reason for this has not yet been investigated.

Conclusions from WOUDC and SHADOZ analysis:

- TES nadir ozone profiles are typically biased high compared to sondes in all three latitude zones, but this bias has been reduced from that determined in Worden et al. (2006) for V001 data.
- The absolute bias is higher between 10-100 hPa, but the % bias is higher for the troposphere.
- Mean ΔO_3 (TES-sonde) % from the surface to 200 hPa are:
  Northern mid-latitude: 4-17%, Tropical: -5-14%, Antarctic: 0-27%
- The main exception to the high bias in ozone occurs in the subtropics between ~100-300 hPa.
- It is important to note the linearity in ozone abundance for TES-sonde comparisons (Figure 5-4). Although TES ozone has biases with respect to sondes, we have confidence that relative variations in TES ozone are meaningful because of this linearity.

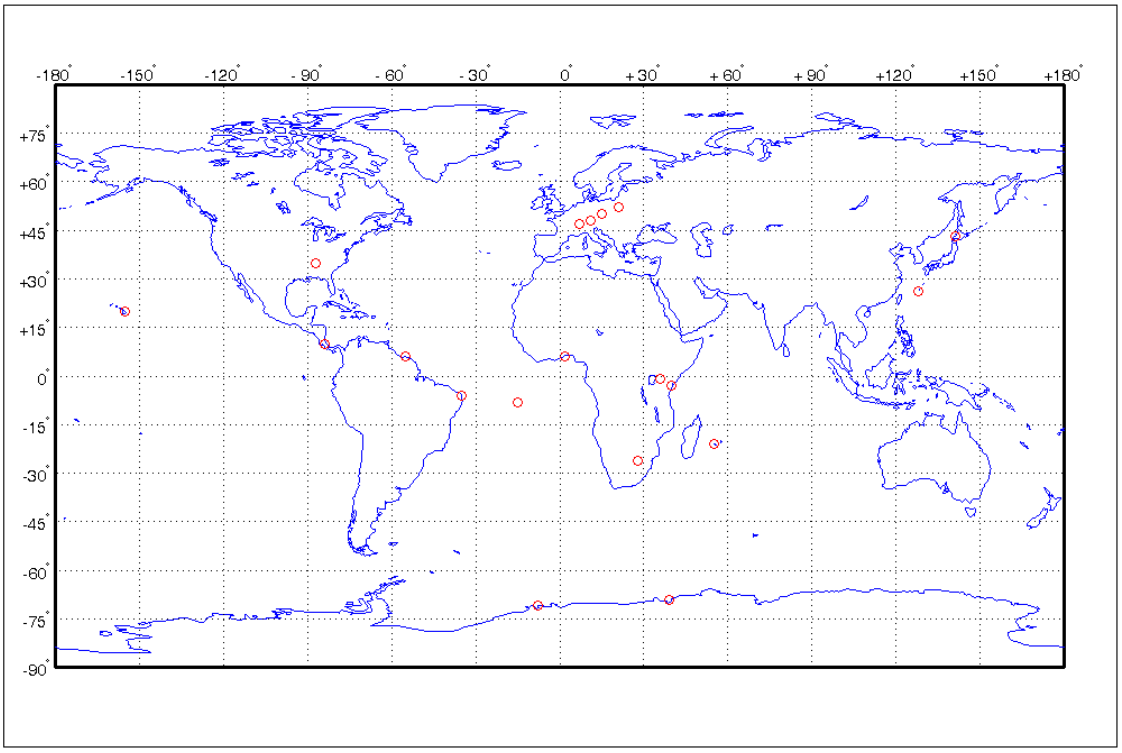

Figure 5-2 WOUDC and SHADOZ Sonde Sites with TES Measurement Coincidences for September 2004 to May 2006.

Distributed by the Atmospheric Science Data Center
http://eosweb.larc.nasa.gov

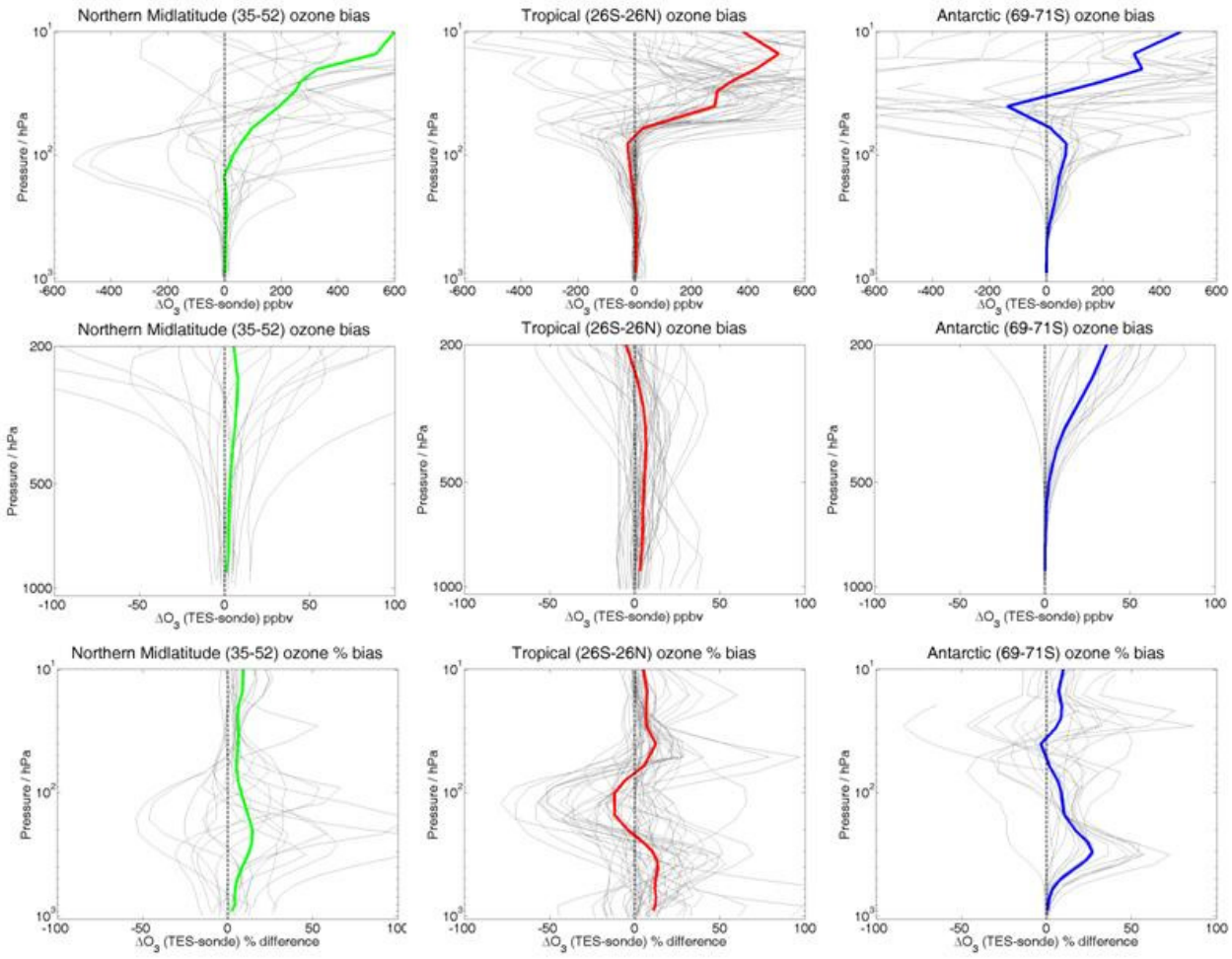

Figure 5-3 TES-Ozonesonde Differences for the Northern Mid-Latitudes, Tropics and Antarctic. Top panels show the difference in ppbv, the middle panels show the same profiles as the top panels in ppbv, but focused on the surface to 200 hPa. Bottom panels show the relative (%) difference for both troposphere and lower stratosphere. The thick red, green and blue lines indicate the zonal averages.

Distributed by the Atmospheric Science Data Center
http://eosweb.larc.nasa.gov

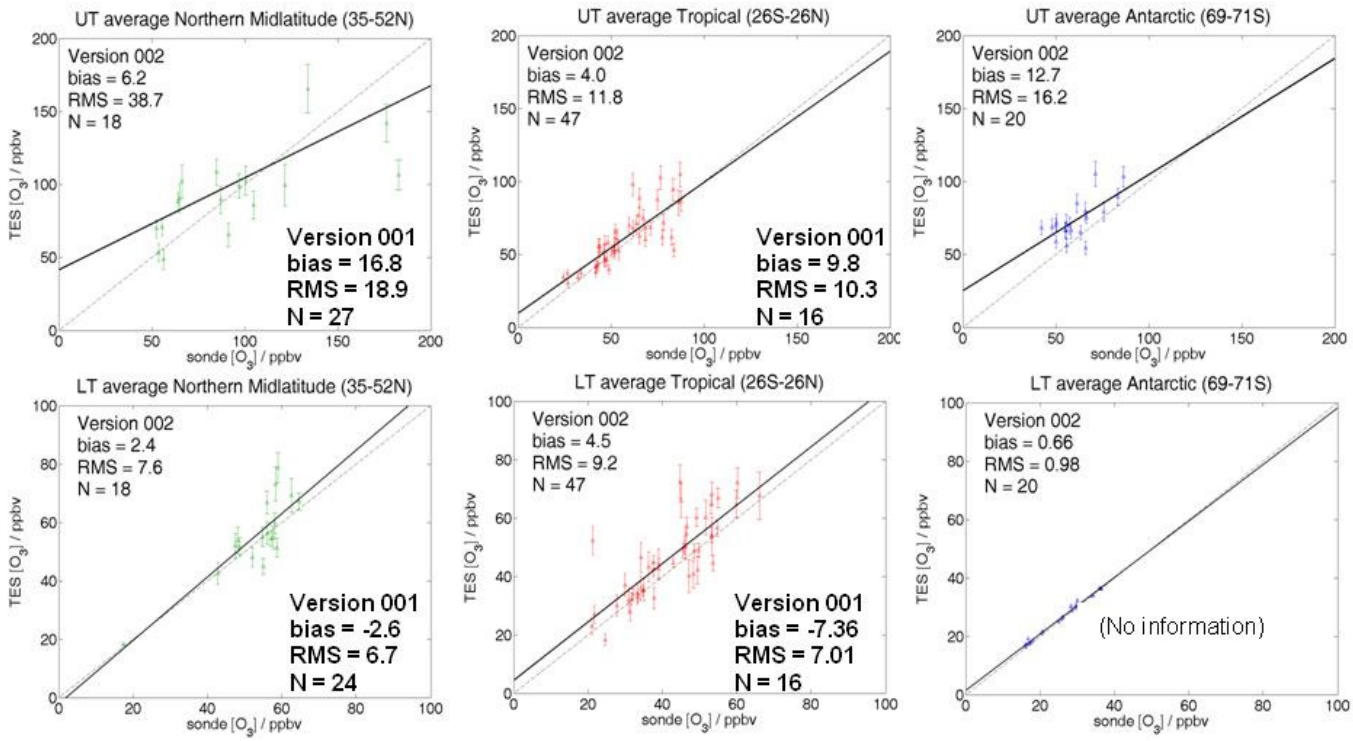

Figure 5-4 TES-Ozonesonde Differences for N. Mid-Latitudes, Tropics and Antarctic. Top panels show average differences for the upper troposphere (500 hPa to 200 hPa or the tropopause, whichever is larger). Bottom panels show average differences for the lower troposphere (surface to 500 hPa). For the Antarctic cases, the comparison in the lower troposphere gives no information due to the lack of TES sensitivity to ozone at those pressures for those latitudes. Bias and RMS values are also given for V001 data, for comparison.

Distributed by the Atmospheric Science Data Center
http://eosweb.larc.nasa.gov

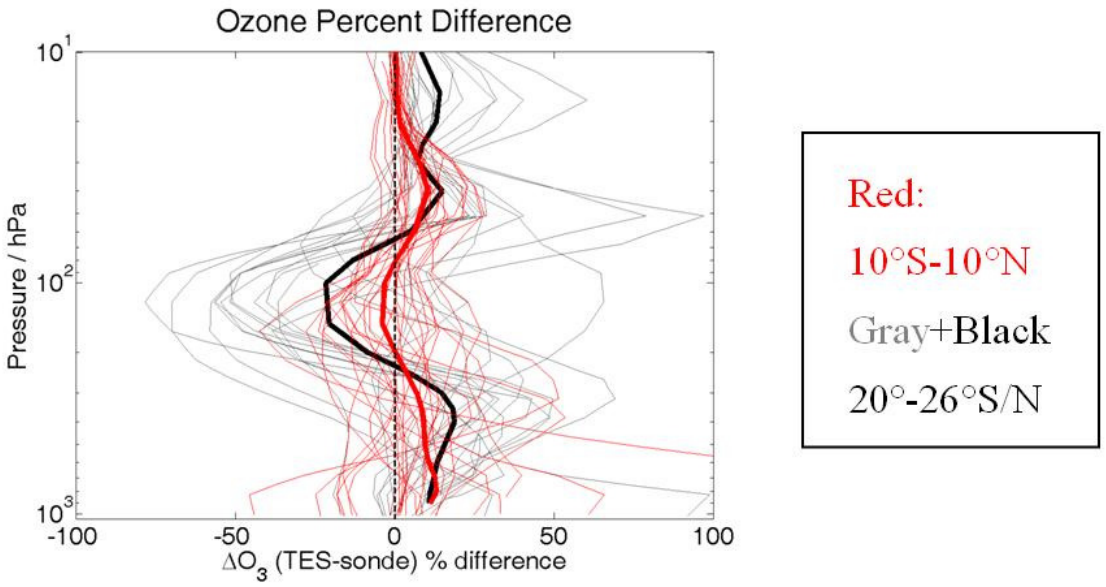

Figure 5-5 Percent Differences in TES-Sonde (with TES Operator). The inner tropics were defined here as coincidences in the 10°S-10°N range and are shown in red. The subtropical (20-26°S/N) coincidences, shown in black are responsible for most of the negative bias between about 100-300 hPa.

5.1.4 Case studies Over Specific Sonde Sites

Ozonesonde campaigns in 2006 with dedicated launches timed for the Aura overpass and corresponding special observations from TES with dense along-track nadir sampling have allowed detailed comparisons and tests of coincidence assumptions.

Two types of TES special observations were used for these campaigns. The TES observations for ARM-SGP and SAUNA were "transects" where the nadir angle changes with scan to allow nearly contiguous footprints with 40 scans covering around 500 km. For the comparisons with IONS-06 ozonesondes launched during the INTEX campaign, "Step and Stare" observations were used for greater coverage with 125 nadir measurements spaced about 40 km apart.

5.1.5 ARM-SGP (36.6°N, 97.5°W) Oklahoma, USA: Identification of "Emission Layer Flag"

Sondes were launched by F. Schmidlin, NASA Wallops from Jan 18 to Feb 16, 2006 for both night and day Aura overpasses at the ARM-SGP site (Southern Great Plains Atmospheric Radiation Measurement facility). The TES comparisons with these sondes have been critical in identifying erroneous retrievals that can sometimes result when the lowest layers of the atmosphere are in emission, *i.e.*, warmer than the surface. The constraints in the retrieval algorithm do not prevent cases with a large ozone abundance in the lowest layers in emission that would radiatively cancel with the layers in absorption above. The retrieval can find a false minimum since the artificially high ozone then suggests higher sensitivity, as seen in the averaging kernel for the lowest layers of these cases. This condition is now identified with the "emission layer flag", set to "bad" when the thermal contrast (T_atm – T_surf) over the lowest 3 layers in our radiative transfer model is > 1K and the ozone in these layers is > 15ppb from the

Distributed by the Atmospheric Science Data Center
http://eosweb.larc.nasa.gov

initial guess. Figure 5-6 shows statistics from the ARM-SGP ozonesonde comparisons (5 night and 4 day transect runs) and demonstrates the effect of the emission layer flag on the night observations, compared to day observations, which did not have emission layer conditions.

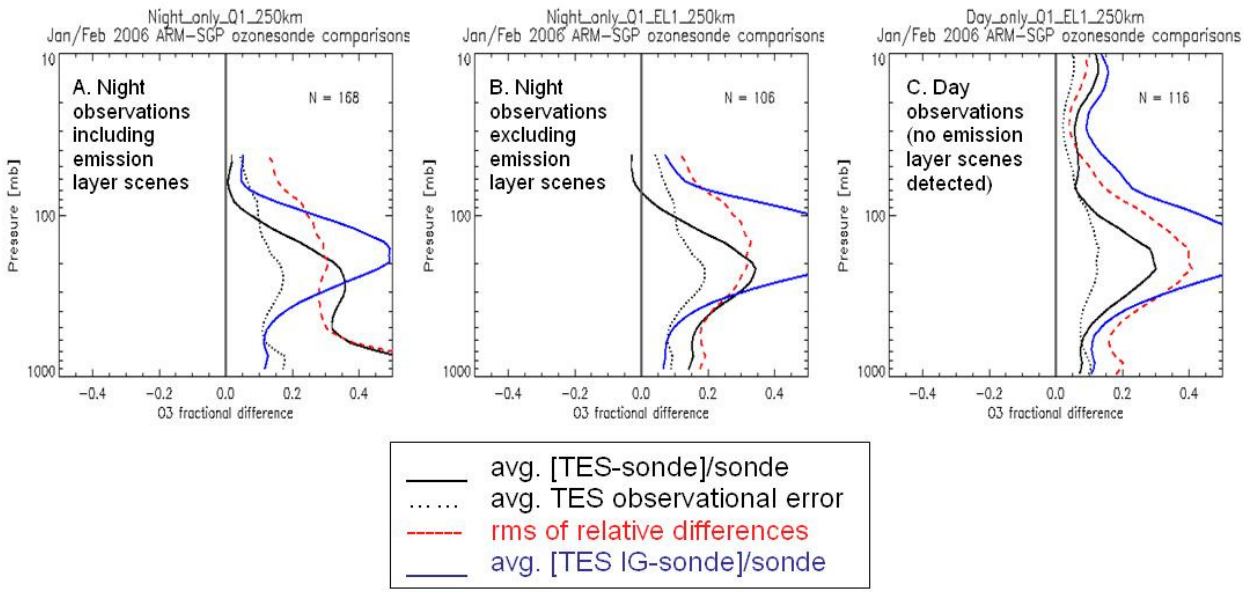

Figure 5-6 Statistics for ARM-SGP TES-Sonde Comparisons. Maximum altitude is determined by the lowest sonde height in the ensemble. Panel A shows the average TES-Sonde (with TES operator) difference and RMS for night observations, screened only by the general quality flag. Note the large values for both average difference and RMS near the surface. Panel B has night observations excluding TES scenes with an emission layer identified. Panel C shows day observations, which did not have any emission layer scenes detected. I.G. indicates initial guess**.**

5.1.6 Sodankyla (67.4°N, 26.6°E) Finland

Sondes were launched as part of SAUNA campaign from March 20 to April 14, 2006. Figure 5-7 shows the location of the TES transects taken during the campaign and a typical curtain plot of averaging kernel diagonals along the transect. The averaging kernels show maximum sensitivity just below the tropopause in these cases. Figure 5-8 shows a TES ozone profile compared to the ozonesonde, the ozonesonde with the TES operator applied and the TES initial guess (same as *a priori*) on the left and the sonde-TES % differences along the TES track as a curtain plot in pressure vs. latitude on the right.

Figure 5-9 shows NOAA-HYSPLIT (Draxler and Rolph, 2003) backward trajectories for both TES measurement locations and sonde site, corresponding to the case shown in Figure 5-8. The larger differences in the curtain plot of sonde-TES are consistent with the changes in the origin of the air masses sampled by TES compared to that sampled by the sonde.

Figure 5-10 gives the statistics of the comparisons as a function of pressure for 3 different coincidence criteria. This figure demonstrates that the average difference for TES-sonde(with TES operator) only varies slightly with the tighter coincidence criteria, while the variance decreases to where it is mostly explained by the estimate for TES observational error (measurement + cross-state errors).

Distributed by the Atmospheric Science Data Center
http://eosweb.larc.nasa.gov

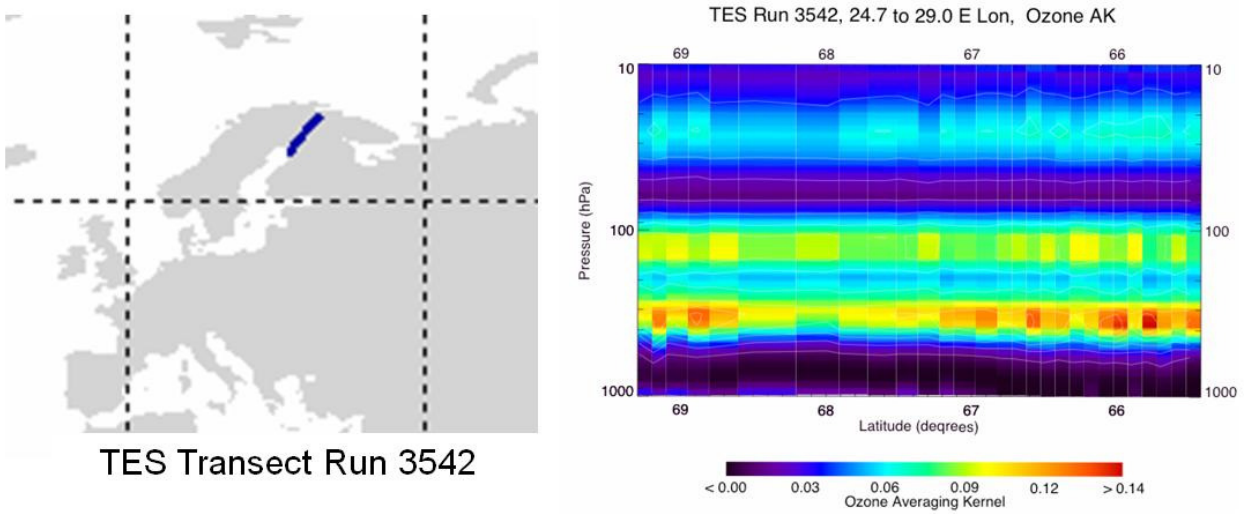

Figure 5-7 Target Locations for TES Transect Observations near Sodankyla and an Example of Averaging Kernel Diagonals vs. Pressure and Latitude Along the Track. The tropopause pressure was around 290 hPa in these measurements.

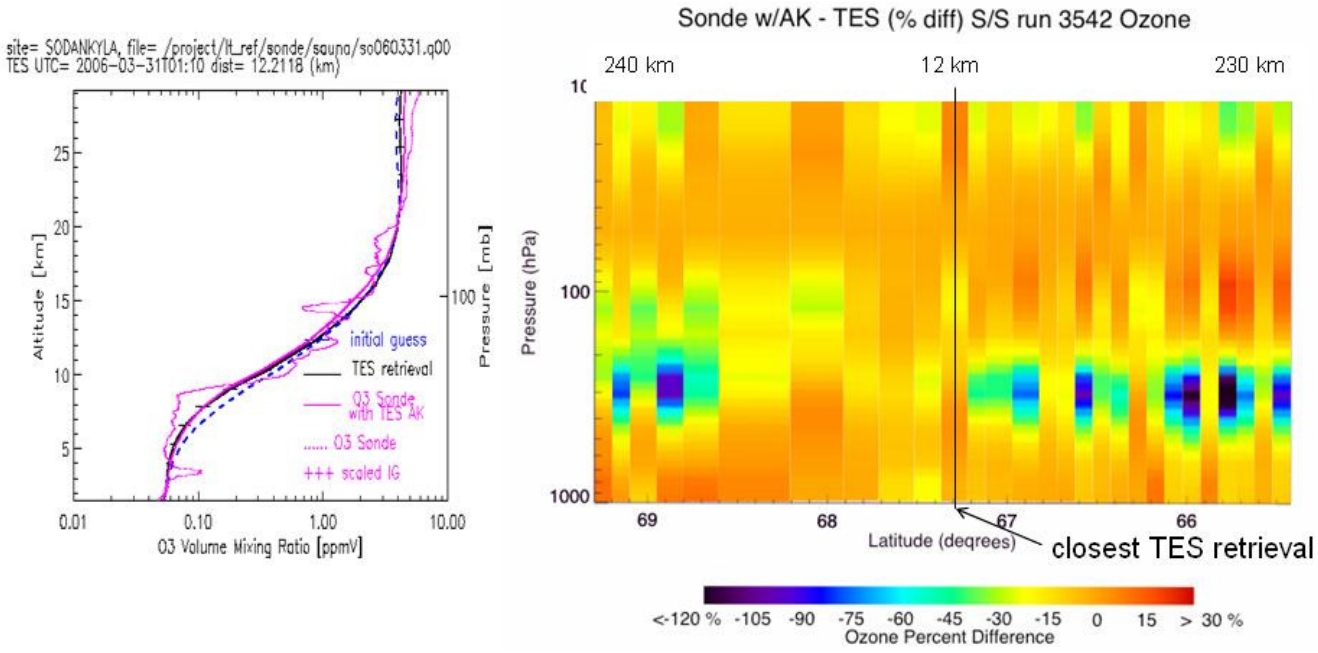

Figure 5-8 Profile Comparison for Closest TES Measurement (12 km) on March 31, 2006 (left) and Curtain Plot of Sonde(w/TES operator) – TES Percent Difference Showing better Agreement Close to the Sonde Site.

Distributed by the Atmospheric Science Data Center
http://eosweb.larc.nasa.gov

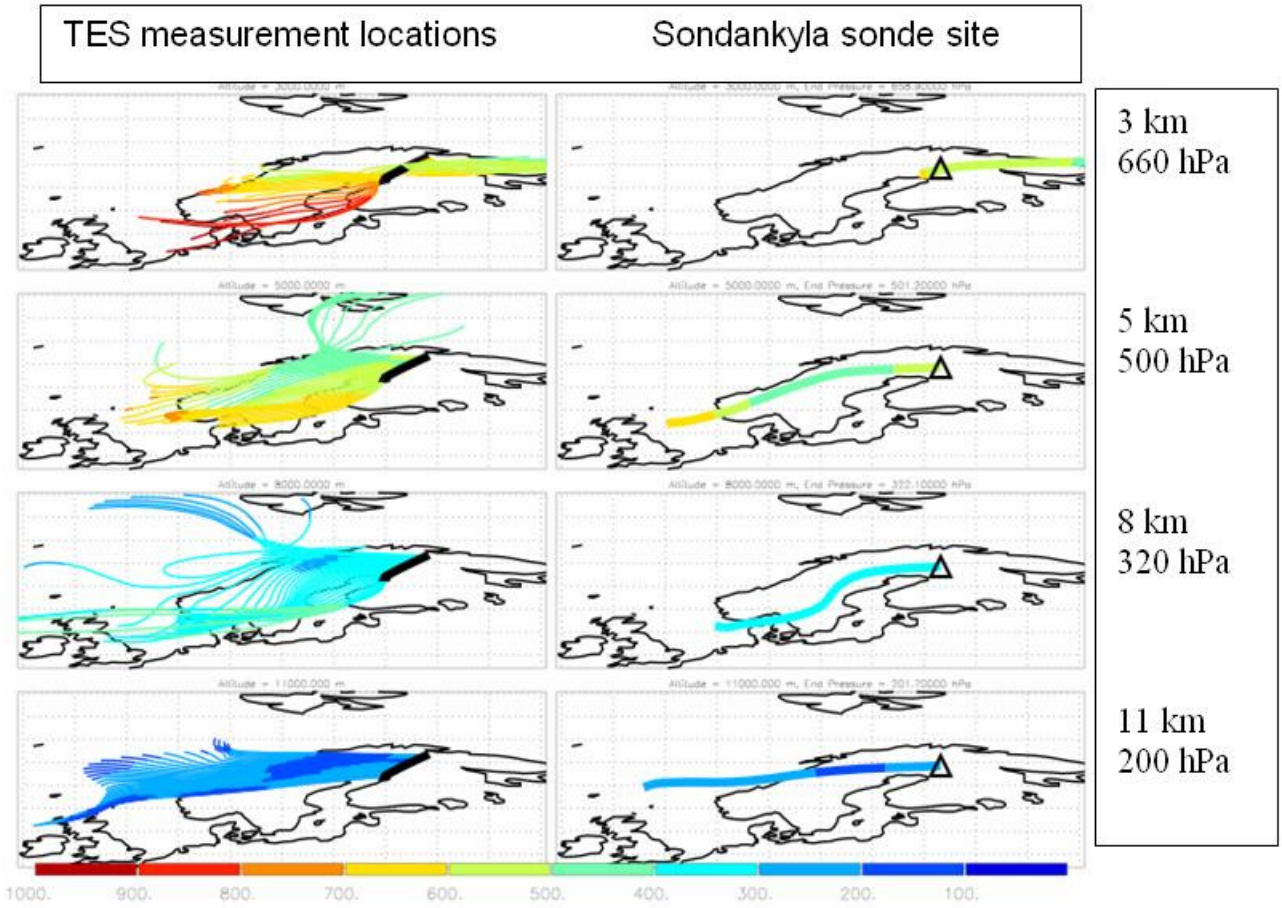

Figure 5-9 72 Hour NOAA-HYSPLIT Backward Trajectories, March 31, 2006, for TES Measurement Locations (Left Panels) and Sodankyla (Right Panels). Pressures of trajectories at the sonde site are shown on the right and colors indicate pressure in hPa along the trajectory.

Distributed by the Atmospheric Science Data Center
http://eosweb.larc.nasa.gov

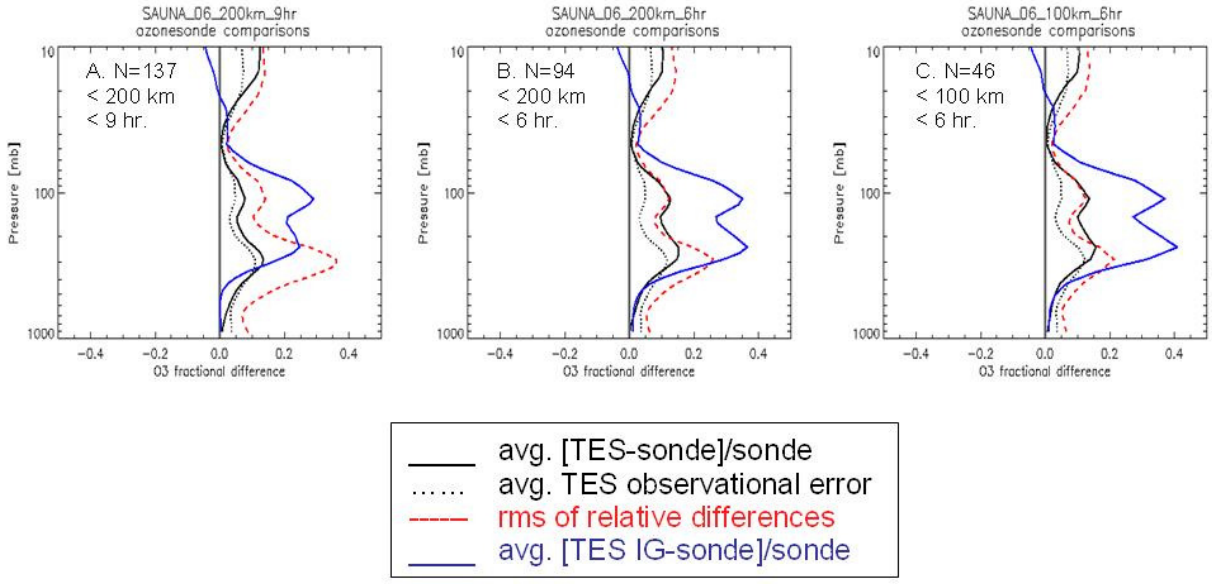

Figure 5-10 Statistics for TES Comparisons to Sodankyla Sondes from the March-April 2006 SAUNA Campaign with Coincidence Criteria as Shown. These plots show that the average fractional difference (avg. [TES-sonde]/sonde) only varies slightly for the different coincident criteria while the rms of fractional differences (red dashed line) decreases to where it is mostly explained by the estimated observational error from TES (black dotted line) for the tightest criteria (panel C: 100 km, 6 hr.).

5.1.7 PNNL (46.2°N, 119.2°W) Richland, Washington, USA

This comparison is with a sonde launched for the IONS-06 campaign on Apr 21, 2006, from the NATIVE (Nittany Atmospheric Trailer and Integrated Validation Experiment) platform at PNNL (Pacific Northwest National Laboratory), A. Thompson (P.I.). Figure 5-11 gives the TES Step/Stare measurement locations and the curtain plot of averaging kernel diagonal along the TES track (between the green bars). The averaging kernel shows that except for the few observations between 43° to 44°N, TES had low sensitivity to the lower troposphere. This is consistent with the retrieved cloud information (effective optical depths > 1 and cloud top pressures around 600 hPa) and demonstrates how application of the averaging kernel accounts for TES sensitivity to clouds. In the presence of optically thick clouds, the TES-sonde comparison gives no information below the cloud, but still allows a valid comparison above. The tropopause for these measurements was around 200 hPa,

Figure 5-12 shows ozone profile comparisons for TES, ozonesonde, ozonesonde with the TES operator and the TES initial guess (same as *a priori*) on the left and a curtain plot of the sonde-TES % differences along the TES track as a curtain plot in pressure vs. latitude on the right. The best TES-sonde agreement appears to be within about 200 km from the sonde site. Figure 5-13 shows NOAA-HYSPLIT (Draxler and Rolph, 2003) backward trajectories for both TES measurement locations and sonde site. Here also the trajectories are consistent with the divergence of the sonde-TES differences observed along the TES track.

Distributed by the Atmospheric Science Data Center
http://eosweb.larc.nasa.gov

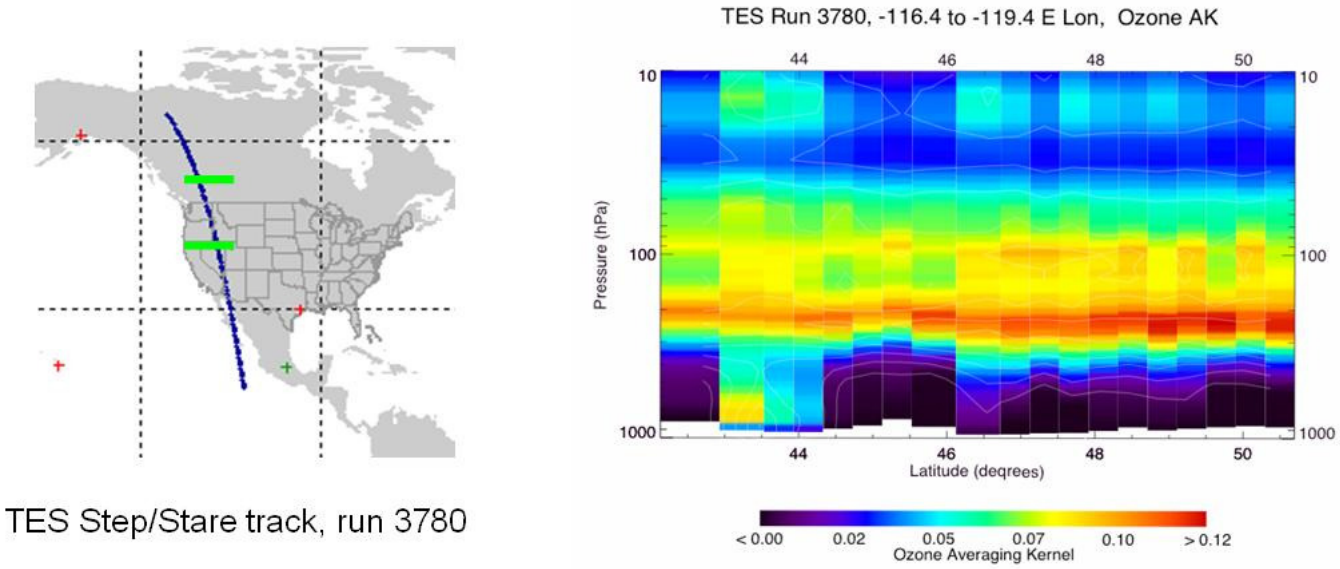

Figure 5-11 TES Measurement Locations (Left) for Closest Run to the IONS NATIVE (PNNL) Sonde on April 21, 2006 and Averaging Kernel Diagonal Curtain Plot (Right) Corresponding to Ozone Profiles Along the Track Between the Green Bars.

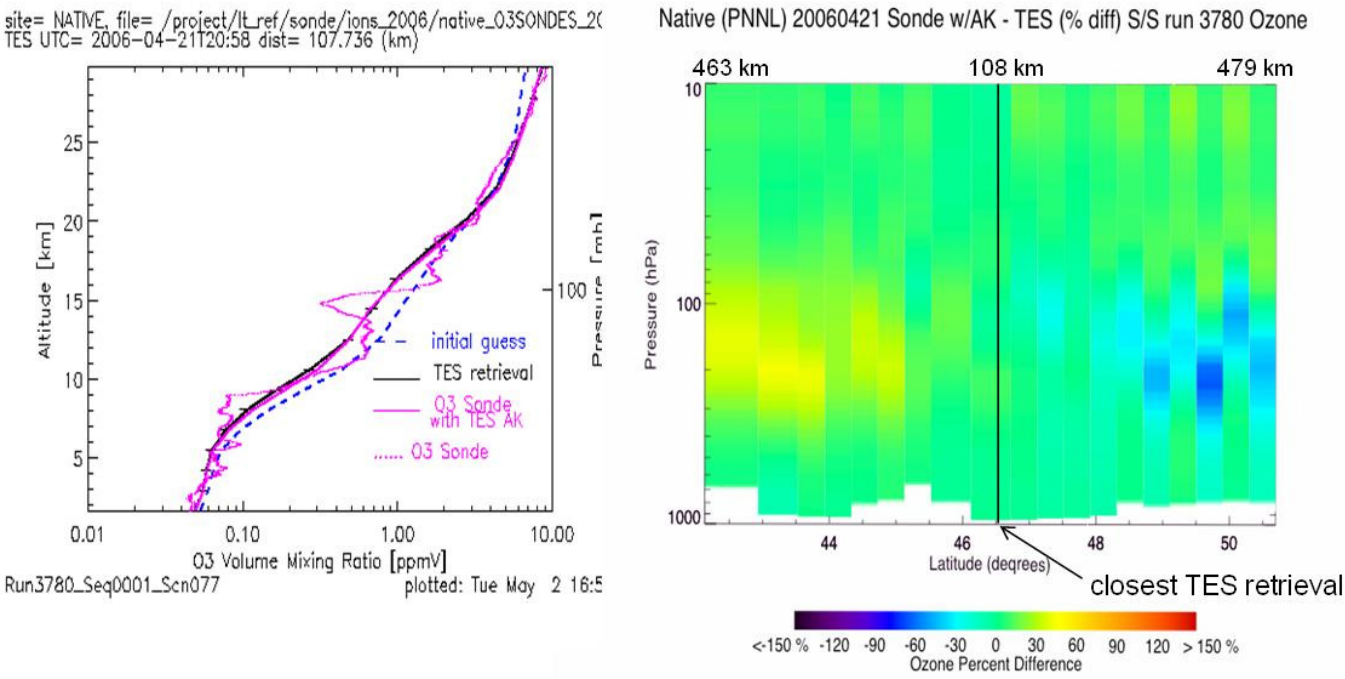

Figure 5-12 Profile Comparison for Closest TES Measurement (108 km) with Sonde, Sonde with TES Operator and TES Initial Guess on April 21, 2006 (left) and Curtain Plot of Sonde(w/TES operator) – TES Percent Difference Showing Better Agreement within about 200 km of the Sonde Site.

Distributed by the Atmospheric Science Data Center
http://eosweb.larc.nasa.gov

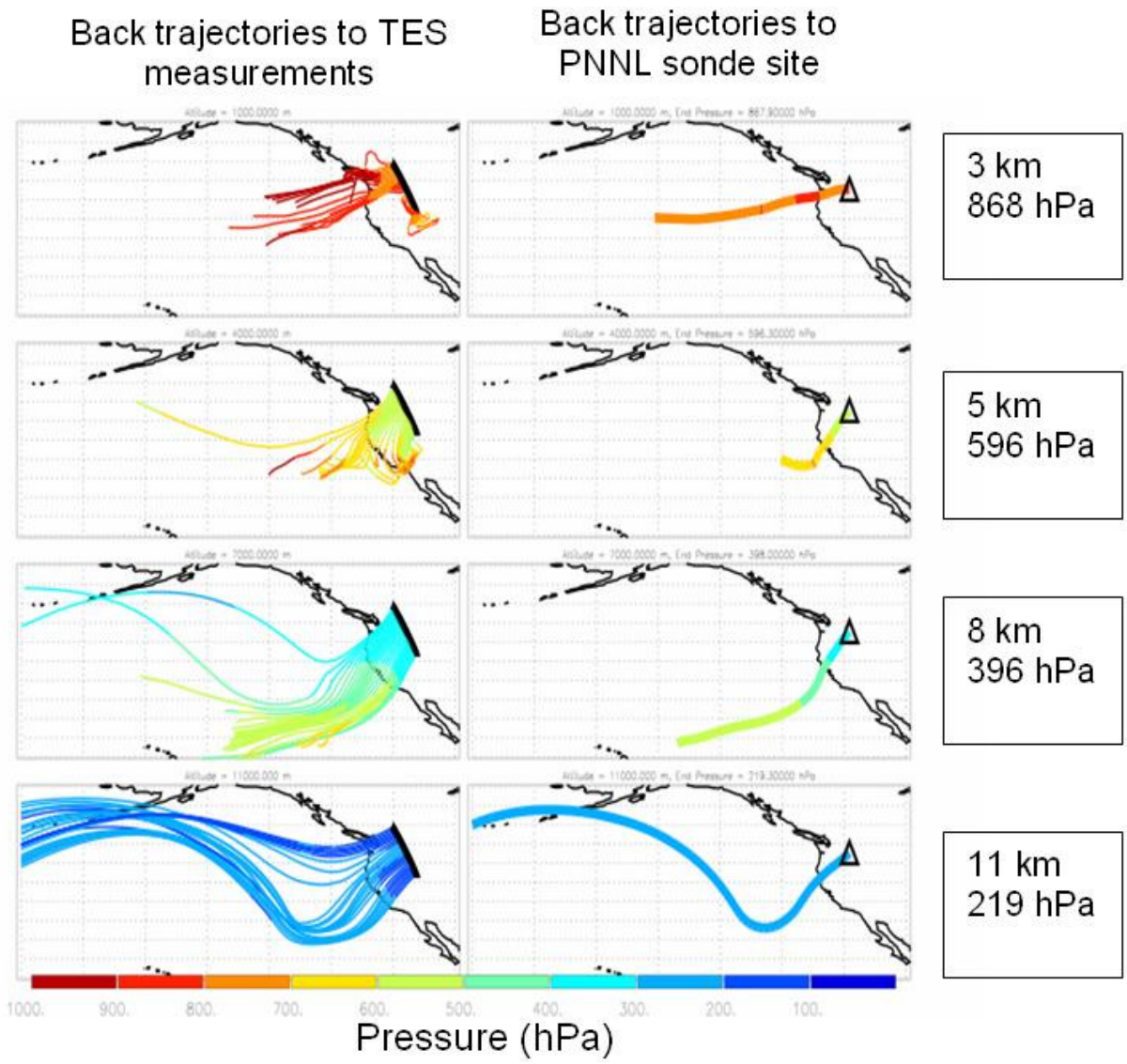

Figure 5-13 72 Hour NOAA-HYSPLIT Backward Trajectories, April 21, 2006, for TES Measurement Locations (Left Panels) and PNNL (right panels). Pressures of trajectories at the sonde site are shown on the right and colors indicate pressure in hPa along the trajectory.

5.1.8 Conclusions from TES-ozonesonde case studies:

- TES data taken near the ARM-SGP site had a high occurrence of emission layer scenes for the night observations. After removing these, the statistics for the night comparisons are much closer to the day comparisons. Both day and night comparisons show a high bias for TES ozone profiles that is larger than the average for northern mid-latitude cases, and is under investigation.
- Sodankyla comparisons represent the highest northern latitude validation obtained so far and exhibit a similar high bias for TES ozone profiles as seen in northern mid-latitude and

Distributed by the Atmospheric Science Data Center
http://eosweb.larc.nasa.gov

Antarctic comparisons with WOUDC sonde data.

- Statistical analysis of Sondankyla comparisons shows that tighter coincidence criteria improve the agreement of the relative difference RMS to the estimated TES observational error, but do not make a significant change to the average relative difference [TES-sonde(with TES operator)]/[sonde(with TES operator)].
- Case studies show that 200 km distance criteria, currently applied for the selection of TES data in sonde comparisons, appears to be reasonable for higher northern latitudes.

5.1.9 References:

[1] K.W. Bowman, C. D. Rodgers, S. S. Kulawik, J. Worden, E. Sarkissian, G. Osterman, T. Steck, M. Lou, A. Eldering, M. Shepherd, H. Worden, M. Lampel, S. Clough, P. Brown, C. Rinsland, M. Gunson, R. Beer, "Tropospheric Emission Spectrometer: Retrieval Method and Error Analysis", *IEEE Trans. Geophys. Remote Sens.,* vol 44, no. 5, pp 1297-1307. May 2006.

[2] Draxler, R.R. and Rolph, G.D. (2003), HYSPLIT (HYbrid Single-Particle Lagrangian Integrated Trajectory) Model access via NOAA ARL READY Website (http://www.arl.noaa.gov/ready/hysplit4.html). NOAA Air Resources Laboratory, Silver Spring, MD.

[3] C. Rodgers and B. Conners, "Intercomparison of remote sounding instruments," *J. Geophys. Res.*, vol. 108(D3), p. 4119, 2003.

[4] C. Rodgers, Inverse Methods for Atmospheric Sounding: Theory and Practice. London: World Scientific, 2000.

[5] J. Worden, S. S. Kulawik, M. Shepard, S. Clough, H. Worden, K. Bowman, and A. Goldman, "Predicted errors of Tropospheric Emission Spectrometer nadir retrievals from spectral window selection," *J. Geophys. Res*., vol. 109, no. D09308, May 2004.

[6] H. M. Worden, J. A. Logan, J. R. Worden, R. Beer, K. Bowman, S.A. Clough, A. Eldering, B.M. Fisher, M. R. Gunson, R. L. Herman, S. S. Kulawik, M. C. Lampel, M. Luo, I. A. Megretskaia, G. B. Osterman and M. W. Shephard, "Comparisons of Tropospheric Emission Spectrometer (TES) ozone profiles to ozonesondes: methods and initial results*", J. Geophys. Res. – Atmospheres*, accepted, 2006.

Distributed by the Atmospheric Science Data Center
http://eosweb.larc.nasa.gov

5.2 Comparison with Lidar Measurements

5.2.1 INTEX-B and DIAL Measurements

Validation of remotely sensed constituent profiles is essential before they may be used for scientific studies. Validation seeks to identify and characterize any systematic biases that may be present in the reported mixing ratio profile. Validation is conducted through comparisons with independent measurements of the same parameters. The validation of tropospheric ozone, which has a large degree both spatial and temporal variability, requires that these independent measurements be as close to temporally and spatially coincident with the satellite observations as possible.

The Intercontinental Chemical Transport Experiment – Phase B (INTEX-B) was an intensive aircraft campaign which took place over a 10 week period from March 1 to May 15 2006. Among the objectives of the campaign were to observe Mexico City pollution outflow and the transport of Asian pollution to the United States, as well as obtaining temporally and spatially coincident measurements of trace gas species for the validation of remote sensing instruments on the AURA satellite platform. Measurements were made using NASA's DC-8 aircraft with a range of *in situ* and remote sensing instruments. The campaign was split into two phases, during the first phase, performed in March 2006, the DC-8 was based in Houston, Texas, where it conducted a number of flights over the Gulf of Mexico, in the hope of observing the outflow of pollution from Mexico City. The second phase took place during April and May 2006 with the objective of observing Asian pollution outflow over the Pacific. During the second phase the DC-8 conducted several flights out of Honolulu, Hawaii and Anchorage, Alaska.

During the course of the INTEX-B campaign TES made 243 Step & Stare special observations over the United States, East Asia and the Pacific (see Figure 5-14) in order to try and set a context for the limited spatial extent covered by the aircraft observations. Of the flights conducted, seven were coincident or near-coincident with TES Step & Stare observations, 3 in Houston, 2 in Hawaii and 2 in Alaska, the flight tracks for these flights are shown in Figure 5-15.

During the INTEX-B campaign the NASA Langley Research Center Airborne Differential Absorption Lidar (DIAL) instrument made profiles of ozone both below and above the DC-8 aircraft. The instrument measure ozone using two lasers in the ultraviolet that are tunable to maximize the range and sensitivity of the measurement. An example of a DIAL ozone curtain and the instrument standard error are shown in Figure 5-16 and Figure 5-17 for a DC-8 flight out of Honolulu on April 23, 2006.

Distributed by the Atmospheric Science Data Center
http://eosweb.larc.nasa.gov

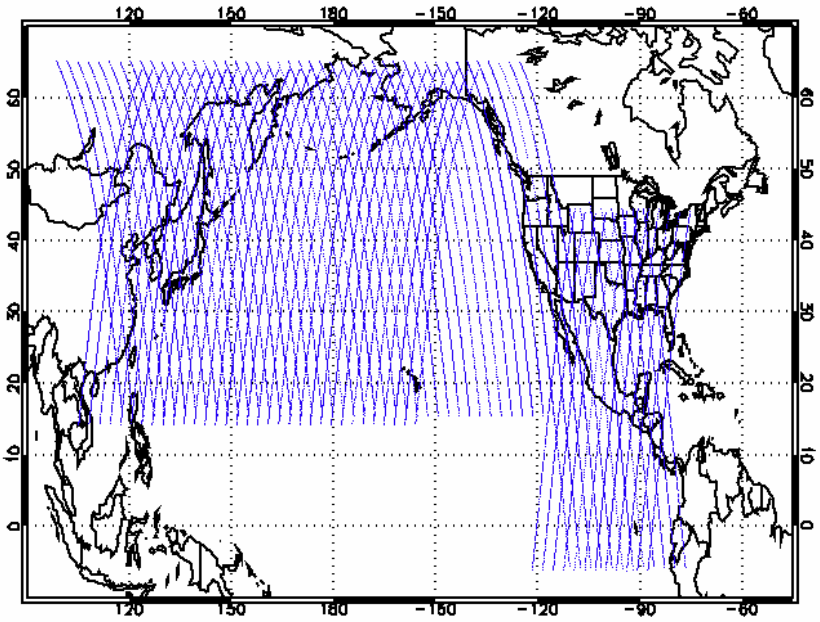

Figure 5-14 The TES step and stare tracks during the INTEX-B campaign.

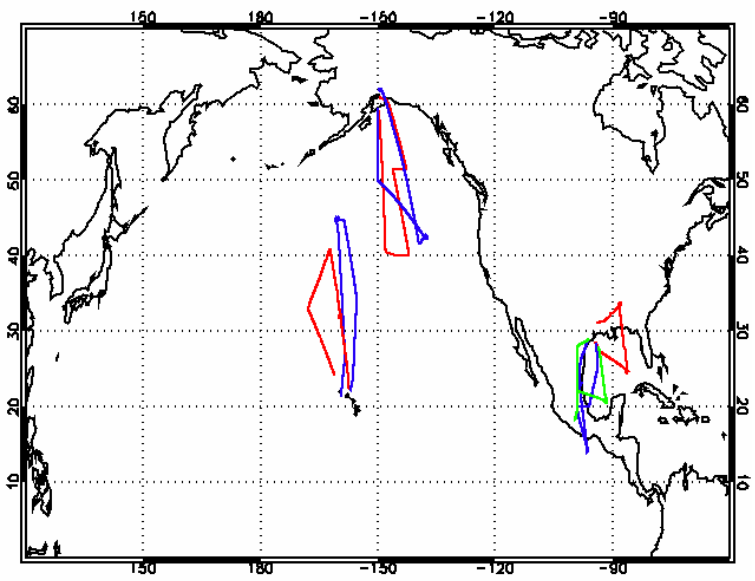

Figure 5-15 The DC-8 flight tracks that provided the best coincidences with TES nadir measurements.

Distributed by the Atmospheric Science Data Center
http://eosweb.larc.nasa.gov

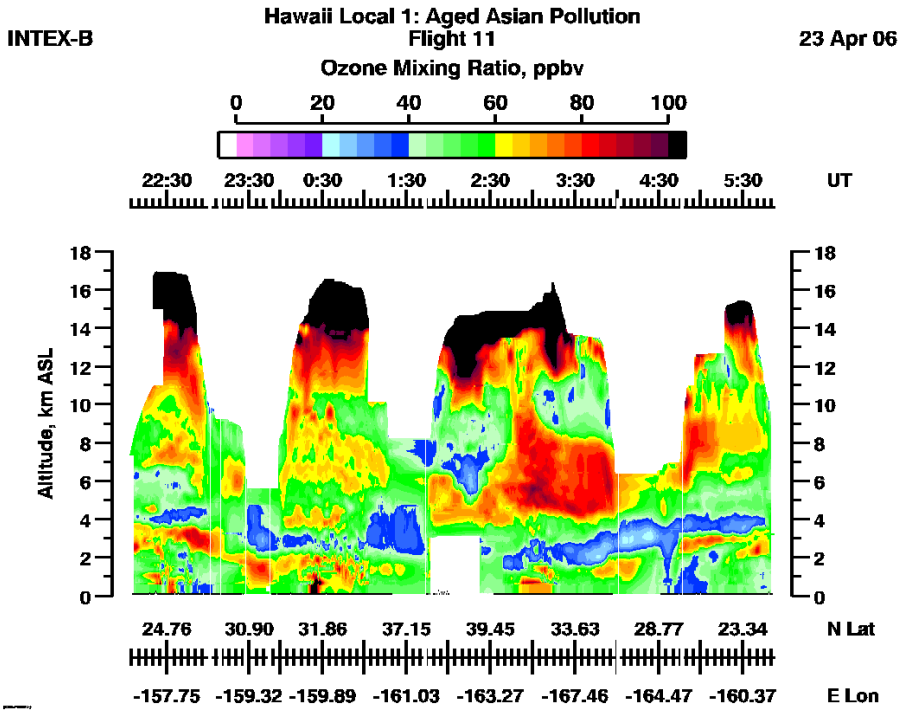

Figure 5-16 A DIAL ozone curtain for the DC-8 flight of April 23, 2006.

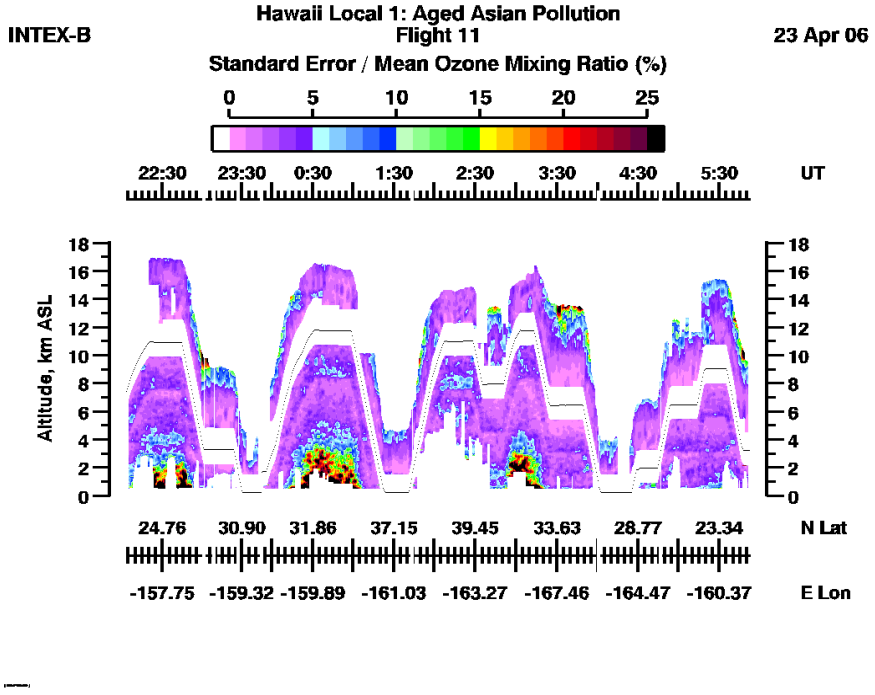

Figure 5-17 The DIAL standard error for the April 23, 2006 DC-8 flight.

Distributed by the Atmospheric Science Data Center
http://eosweb.larc.nasa.gov

5.2.2 DIAL Comparisons with TES

In order to compare profiles obtained from a remote sensing instrument such as TES with *in-situ* data, we must first take into account the limited vertical resolution and the affects of *a priori* information inherent in the retrieved profiles. Averaging kernels intrinsically account for both, and may be used to transform *in-situ* profiles into "TES space" so that they may be directly compared

$$\mathbf{x}_{\mathbf{final}} \equiv \mathbf{x}_{\mathbf{a}} + \mathbf{A}(\mathbf{x}_{\mathrm{DIAL}} - \mathbf{x}_{\mathbf{a}})$$

(Equation 5-3)

An example of how applying the TES averaging kernels affects the DIAL curtain results is given in Figure 5-18. The two panels on the right of Figure 5-18 can be compared directly since the DIAL data is now sampling the atmosphere in a manner similar to TES.

Mean DIAL profiles were calculated to compare to TES special observation profiles. All DIAL observations within 0.15 degrees lat/lon of each TES observation were selected and averaged for comparison with the corresponding TES profile. DIAL profiles were interpolated to the TES pressure grid. In order to apply TES averaging kernels to the DIAL profiles missing data in the DIAL profile were replaced with TES *a priori* information, each profile was also extended to the highest TES pressure level using the *a priori* information used in the TES retrieval. Any profiles which failed the TES QA were discounted from the analysis. Figure 5-19 shows the profile of the difference between TES-DIAL as a function of atmospheric pressure for each of the profiles from DIAL that are coincident with a TES profile. The figure also shows the difference of TES-DIAL for an averaged DIAL profile. The final panel in the figure is the difference profile of TES-DIAL for an average of all coincident DIAL and TES profiles for the Houston based flights during INTEX-B and shows TES to be higher than DIAL by roughly 10-15% over most of the troposphere.

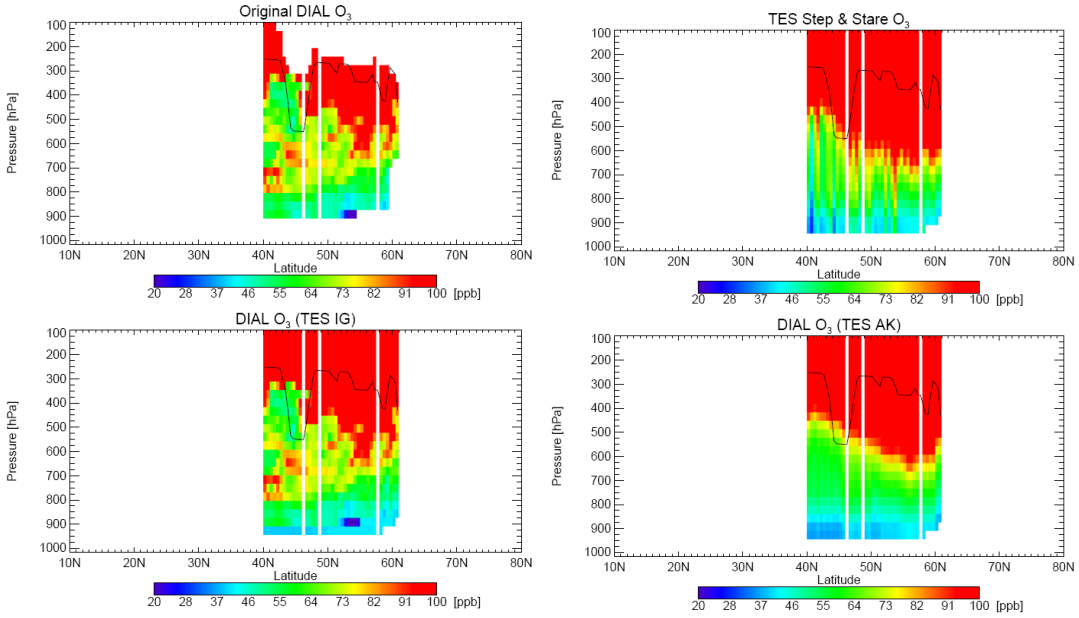

Figure 5-18: The DIAL ozone curtain as measured with the DIAL vertical resolution (upper left). The DIAL ozone curtain with the scaled TES a priori used to extend the profile (lower left).

Distributed by the Atmospheric Science Data Center
http://eosweb.larc.nasa.gov

The TES step and stare curtain (upper right) and the DIAL curtain after application of the TES averaging kernel (lower right).

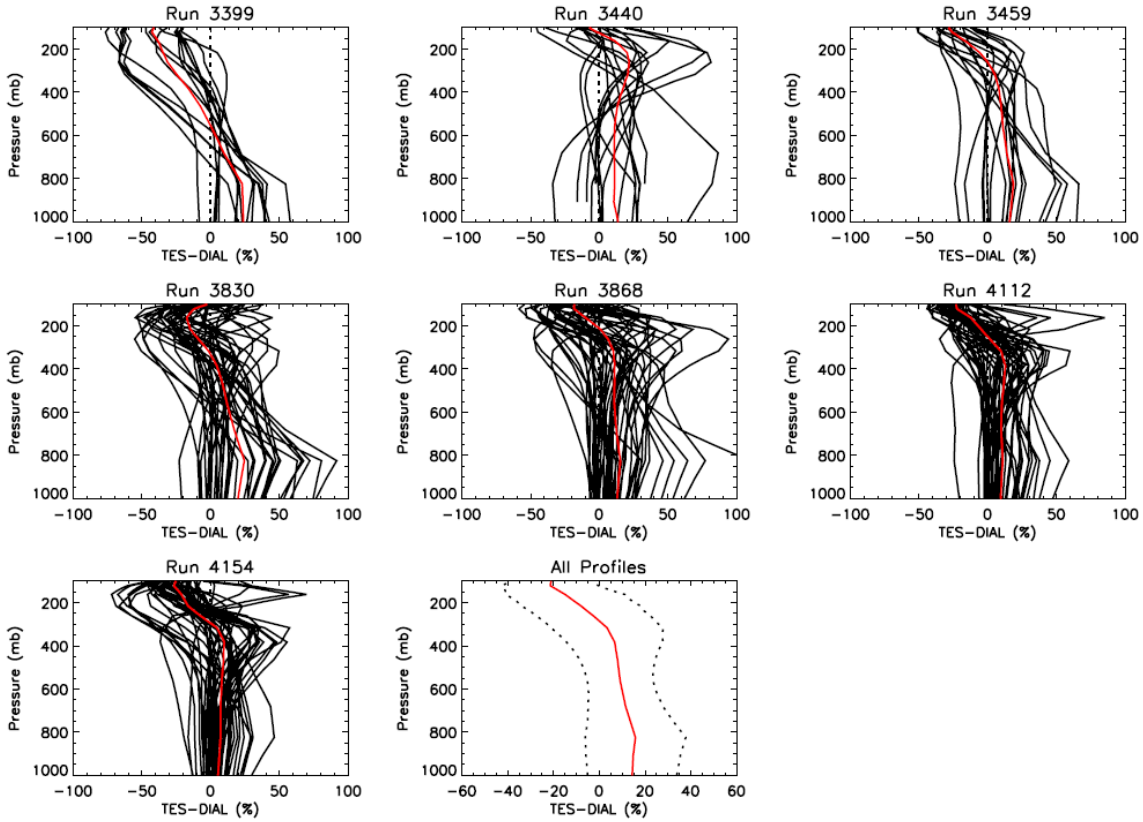

Figure 5-19 Percentage difference between TES and individual (black) and averaged (red) DIAL profiles for different TES step and stare observations. The final plot is the percentage difference between the mean of all TES and DIAL coincident profiles for the Houston based flights of INTEX-B.

5.2.3 Preliminary Conclusions

During the course of INTEX-B 212 coincident profiles were obtained for comparison, these covered the region of the Eastern and Central North Pacific and the Southern United States. A variety of conditions were observed during these observations, from relatively clean air in the Gulf of Mexico to more polluted air in the north eastern Pacific. On average TES exhibits a small positive bias in the middle and lower troposphere of 10-15% and a negative bias of up to 20% in the upper troposphere. Larger differences are observed in cleaner regions than in more polluted regions, this is likely due to the reduced signal available for TES to retrieve profile information. Some of the differences may be due to the temporal mismatch of the DIAL and TES observations since tropospheric Ozone can vary on small spatial and temporal scales.

Distributed by the Atmospheric Science Data Center
http://eosweb.larc.nasa.gov

5.3 Validation of TES Measurements of the Total Ozone Column

5.3.1 TES Total Ozone Column

TES has the measurement sensitivity required to estimate ozone through the regions of the troposphere and stratosphere where the vast majority of total atmospheric column is located. Because of this sensitivity, TES can make a determination of the total column ozone abundance. In order to examine the quality of the total ozone measured by TES, total column ozone amounts determined by TES have been compared to data from the Ozone Monitoring Instrument (OMI) which like TES is on the NASA Aura spacecraft. The OMI data used is version 2 of the "TOMS" (Total Ozone Mapping Spectrometer) type OMI retrievals. In order to make the best comparison with TES nadir measurements, only the OMI data looking straight down were used in the comparisons.

Figure 5-20 is a typical comparison between TES and OMI total column ozone observations over the course of a global survey from April 4-5, 2006. The figure shows that TES captures similar patterns in the ozone column as a function of latitude, but see generally higher amounts of ozone. The percentage difference plot at the bottom of the figure shows that TES is consistently higher than OMI over most latitudes. Figure 5-21 shows the average column value column in 10 degree bins of latitude for both OMI and TES. This figure shows more clearly that TES is higher than OMI for the latitude range of 70°S – 70°N by amounts ranging from 3-5%. The nature of the differences at high latitudes is being investigated.

A more detailed analysis of the validation of the TES ozone column product will be provided in the future including a look at comparisons with Microwave Limb Sounder (MLS), particularly upper tropospheric and stratospheric column comparisons.

5.3.2 TES Tropospheric and Stratospheric Column Values

Because TES is sensitive to ozone in several layers of the atmosphere it is possible to make a determination of the column ozone abundance in the troposphere and stratosphere. In this version of the TES validation report we do not show any of the results of validation of the TES tropospheric column determinations. We are currently working at getting a better characterization of the errors in column values, particularly those associated with the location of the tropopause. The next version of the TES data will have a tropospheric ozone column product and the use of and validation for this product will be discussed.

Distributed by the Atmospheric Science Data Center
http://eosweb.larc.nasa.gov

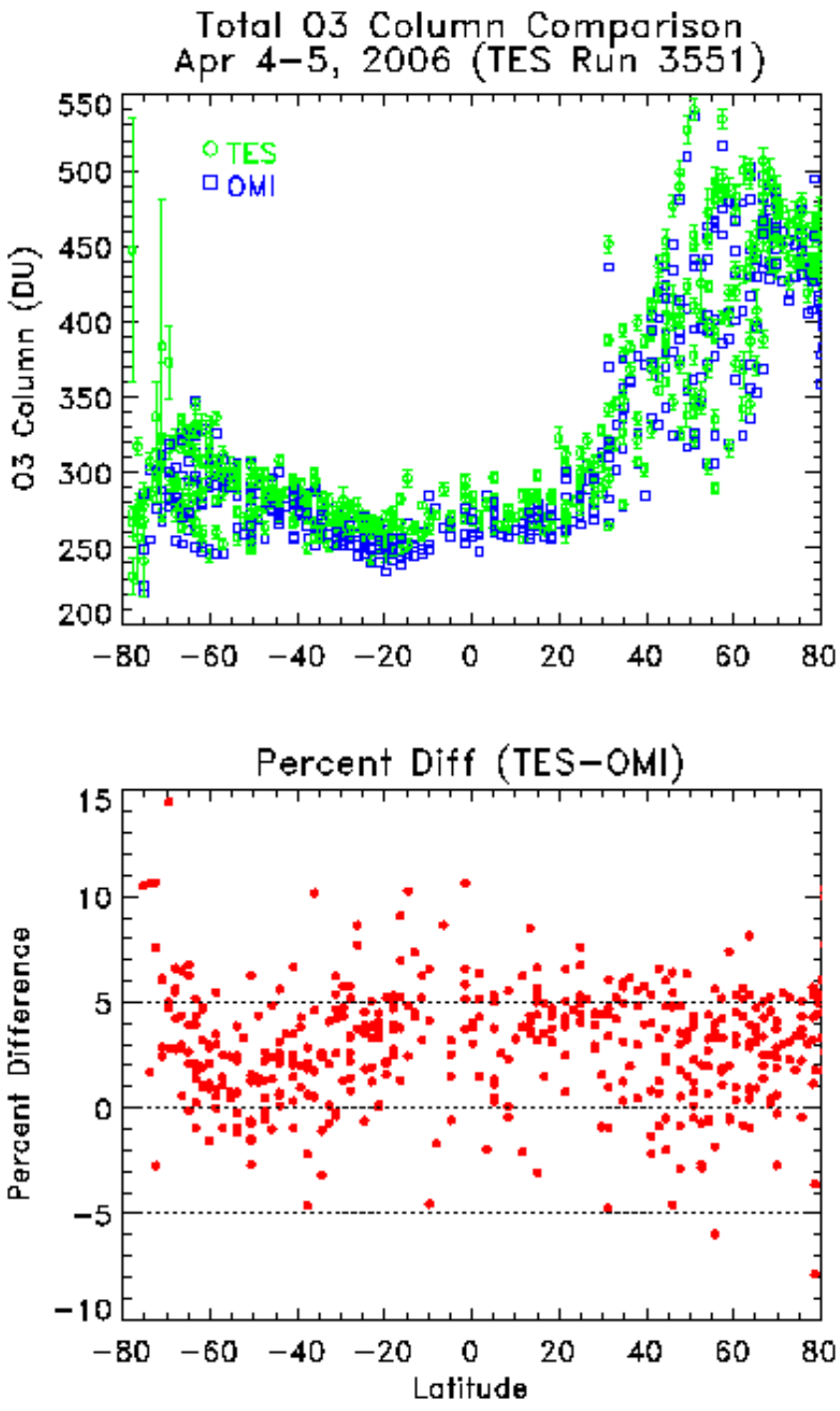

Figure 5-20 TES and OMI measurements of the total ozone column from April 4-5, 2006.

Distributed by the Atmospheric Science Data Center
http://eosweb.larc.nasa.gov

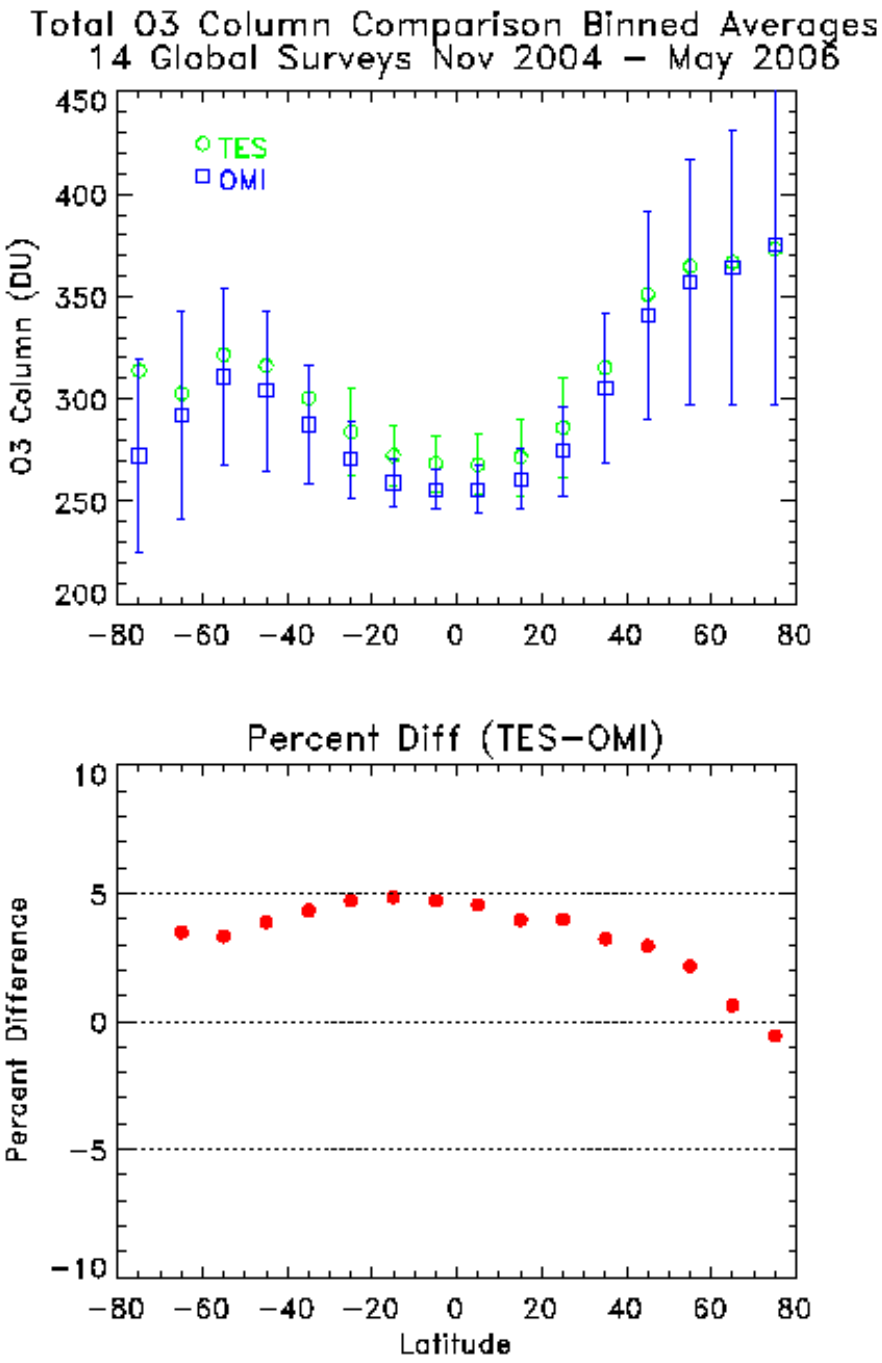

Figure 5-21 The mean value of TES and OMI measurements of the total ozone column in 10 degree bins, clearly showing TES biased high by 3-5% over mid-latitudes and tropics.

Distributed by the Atmospheric Science Data Center
http://eosweb.larc.nasa.gov

6. Validation of TES Retrievals of Carbon Monoxide

In this section we briefly describe the TES instrument performance over two years on orbit and the effect of the optical bench warm-up conducted early Dec 2005 on filter 1A1 and the CO retrievals. A brief overview of the global distributions of TES CO measurements is given different seasons. We present comparisons of TES CO profiles with *in situ* measurements from several aircraft campaigns, including INTEX-B, AVE, and CR-AVE. Validation of TES CO data using MOPITT measurements, as well as comparisons in the upper troposphere of TES CO data to ACE (Atmospheric Chemistry Experiment) and MLS CO are shown. These comparisons not only offer good qualitative checks for TES data, *e.g.,* the characteristics of the CO global distribution or the shapes of their vertical profiles, but also offer initial quantitative validations of TES CO retrievals. An overview of the characterization of TES retrievals, including the roles of *a priori* profiles and the averaging kernels is also provided in this section.

6.1 Instrument performance before and after optical bench warm-up

The signal strength in TES 1A1 filter is not constant over time and the variation of the signal strength is reflected in the CO retrievals. Figure 6-1 displays the normalized integrated spectral magnitude (ISM) (top panel), beam splitter temperature (middle panel), and degree of freedom for signal (DOFS) for latitudes of 30°N-30°S as a function of time (Rinsland et al., 2006). The ISM is a sensitive indicator of the signal levels of the TES detectors and is calculated by integrating a spectrum over wavenumber. It is the primary quantity used to quantify and detect trends in the TES instrument alignment and performance. An overall trend of declining ISM with time and the measured beamsplitter temperature is apparent, with increases in beamsplitter temperatures when the detectors are de-iced periodically. The warming of the TES optical bench on November 29-December 2, 2005 improved the TES beamsplitter alignment, with an integrated spectral magnitude increase for the 1A1 filter by a factor of 3.4 as compared to the pre-warm up value.

Figure 6-2 shows the DOFS before and after optical bench warm-up. The average DOFS in 30°N-30°S was 0.72 prior to the TES optical bench warm up and then increased to 1.45 after the warm up. The latitudinal distributions of DOFS reflect the latitudinal distribution of the surface temperature. TES measurement signal to noise ratios are larger for scenes with higher surface temperatures, *e.g.,* tropics. In the high latitudes or for the scenes covered with clouds, TES CO profile retrievals have relatively less values.

Figure 6-3 illustrates the improvement in total retrieval error and the retrieval precision for TES CO at 511 hPa. In 30S – 30N, the averaged total error was reduced from 19 ppb to 11ppb, and the precision values were reduced from 10 ppb to 5 ppb.

In summary, TES retrievals of carbon monoxide are much improved after the optical bench warm up in early December 2005 as a result of the better alignment of the instrument and increased signal to noise.

Distributed by the Atmospheric Science Data Center
http://eosweb.larc.nasa.gov

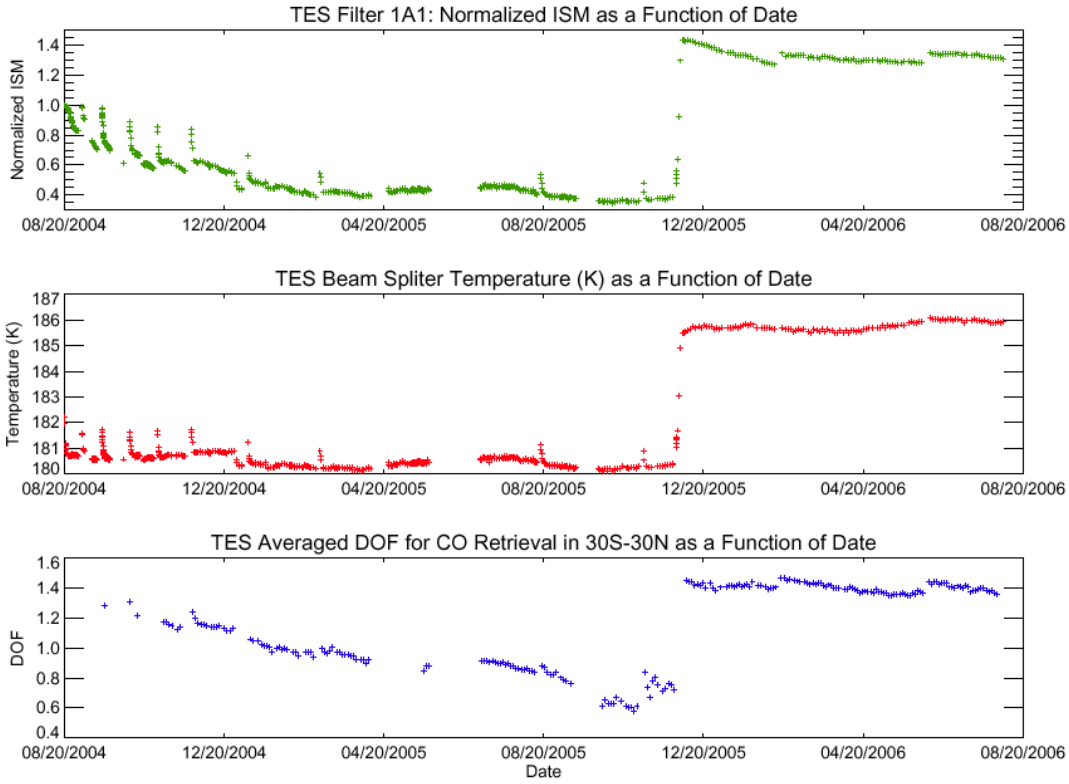

Figure 6-1 Time series of measured normalized Integrated Spectral Magnitude (ISM) (top panel), beamsplitter temperature (middle panel), and average DOFS for 30°N-30°S latitude. The ISM is normalized to 1.0 at the beginning of the time series.

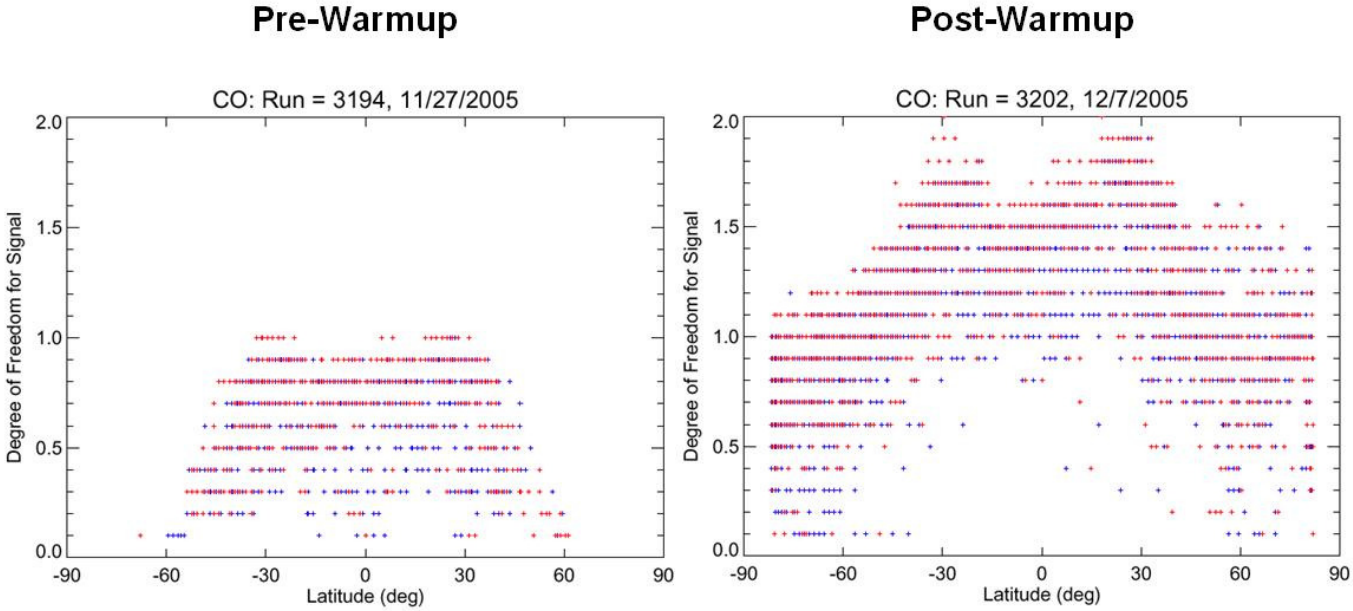

Figure 6-2 Latitudinal distributions of the degrees of freedom for signal (DOFS) of the TES CO retrievals for two global survey runs pre- and post optical bench warm up.

Distributed by the Atmospheric Science Data Center
http://eosweb.larc.nasa.gov

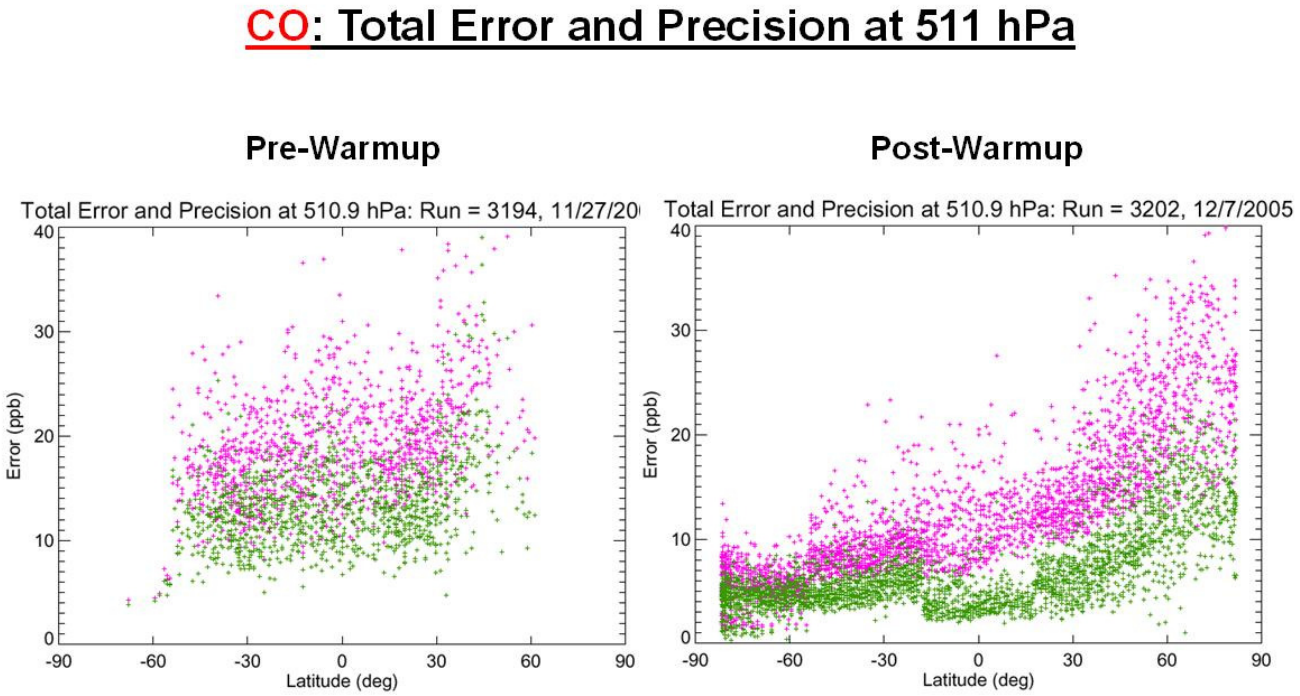

Figure 6-3 Latitudinal Distributions of the Total Errors and The Precisions for TES CO Retrievals in Two Global Survey Runs of Pre and Post Optical Bench Warm-up.

6.2 Global distributions of CO from TES measurements

Carbon monoxide is a by-product of incomplete combustion of fossil fuels and biomass, and is produced by oxidation of methane (CH_4) and other hydrocarbons. The global distributions of TES CO fields reflect this basic understanding, e.g., the enhanced CO regions and their seasonal variations are co-located with the known source regions. Figure 6-4 shows TES CO monthly mean distributions at 681.3 hPa for October 2005, January, April and July 2006. In general, the northern hemispheric (and the tropics) show much more CO than the southern hemisphere due to the known distribution of natural and industrial sources. CO values in the winter/spring are larger than summer/fall due to the longer lifetime in seasons with less photochemical activity.

In central Africa, the enhanced CO corresponding to biomass burning occurs in two time periods, in Dec/Jan/Feb for latitudes north of the equator and in Jul/Aug/Sep south of the equator, corresponding to the local dry seasons. In South America, the biomass burning induced maximum in CO concentration occurred during Aug/Sep/Oct near equator. Enhanced levels of CO over E. China can be related local pollution and can be seen throughout the year in the TES observations. TES also observed enhanced CO over Siberian in July 2006 which is associated with the fire occurred in the last ten days of July as reported by the MODIS Rapid Response System (http://rapidfire.sci.gsfc.nasa.gov/gallery/?2006203-0722

and http://rapidfire.sci.gsfc.nasa.gov/gallery/?2006205-0724).

Distributed by the Atmospheric Science Data Center
http://eosweb.larc.nasa.gov

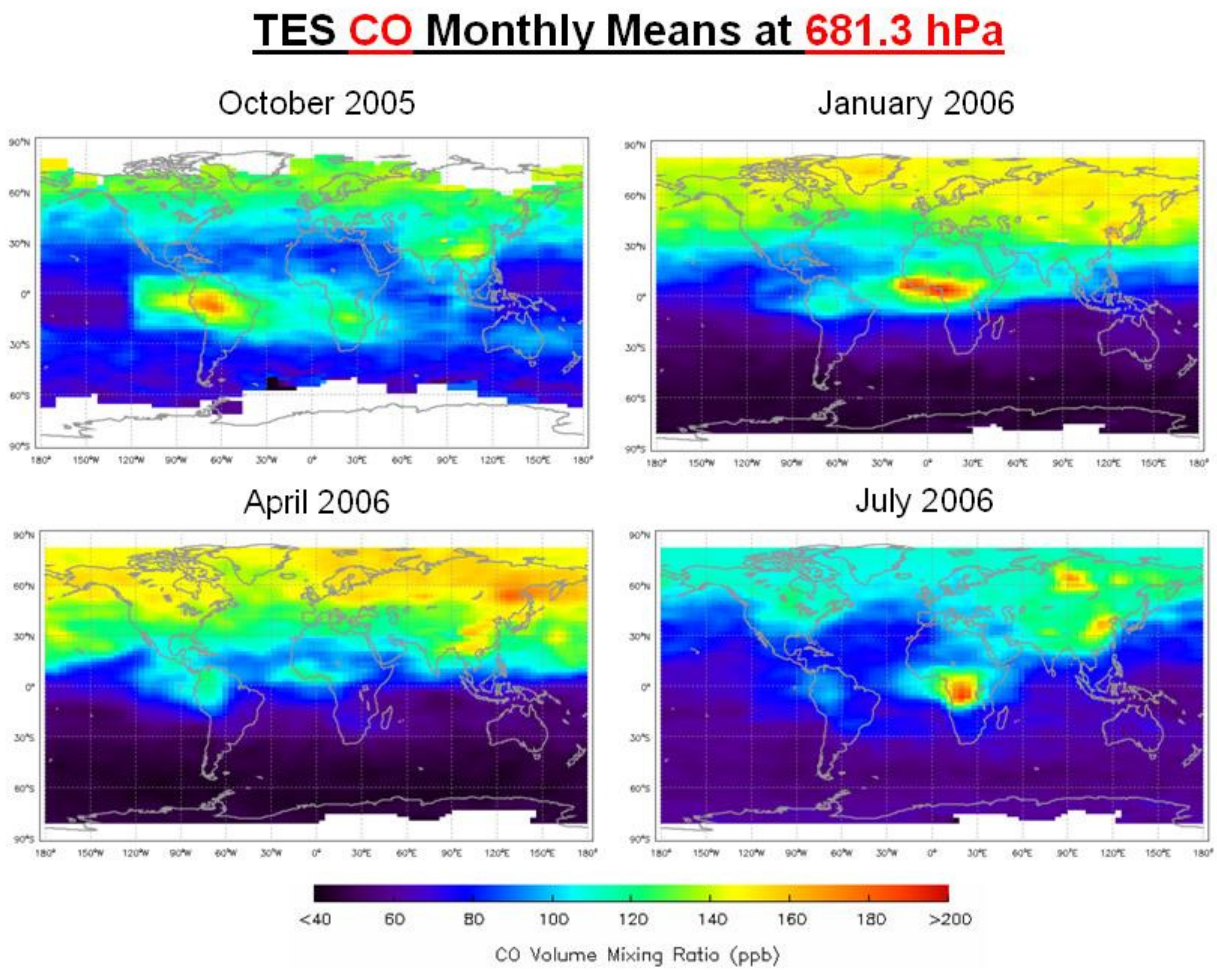

Figure 6-4 TES CO Global Distributions at 681.3 hPa for the Four Typical Months, Oct 2005, Jan, April, and July 2006.

6.3 CO validation: Comparisons to *in situ* Aircraft Measurement

During the past two years, several aircraft campaigns were conducted to study tropospheric chemistry and transport and to provide data for validation of the measurements made by the instruments on the Aura satellite. The TES team participated in the Aura Validation Experiment (AVE) campaigns: Oct-Nov 2004 based near Houston, Jan-Feb 2005 based in Portsmouth, NH (PAVE), and in Jan-Feb 2006 based in Costa Rica (CR-AVE). TES also participated INTEX-B (International Chemical Transport Experiment) based which had deployments in Houston, Honolulu and Anchorage in March-May 2006. The TES CO data from the time periods of theses campaigns are compared with the *in situ* measurements for the aircraft flights when there are the best coincidences between TES measurement location and the aircraft CO profiles.

6.3.1 Comparisons to Argus CO Data in October-November 2004 AVE Aircraft Campaign

During the October-November 2004 AVE mission based in Houston, TX, TES made a series of step and stare nadir observations between equator and 60^{o}N. Table 6-1 lists information about

Distributed by the Atmospheric Science Data Center
http://eosweb.larc.nasa.gov

the aircraft tracks and TES measurements for the five days that were best for comparison of the aircraft and TES data.

Table 6-1 This table Includes Information Pertaining to TES – Aircraft Comparisons for the AVE 2004 Campaign near Houston, TX.

Date		Oct. 31	Nov. 3	Nov. 5	Nov. 7	Nov. 9
TES Run		2262	2282	2290	2298	2305
Distance to Argus (km)	**Takeoff/ Landing**	560-100	160-170	130-20	410-270	700-420
	Diving	10-15	130-150	60-150		20-200
Time from Argus (hours)	**Takeoff/ Landing**	2.0 & 2.5	2.5 & 2.2	1.9 & 2.7	2.0 & 2.5	3.0 & 1.7
	Diving	0.5-1.5	0.4-1.0	0.4-1.3		(-1.0)-0.75
***DOFS* of TES**	**Takeoff/ Landing**	1.3	1.2-1.0	1.2	1.2	1.2-1.3
	Diving	1.3	1.2	1.2		1.1
Cloud OD of TES	**Takeoff/ Landing**	<0.1	<0.1 – 10.	<0.1	<0.1	<0.1
	Diving	<0.1	<0.1	<0.1		<0.6

During the AVE campaign, CO was measured by the NASA Ames Research Center Argus instrument on the WB-57 aircraft. Argus is a two channel, tunable diode laser instrument setup for simultaneous, *in situ* measurement of CO and CH_4 in the troposphere and lower stratosphere. As an example, Figure 6-5 shows the WB-57 flight track in four different views for October 31 flight. The TES nadir measurement footprint locations are shown in the region where WB-57 track overlaps with the Aura track. It is very difficult to obtain coincident profile measurements both in geographic location and time for satellite and *in situ* observations.

TES measurements of CO made on October 31 are presented by a curtain plot shown in Figure 6-6. Overlaid is the flight track along which Argus made *in situ* CO measurements. The *in situ* measurements of CO made by Argus are in good qualitative agreement with the profiles retrieved by TES (Figure 6-7).

All Argus CO profiles taken during takeoff/landing of the WB-57 as well as any spirals are compared with selected TES profiles. For each Argus profile, four to six TES profiles are

Distributed by the Atmospheric Science Data Center
http://eosweb.larc.nasa.gov

selected that are closest in distance to the Argus profile location area. These TES profiles are also filtered to include those with a *DOFS* of about 1.2-1.3 and small effective optical depths corresponding to clear scenes.

Figure 6-8 shows TES CO profiles with retrieval errors and the Argus takeoff/landing profiles for October 31 flight. The Argus profiles are then vertically smoothed with rows of TES CO averaging kernel, also in the figure:

$$x_{Argus_withA} = Ax_{Argus} + (I - A)x_a. \qquad \text{(Equation 6-1)}$$

The percent differences between all TES profiles and these Argus smoothed profiles are shown. The same procedure is used for Argus CO profiles taken during the aircraft profiling period as shown in Figure 6-9 In this case the Argus profiles were extended downward/upward using the TES *a priori* profile, scaled to match the aircraft profile. The resulting profile from the aircraft using the TES *a priori* could then have the TES averaging kernel applied to them for comparison with the TES profiles.

In five days of aircraft flights, a total of 18 Argus CO profiles are compared with 4-6 TES CO profiles for each of them. The percent differences between the Argus and TES measurements for these profiles are summarized in Figure 6-10. Overall, the differences between Argus and TES CO profiles are within TES retrieval errors and equivalent to CO spatial/temporal variability detected in both TES and Argus measurements.

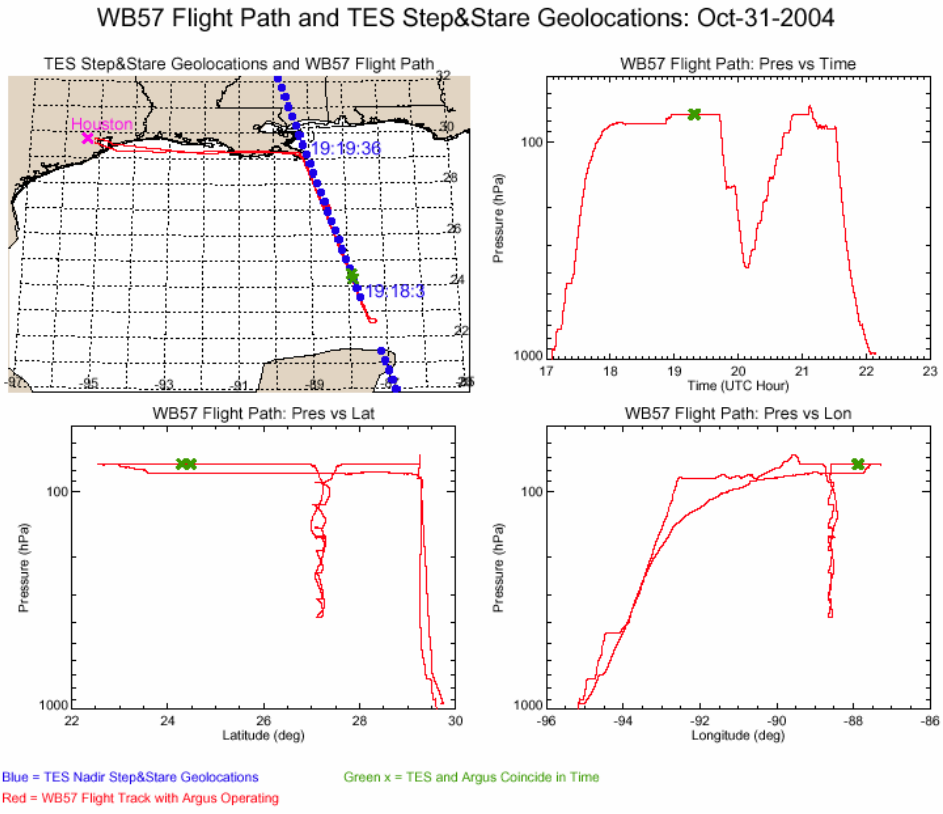

Figure 6-5 One day (October 30, 2004) during the AVE-04 campaign, plots show the WB-57 flight track in red and a fraction of the TES step and stare observation geolocations in blue. The green cross marks the starting and end points of the TES measurements along the aircraft track.

Distributed by the Atmospheric Science Data Center
http://eosweb.larc.nasa.gov

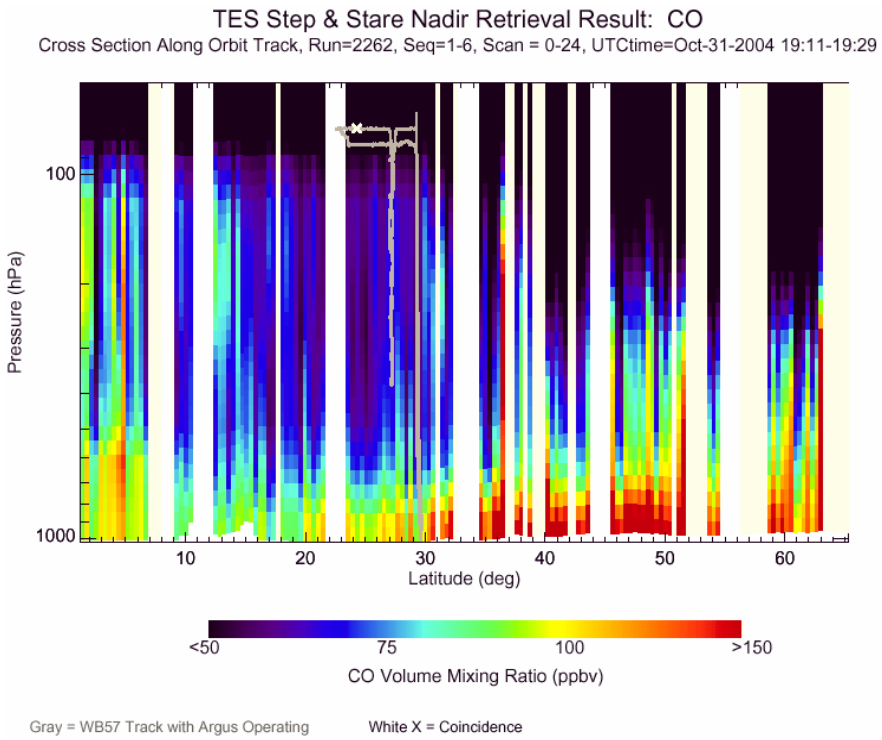

Figure 6-6 The cross section of TES CO profiles along its orbit track from the equator to 63°N latitude, from a step and stare observation on October 31, 2004. The flight pressures of WB-57 as a function of latitude are overlaid in gray.

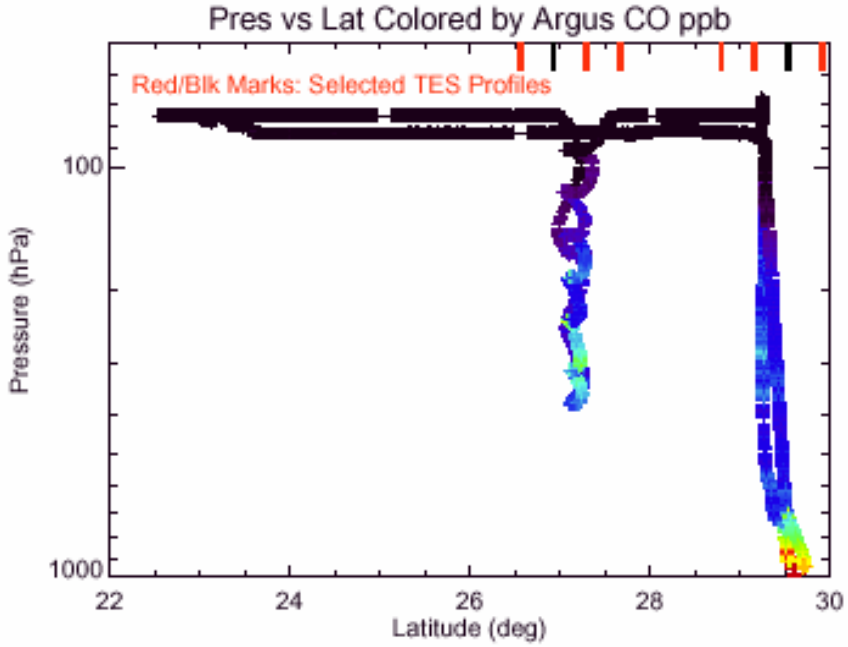

Figure 6-7 The Argus Measurements of CO VMR Plotted along the Flight Track in Comparison to that of TES in **Figure 6-5** for October 31, 2004. Several TES profiles are chosen for comparisons as their latitudes marked by red or black bars on top.

Distributed by the Atmospheric Science Data Center
http://eosweb.larc.nasa.gov

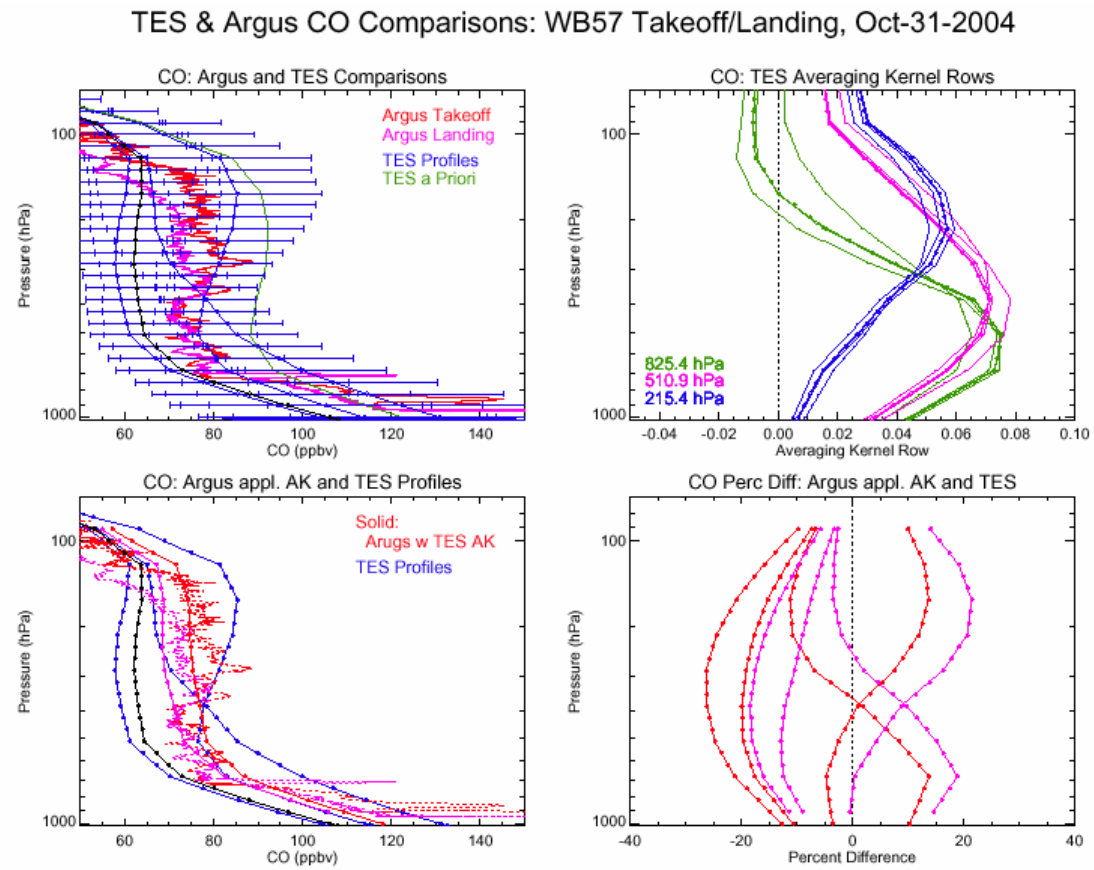

Figure 6-8 CO profile comparisons between TES and Argus measurements made during takeoff and landing of the WB-57 on October 31, 2004. Shown in top left panel are the Argus CO profiles, the four TES CO profiles (blue or black) with error bars, and the TES *a priori* profile (green) used in the retrievals. The top right panel shows the rows of TES averaging kernels at three pressure levels. The bottom left panel shows TES and Argus profiles again and the vertically smoothed profiles for Argus CO measurements with TES averaging kernel and *a priori* profile applied described in detail in the text. The bottom right panel shows the percent differences between the four TES CO profiles and the two vertically smoothed Argus CO profiles.

Distributed by the Atmospheric Science Data Center
http://eosweb.larc.nasa.gov

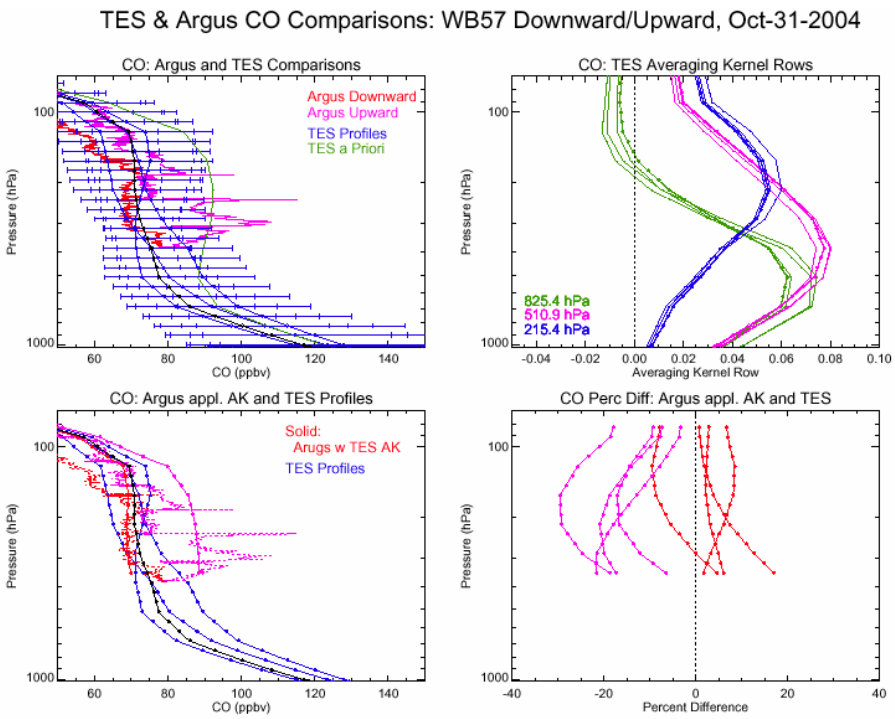

Figure 6-9 Same as **Figure 6-8**, except that the Argus CO Profiles are from the profiling portion of the flight. For this case, before applying the averaging kernel to the Argus profiles, they are extended downward with the TES *a priori* profile.

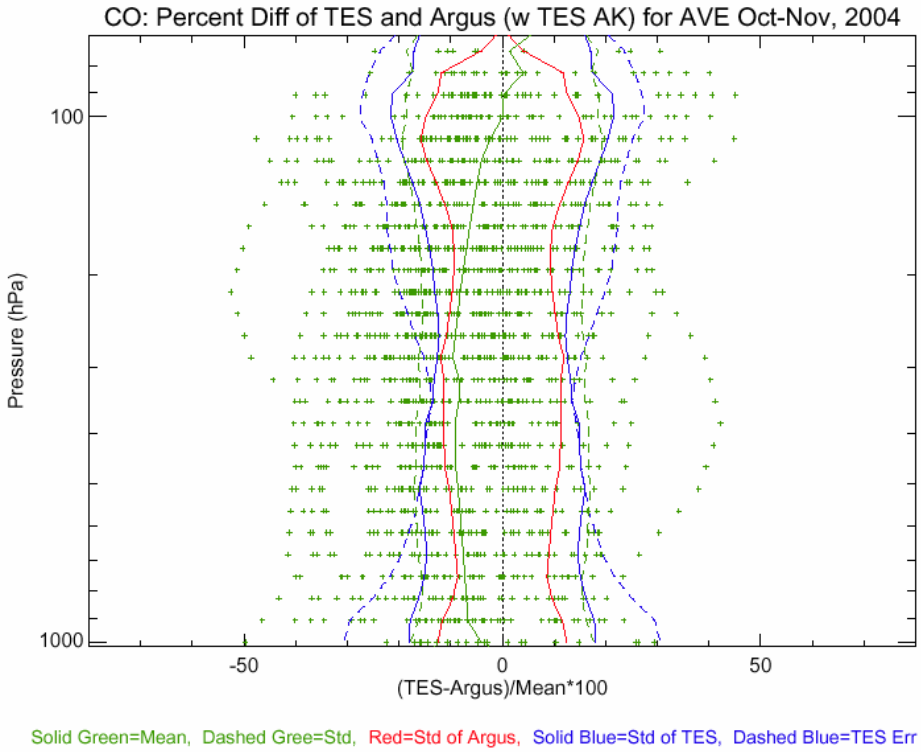

Figure 6-10 Percent Differences between TES and Argus CO Profiles from all Five Days of Measurements during AVE-04 WB-57 Campaign listed in Table 6-1. The solid green is the

Distributed by the Atmospheric Science Data Center
http://eosweb.larc.nasa.gov

mean of all comparisons. The other curves are plotted with respect to zero: the standard deviation (STD) of all percent difference (dashed green), the STD of all Argus measurements (red), the STD of all TES (solid blue), and the averaged percent error for the TES measurements (dashed blue).

6.3.2 Comparisons to ALIAS CO Data in Jan-Feb 2006 CR-AVE Aircraft Campaign

The Aura Validation Experiment campaign in early 2006 was conducted from Costa Rica (CR-AVE). In addition to science objectives for the campaign, most WB-57 aircraft flights were planned for validations of the Aura measurements near tropical tropopause layer (TTL). The CO profiles measured by Aircraft Laser Infrared Absorption Spectrometer (ALIAS) during the take-offs and landings are compared to the TES CO profiles nearest to the airport. Table 6-2 lists the coincidence information between the two instruments and about TES CO measurements. Most *in situ* measurements near the airport were far away from the TES footprints and the time differences were > 1 hr, and some of the comparisons were for next day. Total of 11 ALIAS profiles are used to compare to the TES CO profiles. Most of the TES measurements were in near clear sky with effective cloud OD <0.1 and DOFs ~ 1.5.

Figure 6-11 shows the averaged TES- ALIAS CO profile comparisons and the statistics. The two averaged CO profiles agree within 10% with TES being larger. The variability of the CO fields in the region from the two measurements is ~20%, in agreement with TES retrieval errors.

Table 6-2 ALIAS on WB-57 and TES Measurements during CR-AVE, Jan – Feb 2006.

		Jan 17	Jan 22	Jan 25	Jan 30	Feb 07	Feb 09
WB-57 Flight		Along TES S&S track	MLS	Along TES Transect	Non-Aura	Take-off/ landing near TES GS	MLS
TES Run		SS 3251	GS 3269	TR 3277	GS 3290	GS 3316	GS 3318
Distance btw TES & ALIAS (km)	Take-off	390	160	965	1057	84	84
	Landing	536	43	1146		105	185
Time btw TES & ALIAS (hrs)	Take-off	1	1	1	10	3	13
	Landing	2.5	3	2.5		1	9
TES DOF	Take-off	1.4-1.5	1.6	1.5	1.3	1.5	1.
	Landing	1.4-1.5	1.7	1.5		1.5	1.
TES Cloud OD	Take-off	<-0.1 – 0.5	<0.1	<0.1	0.2	<0.1	~ 9
	Landing	<-0.1	<0.1	<0.1		<0.1	~ 9

Distributed by the Atmospheric Science Data Center
http://eosweb.larc.nasa.gov

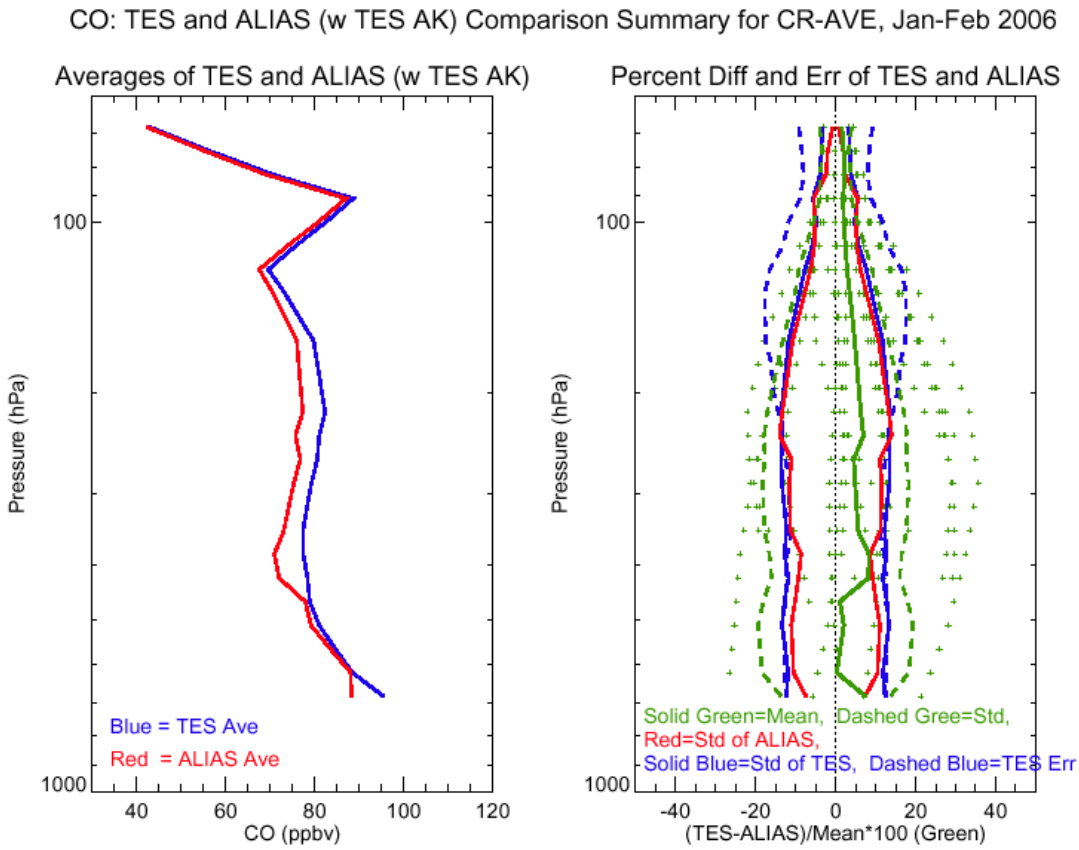

Figure 6-11 The Averaged CO Profiles of TES and ALIAS (Left Panel) and the Averaged Difference between TES and ALIAS CO Profiles (Right Panel, Green). The standard deviations for the TES and ALIAS CO profiles are also calculated, together with the averaged retrieval errors for the TES CO profiles (right panel).

6.3.3 Comparisons to DACOM CO Data in March-May 2006 INTEX-B Aircraft Campaign

During the INTEX-B campaign the DC-8 aircraft was flown out of Houston, Honolulu, and Anchorage. Many DC-8 flight plans were designed to include spirals near TES step and stare nadir observation footprints in order to provide opportunities for validation of TES carbon monoxide and ozone profiles. The total number of aircraft CO profiles collected by the NASA Langley Research Center DACOM instrument that are suitable for validation of TES CO measurements (0-100 km to the TES footprints) is 9 for Houston, 10 for Hawaii, and 1 for Anchorage. Table 6-3, Table 6-4 and Table 6-5 give the distances between the average aircraft location and the TES geolocation, the time difference between the measurements, the TES DOFS for the CO retrievals and the TES effective cloud optical depths for these flights.

Distributed by the Atmospheric Science Data Center
http://eosweb.larc.nasa.gov

Table 6-3 TES and DACOM Information for Flights near Houston, March 2006

		Mar 4	Mar 9	Mar 11	Mar 12	Mar 16	Mar 19	Mar 21
TES Run		SS 3399	GS 3429	GS 3447	SS 3440	SS 3459	GS 3484	SS 3496
Distance btw TES & DACOM (km)	Prof 1	53	24	No coincidences	16	12	43	No coincidences (HIRDLS)
	Prof 2	25	20		16		88	
Time btw TES & DACOM (hrs)	Prof 1	0.8-1.4	0.5-1.1		0.8-1.25	0-0.5	0-0.3	
	Prof 2	1-1.6	0-0.5		1-1.5		0.5-1.5	
TES DOF	Prof 1	1.8	1.3-1.4		1.5	1.5	1.8	
	Prof 2	1.7	1.3-1.4		1.5		1.8	
TES Cloud OD	Prof 1	<0.1	<0.1		>1.0	<0.1-1.0	<0.1	
	Prof 2	<0.1	<0.5		<0.1		<0.1	

Table 6-4 TES and DACOM Information for Flights near Hawaii, April-May 2006

		Apr 17	Apr 23	Apr 25	Apr 28	May 01
TES Run		SS, 3700	SS, 3830	SS, 3868	GS, 3921	SS, 3961
Distance btw TES & DACOM (km)	Prof 1		45	37	6	96
	Prof 2		21	20	60	18
	Prof 3		23		4	102
	Prof 4		23			
	Prof 5		15			
Time btw TES & DACOM (hrs)	Prof 1		1.8-2.3	2.5-3.0	1.5-2.0	5-6
	Prof 2		0.5-1.2	0-0.3	0.5-1.2	1.0-1.5
	Prof 3		0-0.5		0-0.3	0-0.5
	Prof 4		1-1.5			
	Prof 5		1.7-2.2			
TES DOF	Prof 1		1.6	1.4-1.5	1.6	1.3-1.6
	Prof 2		1.5-1.7	1.2-1.3	1.7	1.0-1.3
	Prof 3		1.5-1.6		1.1	0.2-0.7
	Prof 4		1.5-1.6			
	Prof 5		1.0-1.5			

Distributed by the Atmospheric Science Data Center
http://eosweb.larc.nasa.gov

		Apr 17	Apr 23	Apr 25	Apr 28	May 01
TES Run		SS, 3700	SS, 3830	SS, 3868	GS, 3921	SS, 3961
TES Cloud OD	Prof 1		<0.1 & 0.7	<0.1 & 0.7	<0.1	<0.1 & 2
	Prof 2		<0.1 & 1.0	<0.1 & 0.4	<0.1	0.9-2.0
	Prof 3		<0.1 – 1.4		2.3	1.7-4.0
	Prof 4		<0.1			
	Prof 5		<0.1 & 3.0			

Table 6-5 TES and DACOM Information for Flights near Anchorage, May 2006

		May 4	May 7	May 9	May 12	May 15
TES Run		GS	SS 4112	SS 4154	GS 4211	SS
Distance btw TES & DACOM (km)	Prof 1	No coincidences (OMI)	322	10	176	
	Prof 2					
Time btw TES & DACOM (hrs)	Prof 1		1.5-2.0	1.5-2.0	0-0.5	
	Prof 2					
TES DOF	Prof 1		1.35	1.2-1.4	1.1	
	Prof 2					
TES Cloud OD	Prof 1		<0.1 & 0.4	<0.1 & 0.7	2.5	
	Prof 2					

Similar to previous comparisons of TES and aircraft *in situ* measurement of CO, we select 1-4 TES profiles closest to DACOM CO profiles, interpolate the DACOM profile to the TES pressure levels, extend the DACOM profile up and downward by scaled TES *a priori* profile, apply the TES averaging kernel and *a priori* to the DACOM profile, and calculate the differences between TES and the adjusted DACOM CO profiles. Figure 6-12 and Figure 6-13 show the summary of TES and DACOM CO profile comparisons for the Houston phase in March 2006. The correlation plots in the left panel of Figure 6-12 include comparison for all coincident TES profiles, at all appropriate pressure levels and indicate the good agreement between TES and DACOM CO profiles with correlation coefficient of 0.83. If only a single TES profile is considered with its geolocation closest to the averaged DACOM locations (right panel of Figure 6-13), the correlation coefficient improved to 0.89. Figure 6-13 shows the comparisons of the averaged TES and DACOM CO profiles and their differences, compared to their standard deviations and the averaged TES retrieval errors. The difference between the averaged TES and DACOM profiles is much smaller than the variability in the measurements of the two instruments.

The comparisons of TES and DACOM CO measurements during INTEX-B Hawaii and Anchorage periods do not appear to be as good as those from the Houston flights. For example,

Distributed by the Atmospheric Science Data Center
http://eosweb.larc.nasa.gov

the correlation coefficient between TES and DACOM profiles was only 0.55 in Hawaii and even worse for the Anchorage flight. Examination of the individual profiles of the DACOM *in situ* measurements indicate large CO values observed in vertical layers of the flight profiles. This is consistent with the understanding of sources of the CO plumes of and the transport patterns over Pacific Ocean in the spring. TES CO daily maps show much more variability in CO near Hawaii than seen near Houston in March. The large variability in the CO fields and the distance between the TES measurement location and the aircraft make comparisons more difficult for the Hawaii and Anchorage deployments.

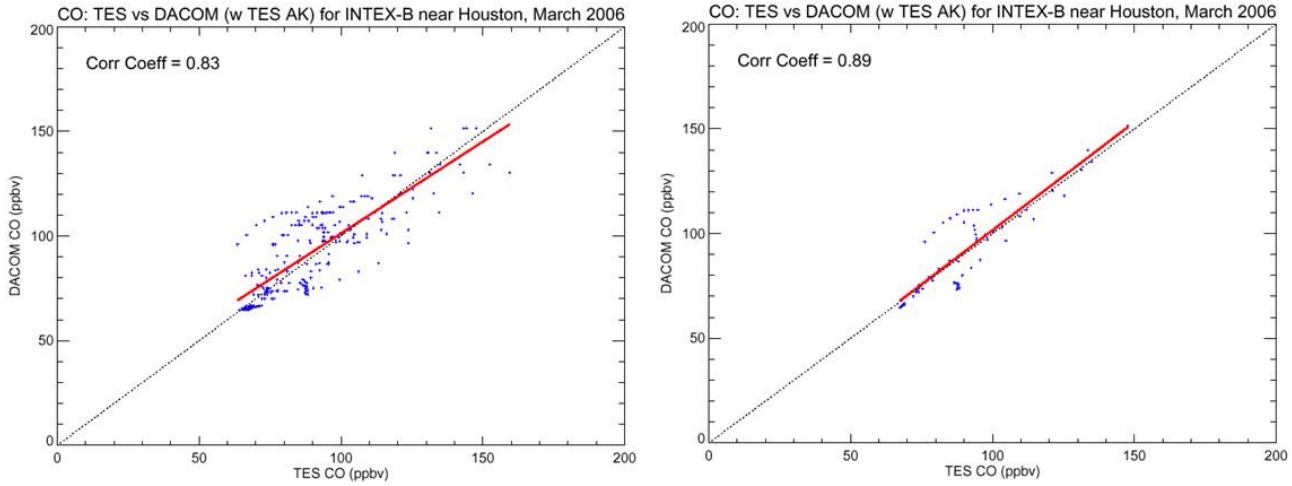

Figure 6-12 The Correlation Plot for TES and DACOM CO Profiles. Data are taken during 1st phase of INTEX-B campaign near Houston, March 2006. Left panel: there are 9 profiles from DACOM *in situ* measurements and 1-4 TES profiles per DACOM profile. Right panel: for each DACOM profile, only the single TES profile is considered closest to the DACOM averaged location. The correlation coefficients are 0.81 and 0.89 for the two comparisons respectively.

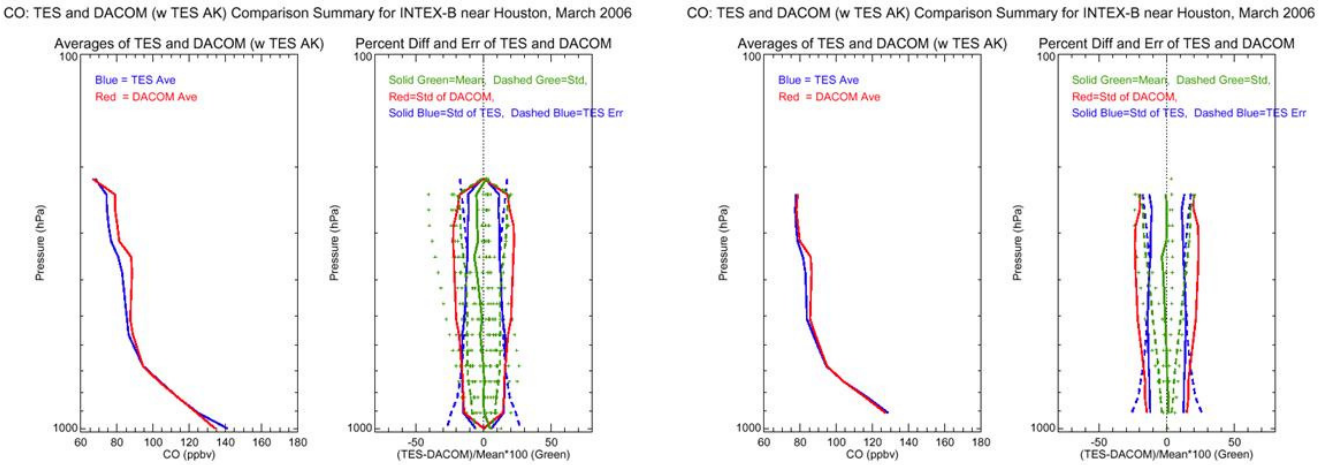

Figure 6-13 Same Data Sets for Figure 5-12. The average profiles of TES and DACOM are overlaid and the averaged different between TES and DACOM CO profiles (green). The standard deviations for the TES and DACOM CO profiles are also calculated, together with the averaged retrieval errors for the TES CO profiles.

Distributed by the Atmospheric Science Data Center
http://eosweb.larc.nasa.gov

6.4 CO validation: comparisons to MOZAIC data set

The MOZAIC program (Measurements of Ozone and water vapor by In-service AIrbus aircraft, http://mozaic.aero.obs-mip.fr) collects CO *in situ* measurement during aircraft departure and arrival flight paths in many of the airports worldwide. Initially, measurements of CO made by MOZAIC aircraft from September 2004 to May 2005 are used for TES validation. Figure 6-14 shows the locations of the airports in the MOZAIC program and those with data used for TES CO comparisons.

For each airport and MOZAIC CO profile, all TES CO retrieved profiles within 250 km and within 24 hours are identified. Similar to the methods described in the previous section, the MOZAIC CO profiles were adjusted using the TES averaging kernel and *a priori*. Figure 6-15 through Figure 6-17 give results for comparisons between TES and MOZAIC profiles at the Munchen airport.

Table 6-6 gives summary of all comparisons for all MOZAIC locations. For most airports, TES and the adjusted MOZAIC profiles agree well. The best agreement is seen in European cities and cities with lower amounts of CO pollution. Those comparisons with poorer agreement are from cities known to be highly polluted and that are associated with larger variability in the CO profiles. We found that TES is generally lower (<10%) than MOZAIC at all pressures in most comparisons. Note that the time period for these comparisons is before the TES optical bench warm up that resulted in improved CO retrievals. Further comparisons between TES and MOZAIC CO data will be performed when the MOZAIC data become available.

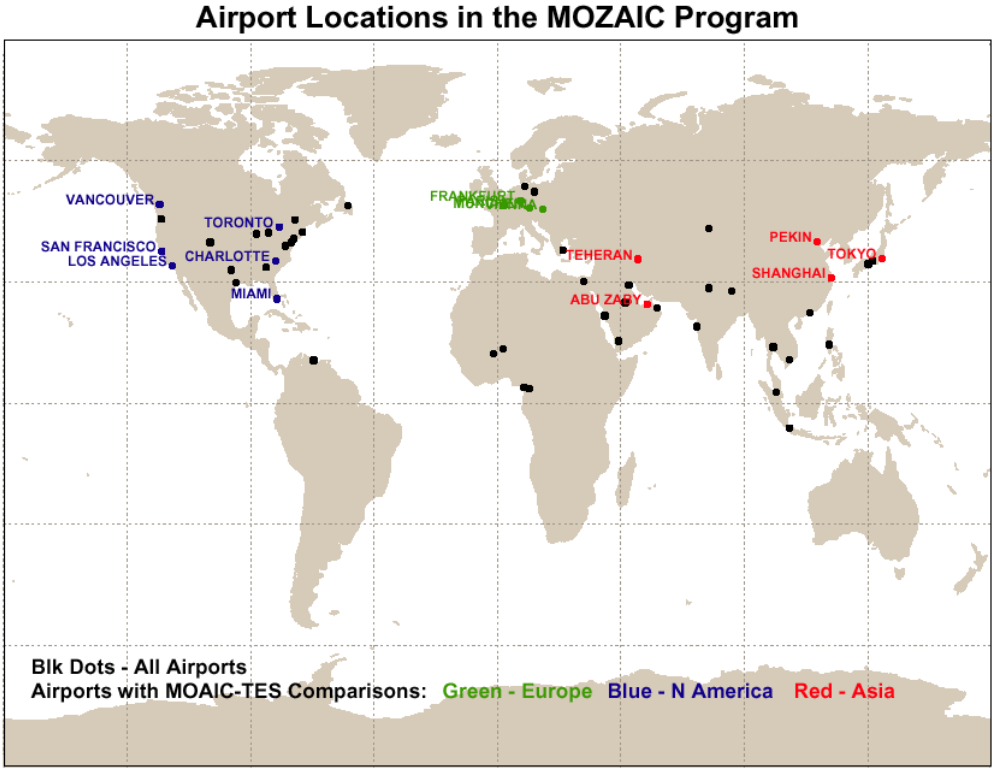

Figure 6-14 Airport Locations in the MOZAIC Program. The colored locations are those having TES coincidences.

Distributed by the Atmospheric Science Data Center
http://eosweb.larc.nasa.gov

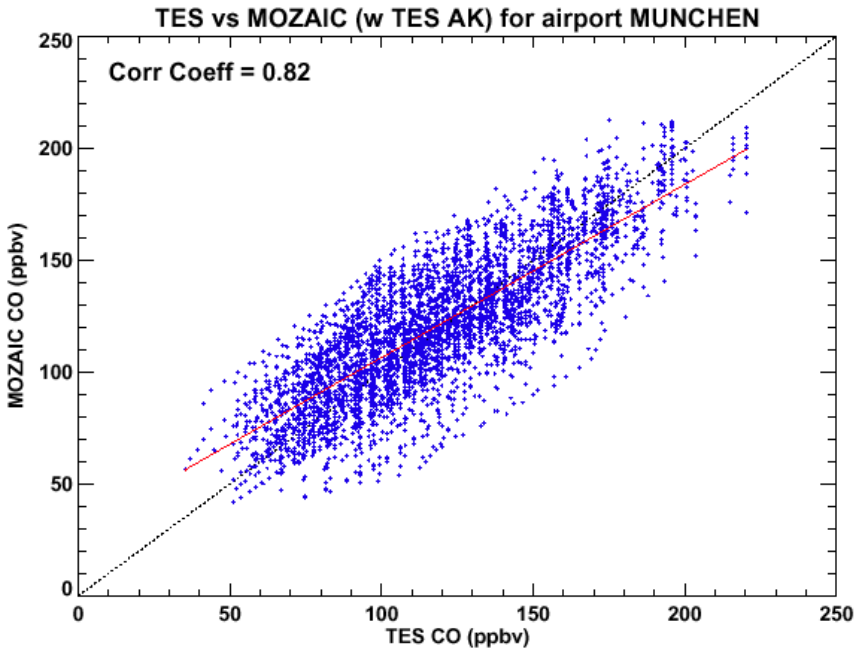

Figure 6-15 Correlation Plot of all TES and MOZAIC CO Comparison Profiles for Airport Munchen. The correlation coefficient is 0.82.

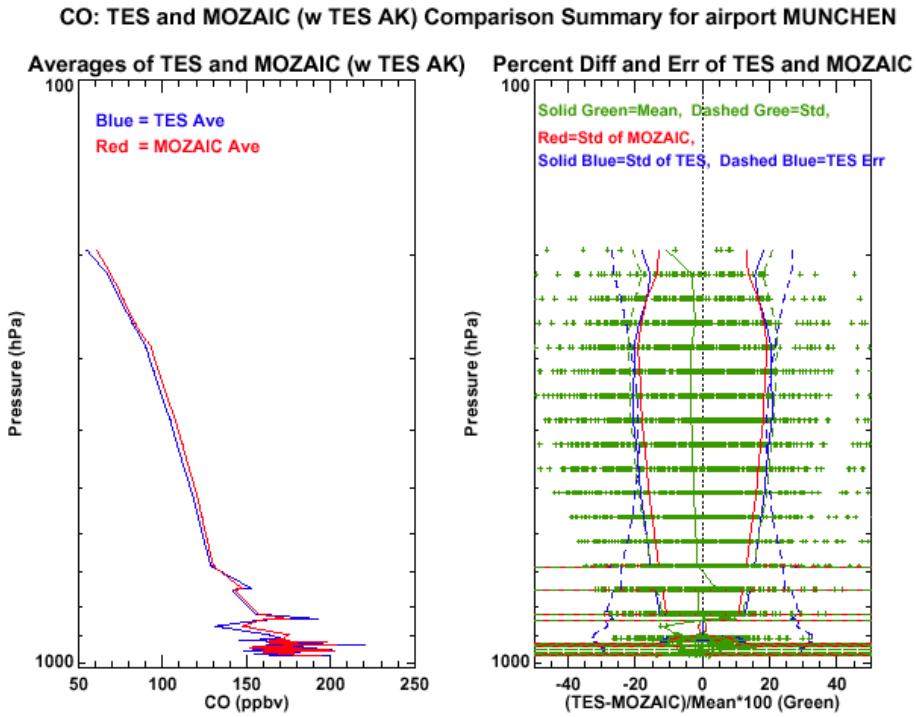

Figure 6-16 Same Data in Figure 5-15. Left panel shows the averages of the TES and MOZAIC CO profiles, and the right panel shows the difference, the standard deviations derived from the two data sets and the average for the TES retrieval errors.

Distributed by the Atmospheric Science Data Center
http://eosweb.larc.nasa.gov

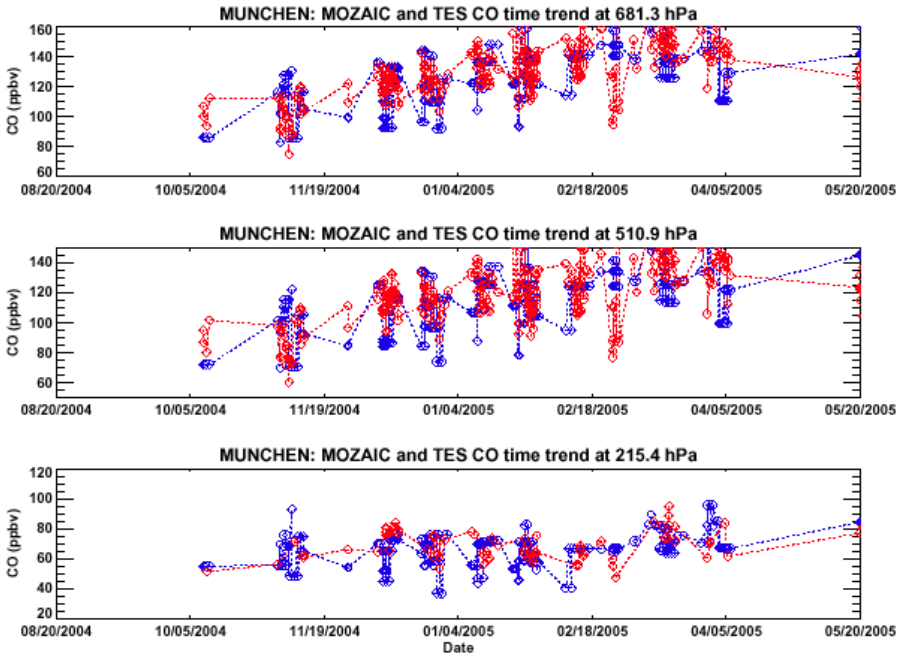

Figure 6-17 Same Data in Figure 5-15. The Time Trends of the TES and MOZAIC CO Data at Three Pressure Levels, 681.3, 510.9, and 215.4 hPa.

Table 6-6 Summary for TES-MOZAIC CO Comparisons, Sept 2004 – May 2005

Airport	Num TES-MOZ	Corr Coeff	TES-MOZ (%)	Sdv of MOZ (%)
PARIS	32	0.81	~ 5	15
FRANKFURT	93	0.85	<+/- 5	10-20
VIENNA	81	0.88	- (0-5)	10-15
MUNCHEN	193	0.82	< -5	10-20
TORONTO	49	0.81	-(5-10)	5-15
LOS ANGELES	27	0.63	- (0-5)	10-20
VANCOUVER	59	0.72	- (0-10)	10-20
SAN FRANCISCO	15	0.39	< 5	20-30
CHARLOTTE	12	0.78	< -5	5-15
MIAMI	8	0.81	- (0-10)	5-15
TOKYO	45	0.74	< -5	15-25
ABU ZABY	44	0.61	~ -5	10-20
TEHERAN	13	0.71	~ (-10)	10-15
PEKIN	14	0.81	- (0-10)	25
SHANGHAI	18	0.19	- (0-20)	15-50

Green – Europe, Blue - N America, Red - Asia

Distributed by the Atmospheric Science Data Center
http://eosweb.larc.nasa.gov

6.5 CO Validation: Comparisons to MOPITT Data

The retrieval results of TES 16-orbit global survey measurements in Sept 20-21, 2004 (Run ID 2147) have been examined extensively by the TES science team (M. Luo et al., 2006). Figure 6-18 illustrates CO total column amounts at TES nadir footprints for Run ID 2147. Over 70% of the profiles met the requirements for a successful retrieval according to the current quality criteria. In the future, TES Level 2 retrievals and column values will be mapped to a uniform latitude/longitude grid for each global survey (TES Level 3 products). An illustration of this is provided in Figure 6-19 for the CO column. Enhanced tropospheric CO is observed over parts of S. America and Africa, and along the east coast of Asia. These are associated with the well known seasonal biomass burning or pollution source regions. The degree-of-freedom for signal from TES CO retrievals are plotted as a function of latitude in Figure 6-20. Values for the *DOFS* of 0.5-2 are achieved, meaning TES measurements provide 0.5-2 pieces of independent vertical information for tropospheric CO. The better *DOFS* normally occurred for the daytime tropics with high surface temperatures and clear sky conditions where fewer scan signals were rejected due to clouds.

The CO profiles from MOPITT instrument on Terra are gathered for the same time period of the TES global survey on Sept.20-21, 2004. Figure 6-21 shows the MOPITT measurement of CO total column overlaid with TES geolocations. It is immediately realized that TES (Figure 6-18) and MOPITT (Figure 6-21) global CO agree well qualitatively, *e.g.,* they both detected enhanced CO near the polluted sources. In examining the model field of CO, *e.g.,* the MOZART simulation used as *a priori* for TES CO retrievals, TES and MOPITT measurements revealed some more detailed CO distributions.

Figure 6-22 shows a comparison of the TES and MOPITT CO total column values as a function of latitude for the TES global survey time period in Sept.20-21, 2004. The reported percent errors for the two instruments are plotted as functions of latitude. The global averages of total column errors for CO are 8.7% for TES and 11.7% for MOPITT respectively. Again, we see general good agreement between the two instruments at most latitudes with the exception of southern high latitudes, where the column CO amounts measured by TES are slightly lower than that of MOPITT. This is believed to be due to the effect of the *a priori* in CO retrievals which will be demonstrated below for different pressure levels.

Quantitative comparisons between TES and MOPITT CO at low, mid and upper troposphere and total column for this day are presented in the paper M. Luo et al. 2006. Table 6-7 lists the comparison summary. Two steps are performed in the comparison, adjusting TES CO profiles to MOPITT *a priori* profile, and applying TES averaging kernels to MOPITT retrieved profiles. The final comparison is to compare TES retrieved CO profiles adjusted to MOPITT *a priori* and the MOPITT retrieved CO profiles adjusted to MOPITT averaging kernel. The agreement between the two CO fields becomes much better in all tropospheric levels and the total column, especially in the lower and upper troposphere where both instruments do not have much sensitivity in their measurements.

It is concluded in the paper (M. Luo et al., 2006) that no systematic differences are found as a function of latitude in the final comparisons between TES and MOPITT CO. These results show that knowledge of the *a priori* profiles, the averaging kernels, and the error covariance matrices in the standard data products provided by the instrument teams and understanding their roles in

Distributed by the Atmospheric Science Data Center
http://eosweb.larc.nasa.gov

the retrieval products are essential in quantitatively interpreting both retrieved profiles and the derived total or partial columns for scientific applications

Table 6-7 Comparisons of Global Averages of TES and MOPITT Reported CO Volume Mixing Ratios at Three Pressure Levels and Total Column for Data taken in September 20-21, 2004.

	850 hPa		500 hPa		150 hPa		Total Column	
	% diff	% rms	% diff	% rms	% diff	% rms	% diff	% rms
Direct comparison of TES and MOPITT CO	-18%	36%	-3%	24%	-4.5%	35%	-11%	22%
TES CO adjusted to MOPITT *a priori* compared to MOPITT CO	-5%	35%	-3.8%	23%	-7%	24%	-5.4%	22%
TES CO adjusted to MOPITT *a priori* compared to MOPITT CO adjusted to TES averaging kernel	-0.2%	15%	-4%	23%	-4.8%	18.7%	-4.4%	16%

%diff is the global average of the differences between the matched TES and MOPITT points (TES minus MOPITT) divided by the average of the global averages of TES and MOPITT CO VMRs. %rms is the root mean square (rms) of the differences between the matched TES and MOPITT points (TES minus MOPITT) divided by the average of the global averages of TES and MOPITT CO VMRs.

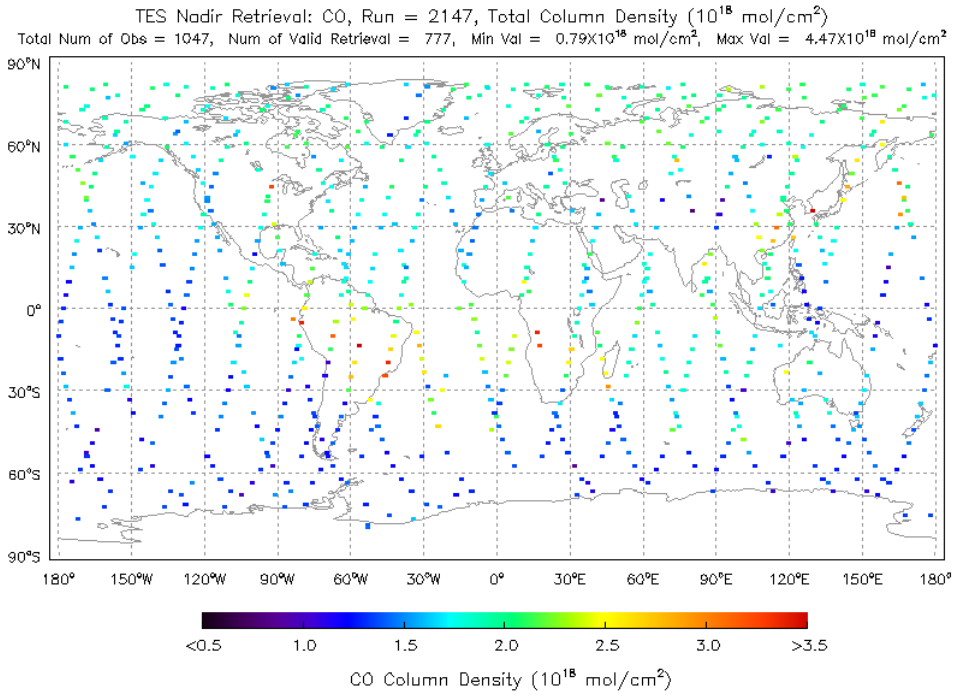

Figure 6-18 Total Column of TES CO shown as enlarged nadir footprints for TES Run ID 2147 (September 20-21, 2004). Elevated CO over and near the coasts of S. America and Africa are observed due to extensive biomass burnings in both regions. Larger CO values also showed up in expected pollution regions in E. Asia.

Distributed by the Atmospheric Science Data Center
http://eosweb.larc.nasa.gov

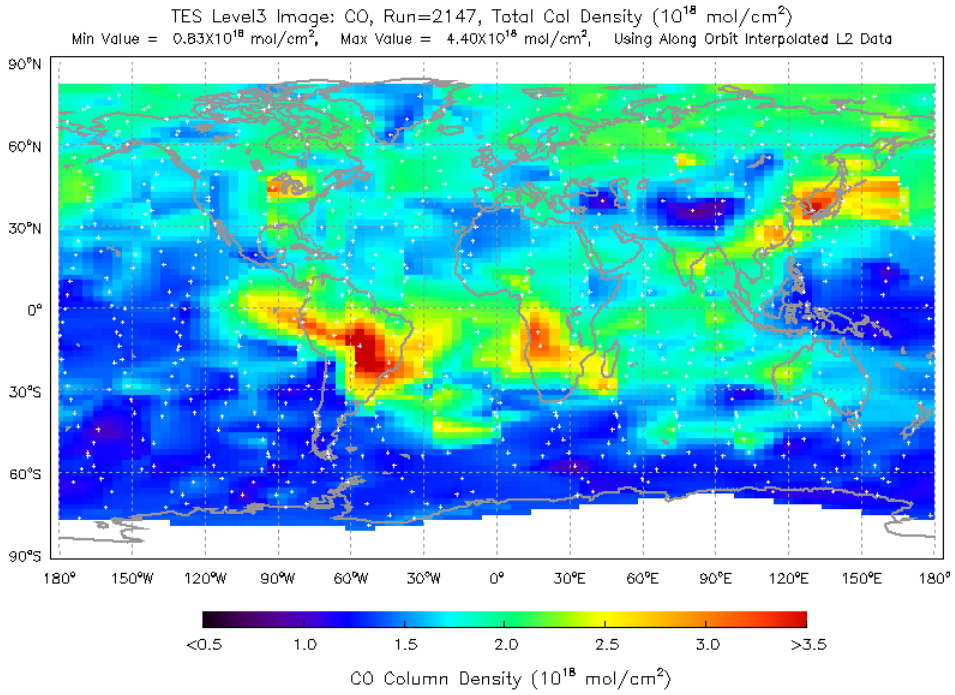

Figure 6-19 TES CO Column from **Figure 6-18** mapped to uniform grids in latitude and longitude, using Delaunay triangulations and the 2-D linear interpolation method. White marks are TES geolocations. The features in CO global distributions are more clearly displayed.

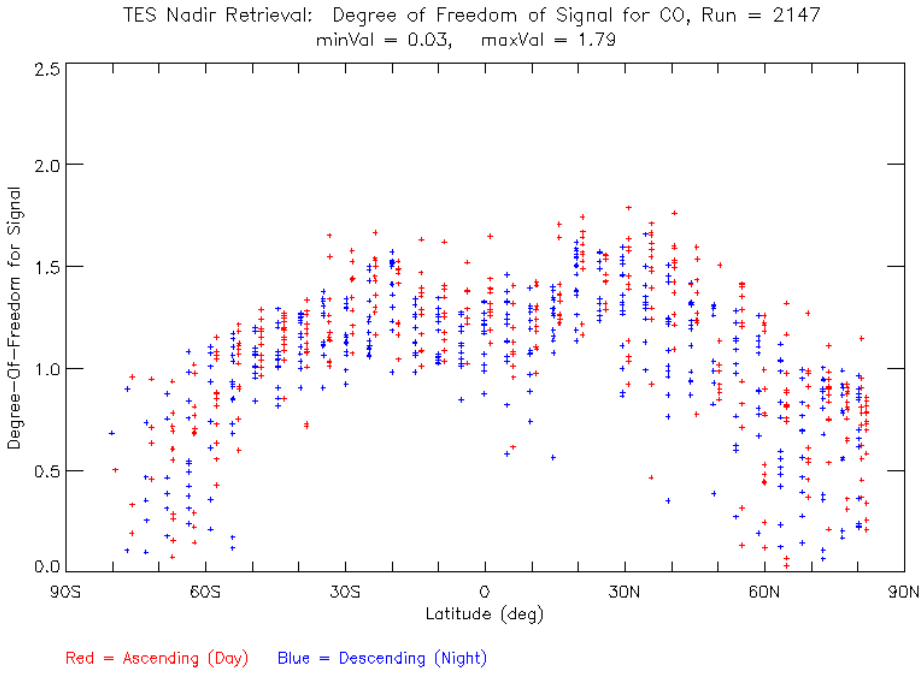

Figure 6-20 Degree of freedom for signal as a function of latitude for TES nadir CO retrieval on Sept. 20-21, 2004.

Distributed by the Atmospheric Science Data Center
http://eosweb.larc.nasa.gov

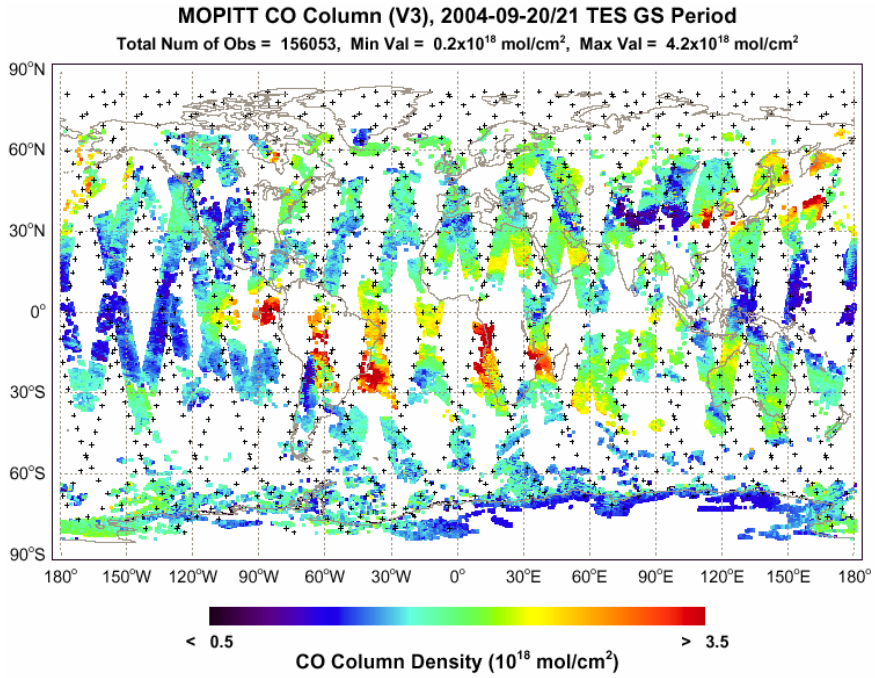

Figure 6-21 Terra-MOPITT CO total column observed in TES global survey period of Run ID 2147, Sept.20-21, 2004. Black marks are TES geolocations. Orbits of Terra and Aura have equator ascending crossing times of about 9:30 am and 1:45 pm respectively.

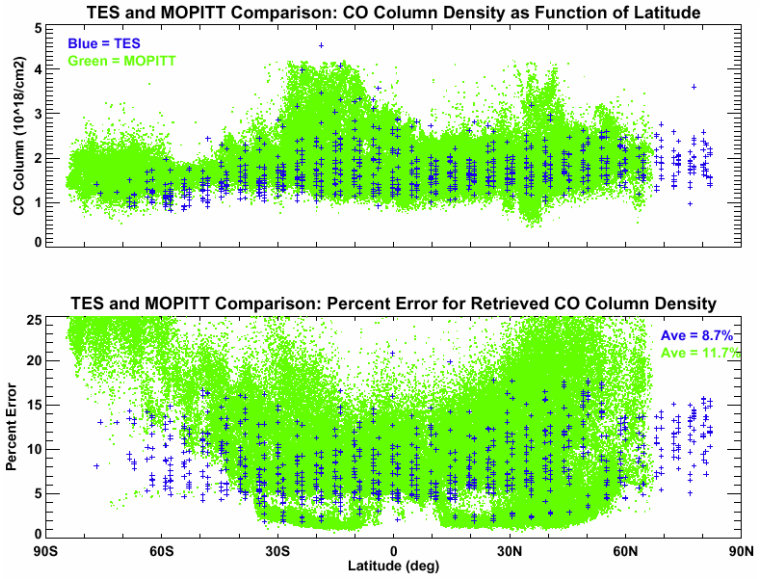

Figure 6-22 The top panel shows the comparisons of TES and MOPITT total CO columns as functions of Latitude for TES Run ID 2147, Sept.20-21, 2004. Note that TES CO column is visibly lower than that of MOPITT in Southern high latitudes. The bottom panel is the percent errors in TES and MOPITT CO columns. The global average values of their percent errors are 8.7% for TES and 11.7% for MOPITT, respectively.

Distributed by the Atmospheric Science Data Center
http://eosweb.larc.nasa.gov

6.6 CO validation: comparisons to ACE and MLS data

Both the Atmospheric Chemistry Experiment (ACE) and Microwave Limb Sounder (MLS) are limb viewing instruments and the sensitivity of the retrievals of CO by the two instruments are limited to the upper troposphere. Preliminary validation results between TES/ACE and TES/MLS are shown in the following section.

6.6.1 Comparisons to ACE

ACE is a Canadian satellite mission launched Aug 13, 2003. The ACE-FTS instrument operates primarily in solar occultation providing altitude profile information (typically 10–100 km) for temperature, pressure, and the volume mixing ratios of dozens molecules of atmospheric interest, as well as atmospheric extinction profiles over the latitudes 85°N to 85°S. Figure 6-23 gives the time trend of ACE latitude coverage for its sunrise and sunset measurements.

For each ACE CO profile, we select the corresponding TES CO profile within 24 hrs and closest in distance. Figure 6-24 shows some examples of the CO profile comparisons. Figure 6-25 illustrates time trend of the CO comparisons at 316.2 hPa for data between 30S and 30N latitude. These comparisons and those for other pressure levels (215.4 and 146.8 hPa) and latitudes indicate there is no obvious bias in the two CO data sets. The comparisons will be updated using more ACE and TES in the future.

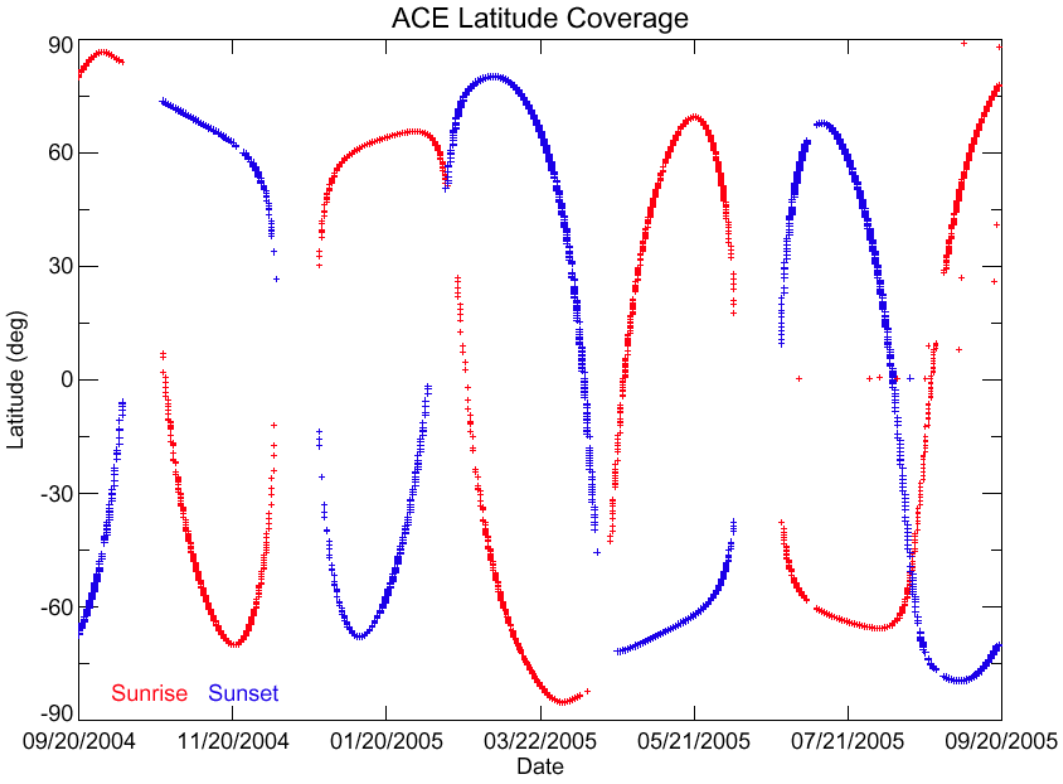

Figure 6-23 Time Trend of Latitude Coverage for ACE.

Distributed by the Atmospheric Science Data Center
http://eosweb.larc.nasa.gov

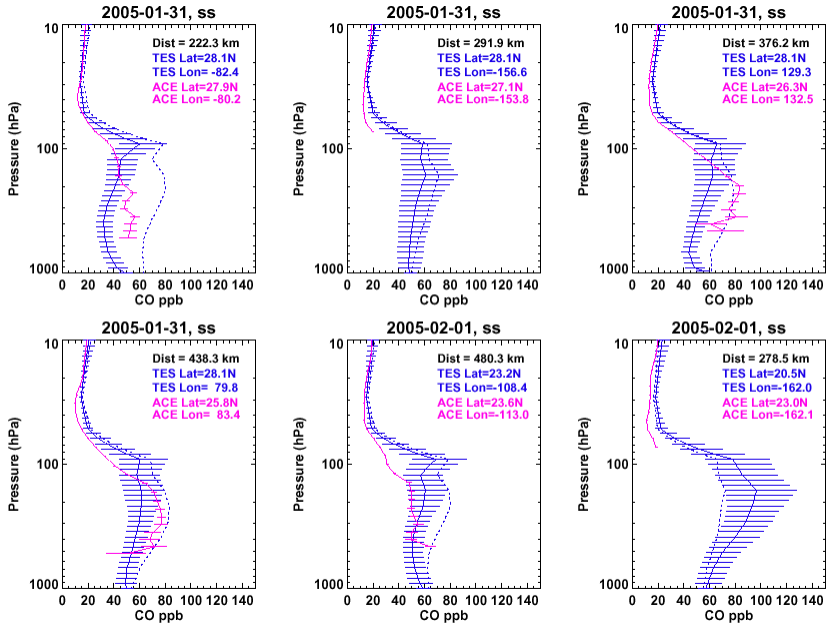

Figure 6-24 Examples of TES-ACE CO Profile Comparisons. Solid blue is TES retrieved profile and dotted blue is TES *a priori* profile. Solid magenta is ACE retrieved profile.

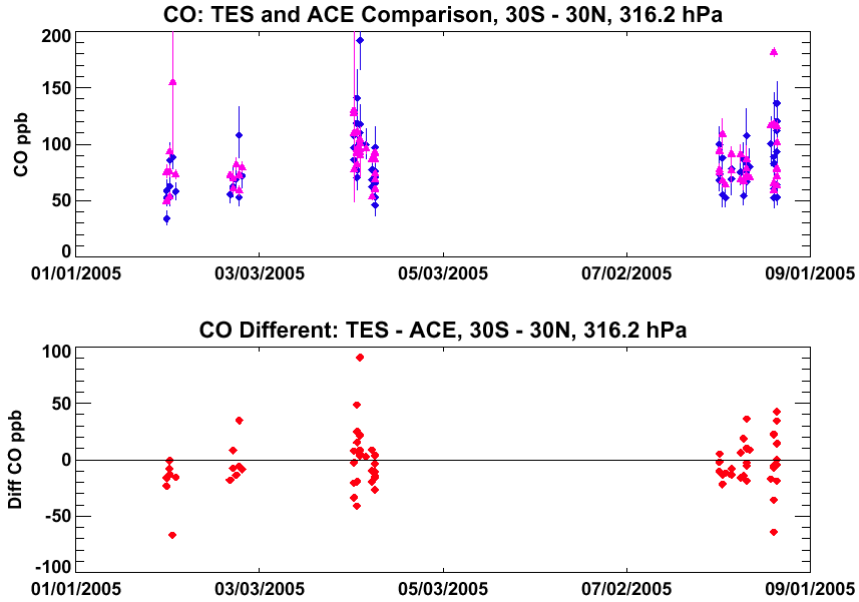

Figure 6-25 Time Trend of TES and ACE CO Comparisons at 316.2 hPa for Data in 30S-30N Latitude.

6.6.2 Comparisons to MLS

The JPL MLS instrument is a limb viewing instrument sensing the microwave thermal emissions in the atmosphere. The retrievals of CO profile from MLS measurements are available above the upper troposphere, for pressure levels < ~215 hPa. We made preliminary comparisons between

Distributed by the Atmospheric Science Data Center
http://eosweb.larc.nasa.gov

TES V2 and MLS V1.5 CO data. This version of MLS CO data is too high relative to the aircraft measurements and model simulations (Filipiak et al., 2005). Figure 6-26 shows a side-by-side comparison of TES and MLS CO at 215.4 hPa. A new version of MLS data (V2) will be available in the near future and its comparison to TES CO is expected to be much improved.

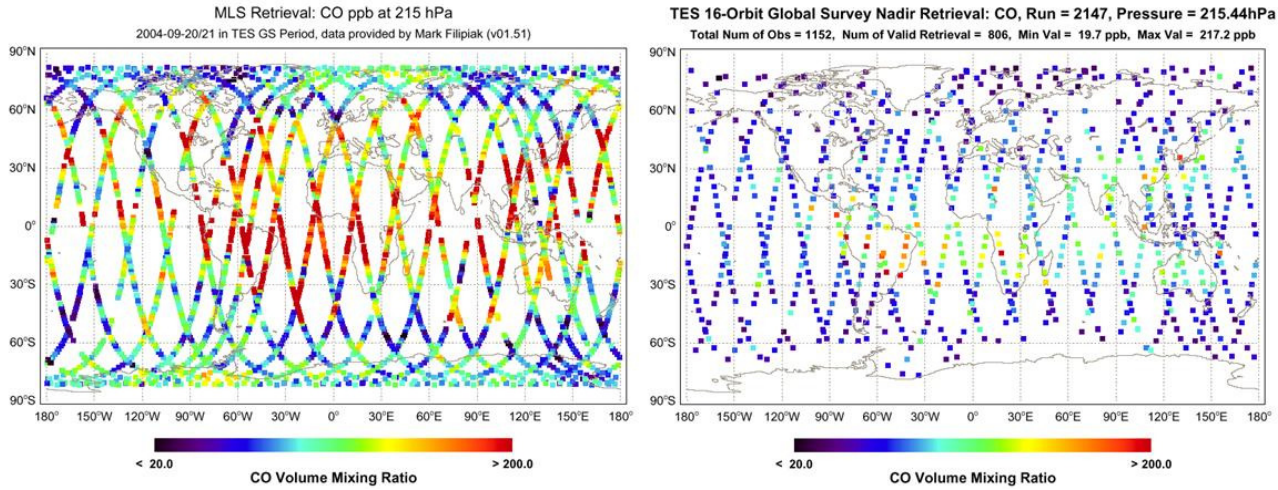

Figure 6-26 Comparison of TES and MLS Global Retrievals of CO at 215.4 hPa, September 20-21, 2004.

6.7 CO validation: summary and future works

Much progress has been made in validating TES CO profile retrievals. Table 6-8 gives a brief summary of the CO validation sources, the activities, and the preliminary conclusions. TES CO profiles are and will be compared to all satellite CO data from currently operating instruments, MOPITT, AIRS, ACE and MLS. These comparisons show general agreement in patterns of CO global distributions in the troposphere. The enhanced CO data in the lower troposphere can be closely related to the known burning or pollution sources. The direct comparisons of the retrievals from the remote sensing radiance measurements are not proper though, since the retrievals are influenced by the *a priori* assumptions used by different instrument teams. In comparisons to the MOPITT CO data, we illustrated the method of adjusting the comparison profiles with common *a priori* profiles and using the TES averaging kernels. This method will be used for future TES – AIRS CO comparisons.

The comparison of TES CO retrievals with *in situ* aircraft measurement cannot be made directly either. We presented that the TES CO averaging kernels and *a priori* profiles need to be applied to the *in situ* profiles before comparing to the TES retrieved CO profiles. Good agreement between the averaged *in situ* and TES CO profiles is obtained, within 10% and much less than the variabilities of TES and the aircraft CO measurements in the region. In general, the agreement is better for regions where CO fields have less variability. The MOZAIC data set includes a variety cities in different regions and for an extended term time period and therefore is potentially very valuable for validation of TES CO profiles.

Distributed by the Atmospheric Science Data Center
http://eosweb.larc.nasa.gov

Table 6-8 A summary list for TES CO validation activities. Red marks the future works.

Comparison Sources	Progress	Results / problems
MOPITT	• Data from Sept 20-21, 2004. JGR paper under review • Monthly	• Good agreement in global patterns • Influence of *a priori* constraints on CO retrievals of both instrument. The agreement much improved after adjusting the retrieval with *a priori* info. • MOPITT will release V4 data
ACE MLS AIRS	• Time trends with ACE data in upper trop • One day 2004 data with MLS in upper trop • AIRS in preparation	• Good agreement with ACE • MLS being too high • Understand AIRS AK
AVE (Argus) CR-AVE (Alias)	• Comparisons made AVE-04; paper will go to special JGR issue	• Agreement within CO area variability and the estimated errors of 10-20%.
INTEX-B (DACOM)	• Comparisons made; paper will go to special JGR issue	• Agreement within CO area variability and the estimated errors of 10-20%. in Houston area.
MOZAIC	• Comparisons made Sept 04 – May 05	• Agreement within CO area variability and estimated errors of 10-20% in most airports. • Waiting for data after May 2005.

6.8 References

[1] Filipiak, M.J., R.S. Harwood, J.H. Jiang, Q. Li, N.J. Livesey, G.L. Manney, W. G. Read, M.J. Schwartz, J.W. Waters, D.L. Wu, "Carbon Monoxide Measured by the EOS Microwave Limb Sounder on Aura: First Results," *Geophys. Res. Lett. 32*, No. 14, L14825, doi:1029/2005GL022765, 28 July 2005

[2] C. P. Rinsland, M Luo, J. A. Logan, R. Beer, H. Worden, S. S. Kulawik, D. Rider, G. Osterman, M. Gunson, A. Eldering, A. Goldman, M. Shephard, S. A. Clough, C. Rodgers, M. Lampel, and L. Chiou, Nadir Measurements of Carbon Monoxide (CO) Distributions by the Tropospheric Emission Spectrometer (TES) Instrument onboard the Aura Spacecraft: Overview of Analysis Approach and Examples of Initial Results, *Geophys. Res. Lett.,* in press, 2006.

[3] M. Luo, C. P. Rinsland, C. D. Rodgers, J. A. Logan, H. Worden, S. Kulawik, A. Eldering, A. Goldman, M. W. Shephard, M. Gunson, and M. Lampel, Comparison of carbon monoxide measurements by TES and MOPITT - the influence of *a priori* data and instrument characteristics on nadir atmospheric species retrievals, submitted to JGR, June 2006.

Distributed by the Atmospheric Science Data Center
http://eosweb.larc.nasa.gov

7. Validation of TES Retrievals of Temperature

7.1 Comparisons of TES Temperature with AIRS, Aircraft, and Sondes

Validation of TES temperature is important not only for its own merits, but also because ozone is retrieved jointly with temperature and water vapor. Retrieval improvements in any one of these species could impact the other two. This section focuses on v002 temperature retrievals with the standard retrieval quality flags. As discussed elsewhere in this validation report, the retrieval algorithm for TES v002 (R9) data has undergone significant improvements.

In 2005, the first TES validation report version 1.00 dealt with v001 (R7) TES temperature retrievals. TES v001 temperature exhibited an upper tropospheric warm bias of typically 2 K relative to AIRS and other measurements. In the lower to middle troposphere (900 to 300 hPa), TES v001 had a cold bias of less than 1 K relative to AIRS. As described below, the main difference between v001 and v002 is that the sign of the TES bias has reversed.

7.1.1 TES Temperature Comparisons with AIRS

TES nadir retrievals have spatial overlap with AIRS nadir retrievals and a temporal difference of only 15 minutes, so AIRS provides an ideal dataset for comparisons with TES. Nine TES v002 global surveys have been compared with AIRS temperatures. See Table 7-1, below.

Table 7-1 Nine TES v002 Global Surveys Compared with AIRS Temperatures

Runid	3130	3141	3149	3172	2949	2960	2963	2967	2983
Date	10/4/05	10/12/05	10/18/05	11/9/05	7/6/05	7/12/05	7/14/05	7/16/05	7/24/05

The coincidence criteria were retrievals within 0.3° latitude and 0.3° longitude on the same dates and orbits (thus ensuring time coincidence within 15 minutes). Since the combined AIRS/AMSU footprint is 45 km in diameter, these criteria allow for retrievals that spatially overlap the TES 8 km by 5 km nadir retrievals. The versions of temperature data compared were TES v002 and AIRS v4.0, with the AIRS quality flag QA_TEMP_BOT = 0 and the standard TES quality flags. Cloud conditions for these retrievals spanned the range of TES effective optical depths from 0.01 to 10. TES retrievals were interpolated to the closest AIRS standard retrieval pressures levels for a direct comparison of temperature. The results, shown below in Figure 7-1, indicate that TES v002 temperatures have an upper tropospheric cold bias of 0.5 to 1.2 K relative to AIRS at 100-600 hPa. In the stratosphere, TES v002 has a warm bias of up to 0.7 K relative to AIRS at 20-100 hPa. These biases are similar in the latitude ranges 90 S to 90 N, 60 S to 60 N, and 30 S to 30 N (Figure 7-2 (a-c)), indicating that there is very little apparent latitudinal bias in temperature.

7.1.2 TES Temperature Comparisons with Aircraft in the Tropics

Aircraft and sondes are reliable sources of temperature measurements to compare with TES retrievals. Not only do they have documented accuracy, but they also provide local

Distributed by the Atmospheric Science Data Center
http://eosweb.larc.nasa.gov

meteorological context for TES retrievals. The challenge is incomplete spatial overlap between the aircraft or sonde measurements and satellite footprint. The aircraft comparisons shown here are from the deep tropics, where tropospheric temperature profiles do not have much spatial variability.

During January and February 2006, the Costa Rica Aura Validation Experiment (CR-AVE) was carried out from San Jose, Costa Rica. On a series of 12 flights of the high-altitude WB-57F aircraft, both remote sensing and *in situ* instruments measured atmospheric properties in the tropical troposphere and lower stratosphere. The Microwave Temperature Profiler (MTP) provided temperature retrievals from the WB-57F aircraft during the second half of CR-AVE. MTP measures oxygen emission lines above and below the aircraft to retrieve temperature profiles from the lower troposphere to the middle stratosphere. The MTP retrieval process uses local radiosonde profiles, and is not completely independent of those measurements. The best comparisons between TES and MTP were on two global surveys near Costa Rica: 7 February and 9 February 2006. Flight tracks for these days are shown in Figure 7-3 and Figure 7-4, respectively. Comparisons were made for the closest spatial approach of the aircraft to the TES global survey points. The TES Global Survey retrieval at 69233 seconds UTC (9.8 °N, 84.7 °W) was flagged as bad L2 data and not included in this comparison. Figure 7-5 and Figure 7-6 show the comparison between MTP (red) and TES (blue). The most pronounced features are a TES cold bias in the upper troposphere and a TES warm bias in the middle stratosphere.

During CR-AVE, *in situ* measurements of temperature were carried out by the NASA Ames Meteorological Measurement System, or MMS, on the WB-57F aircraft. On 22 January 2006, the aircraft takeoff and climb-out profiled temperature from the ground up to 15 km altitude within 60 km of the TES Step and Stare special observation. On 7 February 2006, the aircraft performed a spiral descent at the end of the flight within 200 km of the nearest TES Global Survey retrieval with good quality. Figure 7-7 (a-c) shows comparisons of these MMS profiles with TES. The TES averaging kernel has been applied to the *in situ* temperature profiles. TES temperature retrievals have a cold bias in the upper troposphere at 100 to 300 hPa relative to MMS.

7.1.3 TES Temperature Comparisons with Sondes

During 2006, TES special observations were scheduled at the DOE Atmospheric Radiation Measurement (ARM) sites at Southern Great Plains, Oklahoma, the North Slope of Alaska, and the Tropical Western Pacific. With coincidence criteria of 2 hours and 250 km, these special observations were compared with radiosondes (RS90 and RS92 types). As shown below in Figure 7-8, a TES cold bias of ~1 K is seen in the upper troposphere relative to these sondes. In contrast, the bias between GMAO GEOS-4 and the sondes is much smaller.

Another set of sondes were launched from Heredia, Costa Rica, and San Cristobal, Galapagos, as part of the Ticosonde mission in January and February 2006. Figure 7-9 (a-c) shows comparisons between the closest sondes (with TES averaging kernel applied) and TES retrievals on three days. The comparisons on 22 January and 25 January both indicate a TES cold bias in the upper troposphere. On 7 February 2006, the temperature differences are greater, but so is the distance between the sonde and the TES retrieval.

7.1.4 Summary

TES temperature retrievals have been compared with both remote sensing and *in situ*

Distributed by the Atmospheric Science Data Center
http://eosweb.larc.nasa.gov

measurements. In all cases, TES temperature has a cold bias in the upper troposphere of typically 0.5 to 2 K. A TES warm bias is sometimes observed in the stratosphere.

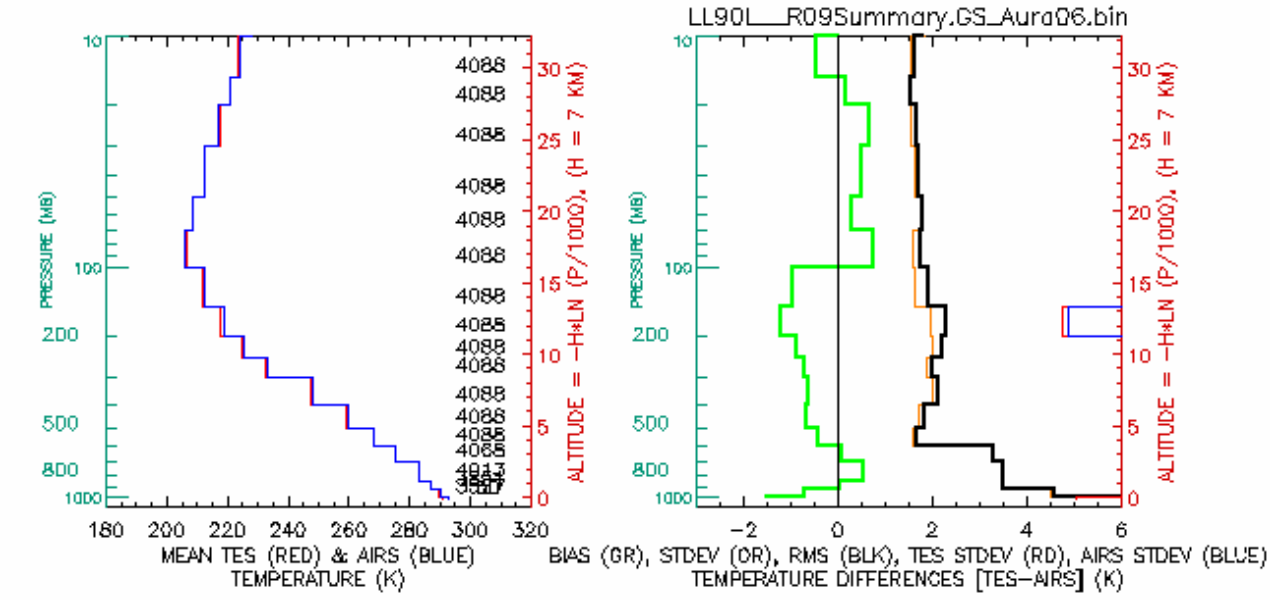

Figure 7-1 Comparison of TES v002 Global Surveys with AIRS v4.0 from matched Temperature Retrievals. The temperature bias (green) is TES minus AIRS.

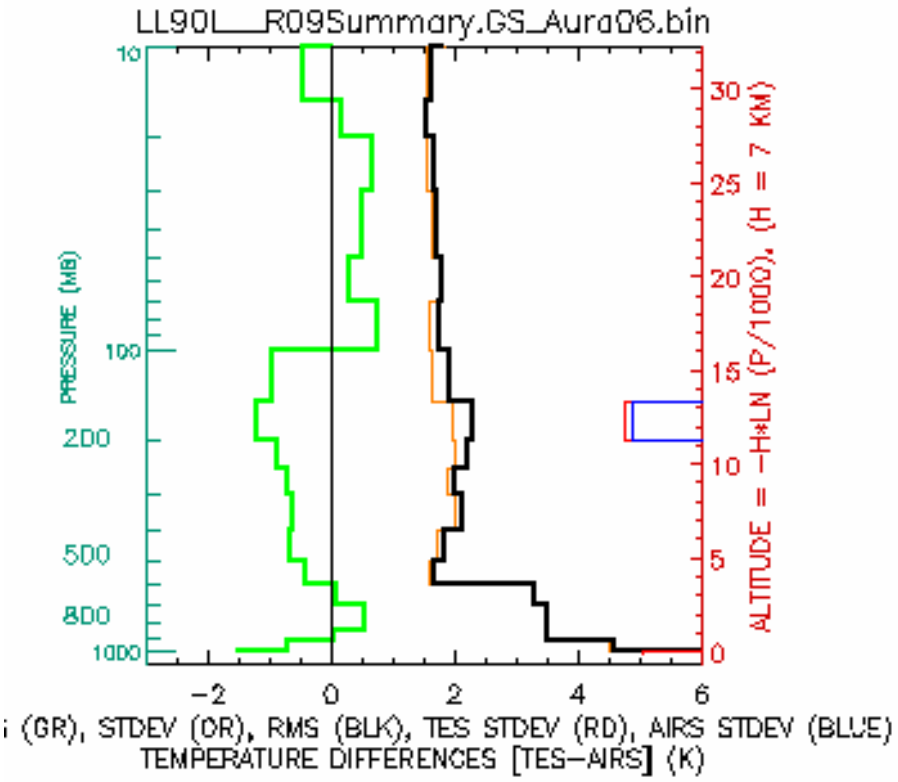

(a)

Distributed by the Atmospheric Science Data Center
http://eosweb.larc.nasa.gov

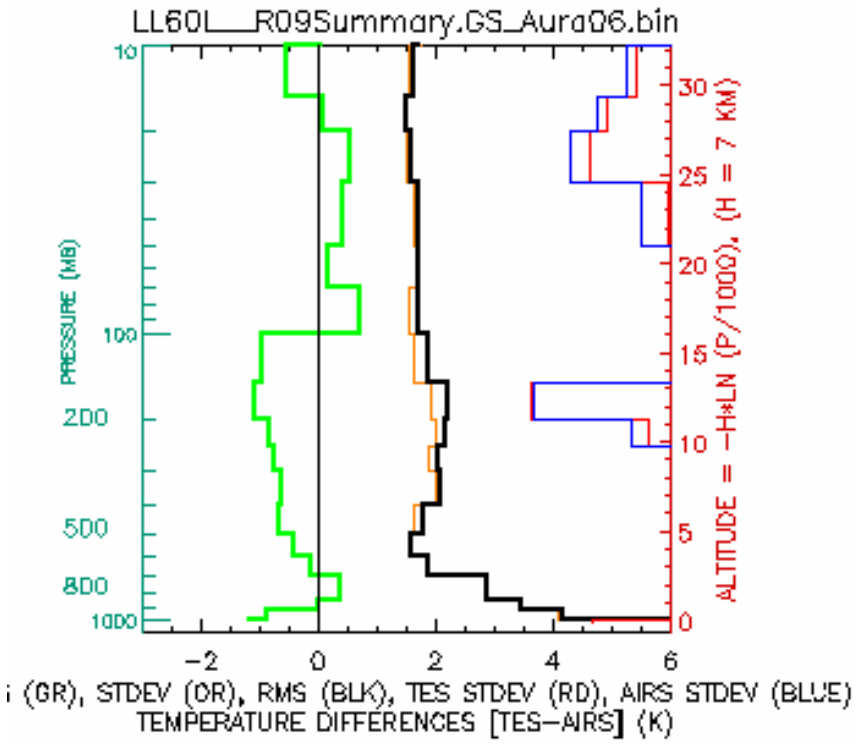

(b)

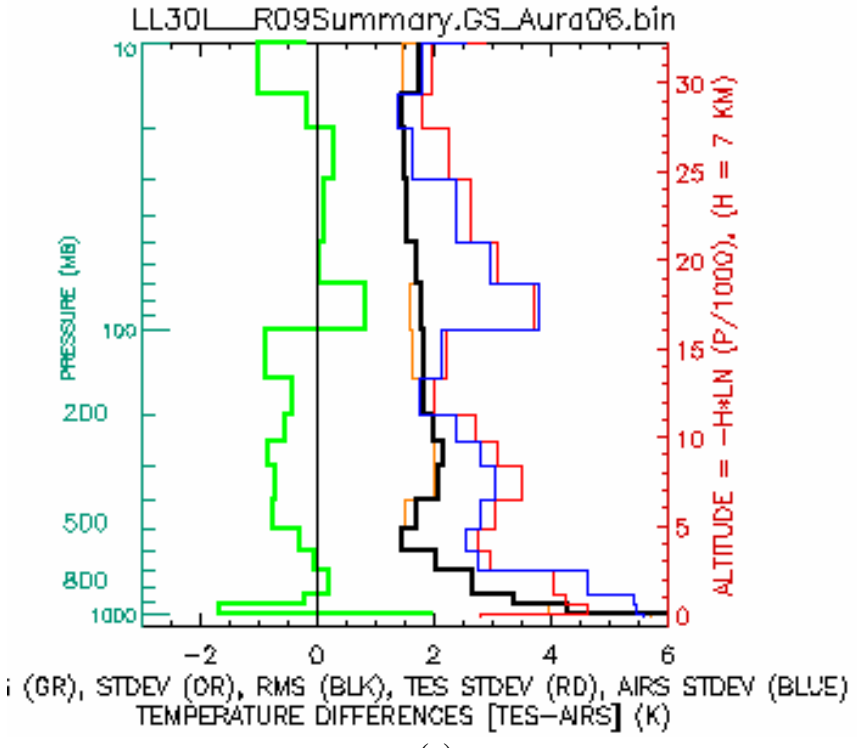

(c)

Figure 7-2 (a) Comparison of TES v002 and AIRS v4.0 from matched Temperature Retrievals over all Latitudes, 90 S to 90 N. (b) Comparison of TES v002 and AIRS v4.0 from matched Temperature Retrievals from 60 S to 60 N. (c) Comparison of TES v002 and AIRS v4.0 from matched Temperature Retrievals in the Tropics, 30 S to 30 N.

Distributed by the Atmospheric Science Data Center
http://eosweb.larc.nasa.gov

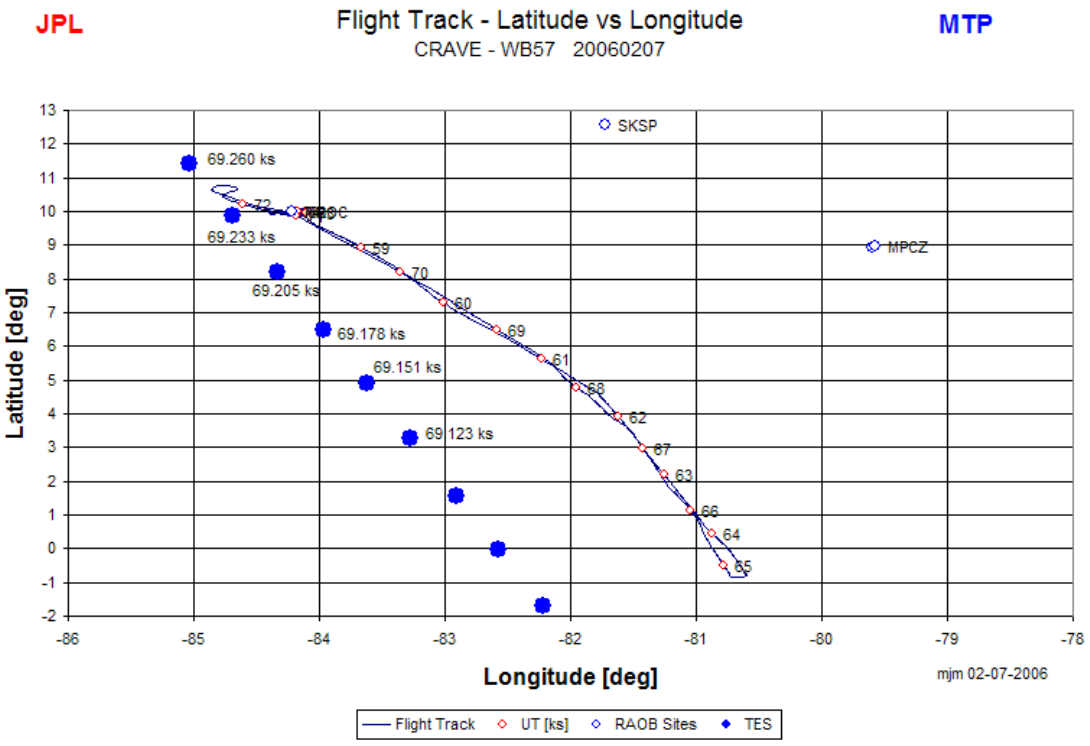

Figure 7-3 Flight track of the WB-57F Aircraft (Black) and TES Global Survey Locations (Blue Dots) on 7 February 2006.

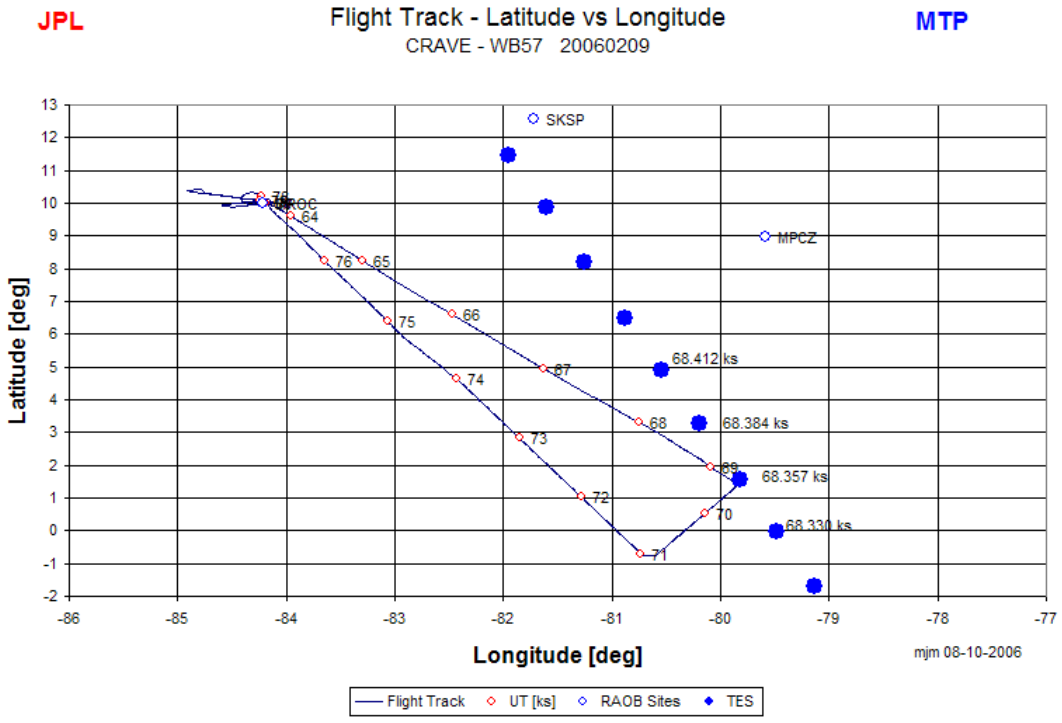

Figure 7-4 Flight Track of the WB-57F Aircraft (black) and TES Global Survey Locations (blue dots) on 9 February 2006.

Distributed by the Atmospheric Science Data Center
http://eosweb.larc.nasa.gov

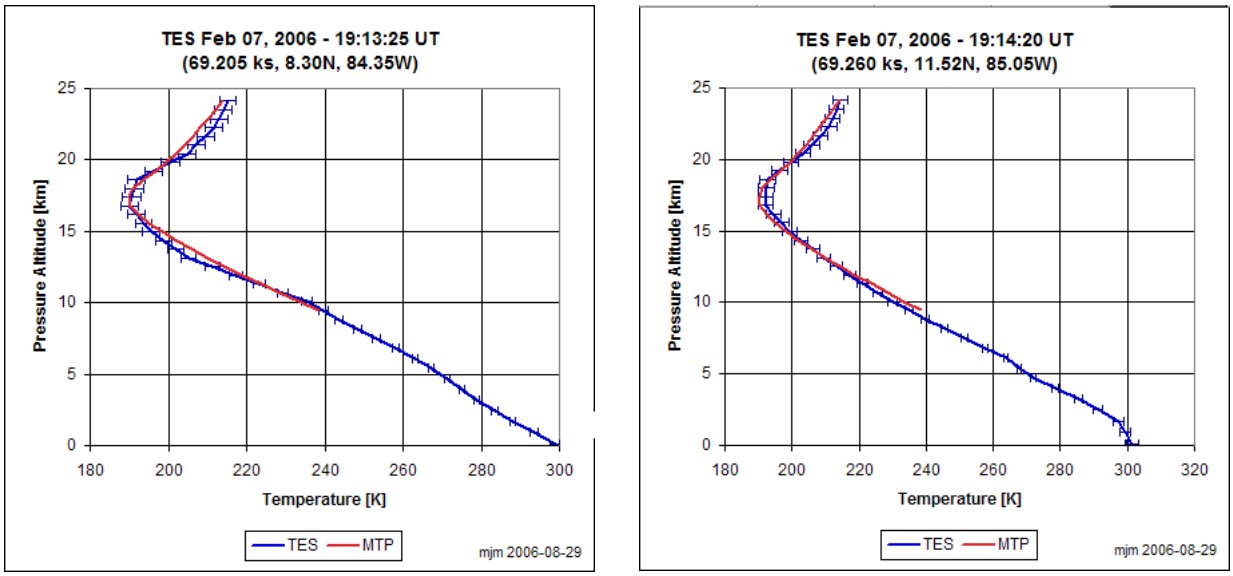

Figure 7-5 Nearby Temperature Profiles from MTP (red) and TES (blue) on 7 February 2006.

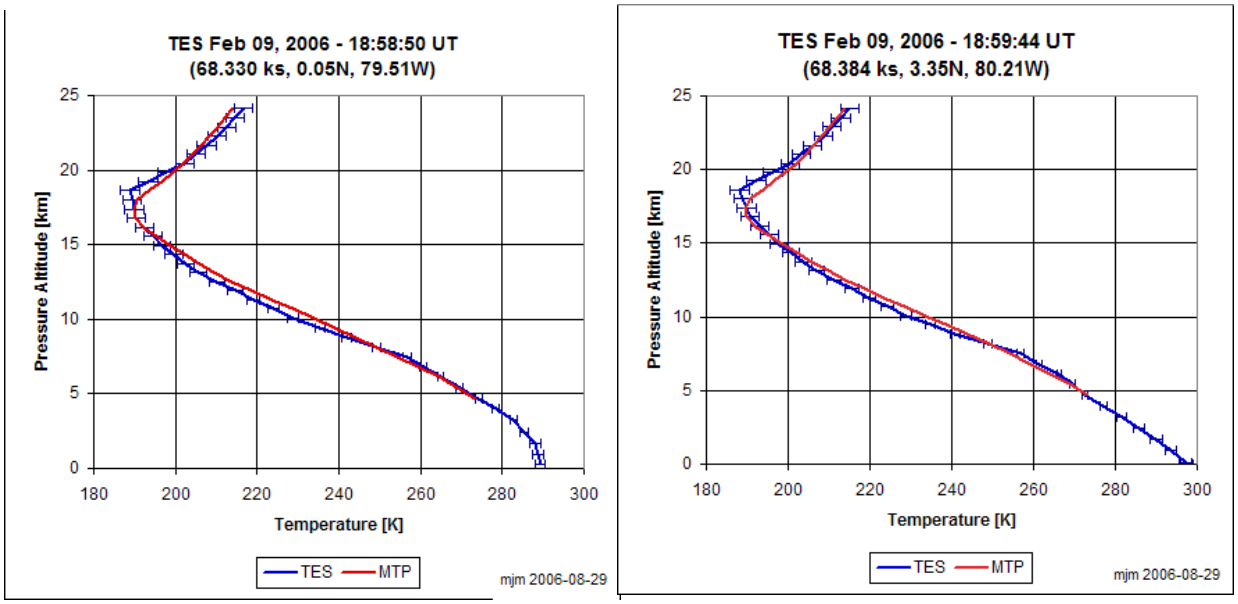

Figure 7-6 Nearby Temperature Profiles from MTP (red) and TES (blue) on 9 February 2006.

Distributed by the Atmospheric Science Data Center
http://eosweb.larc.nasa.gov

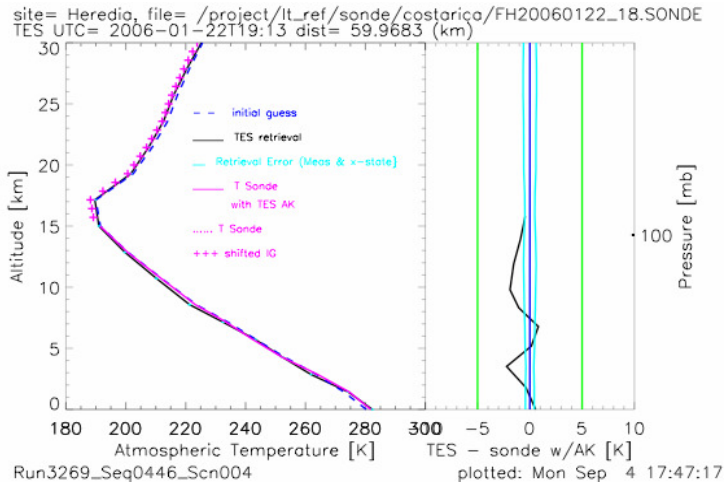

(a)

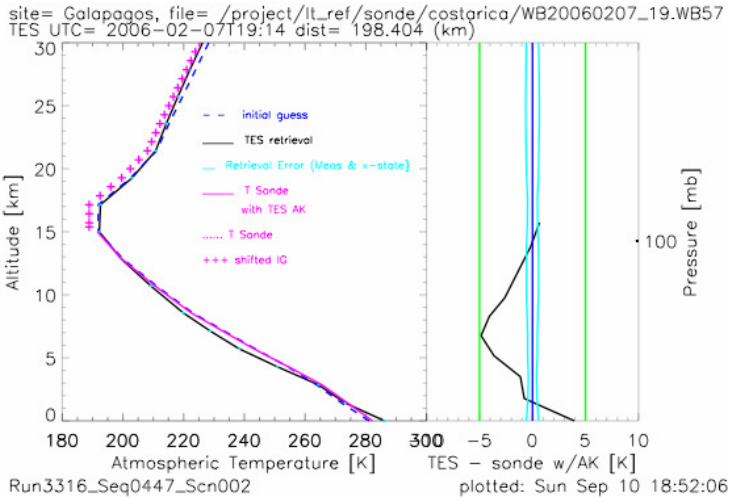

(b)

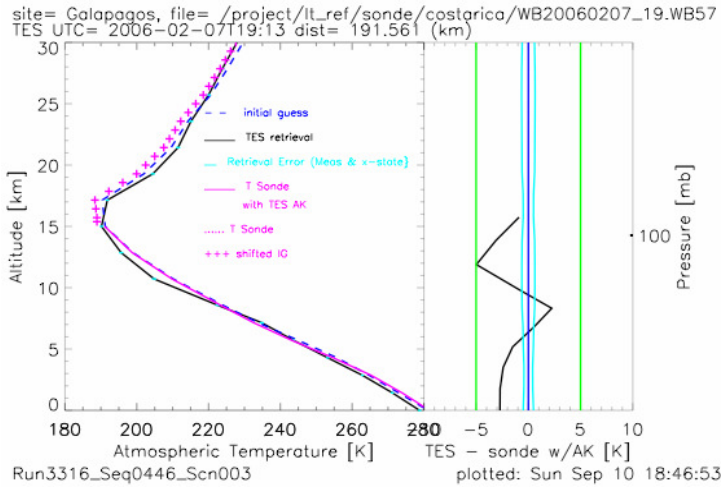

(c)

Figure 7-7 (a-c) Comparisons of TES Temperature with Aircraft *in situ* Temperature from the WB-57F during CR-AVE

Distributed by the Atmospheric Science Data Center
http://eosweb.larc.nasa.gov

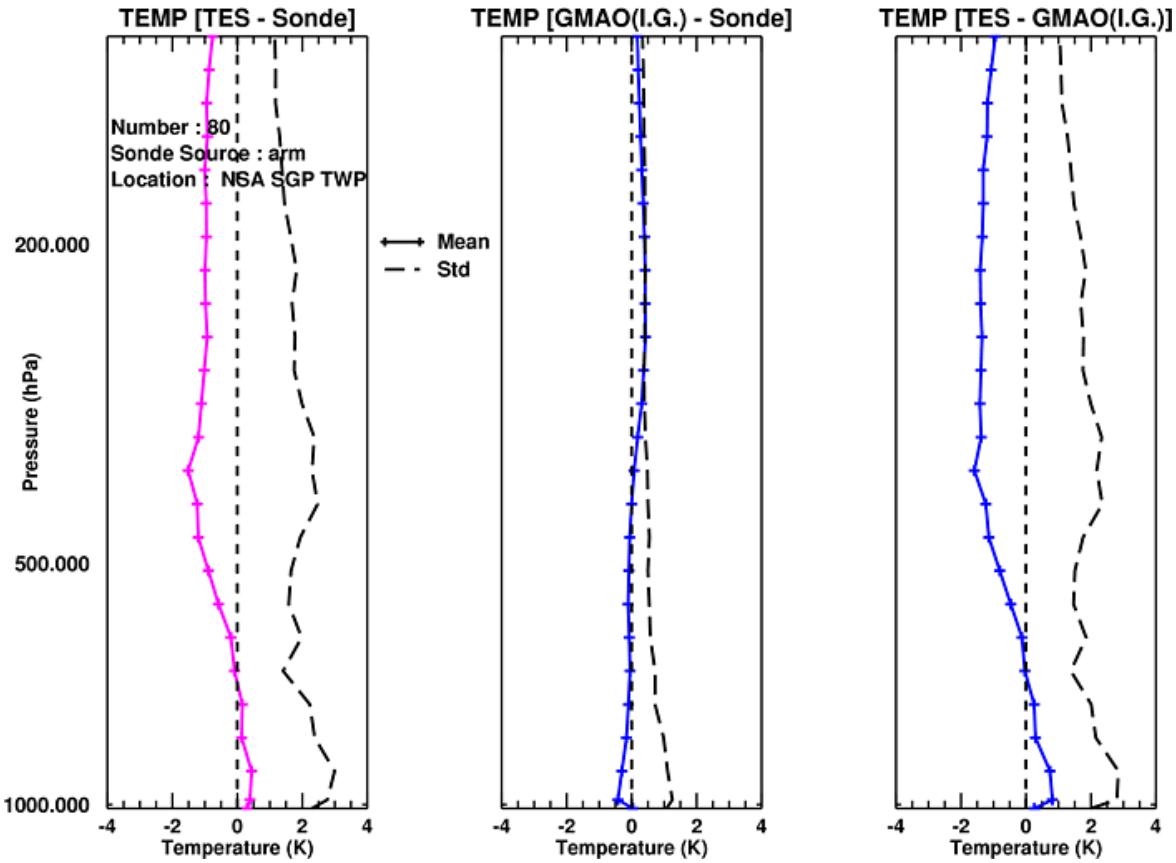

Figure 7-8 Comparison of TES Temperature Retrievals with ARM Site Radiosondes and GMAO GEOS-4.

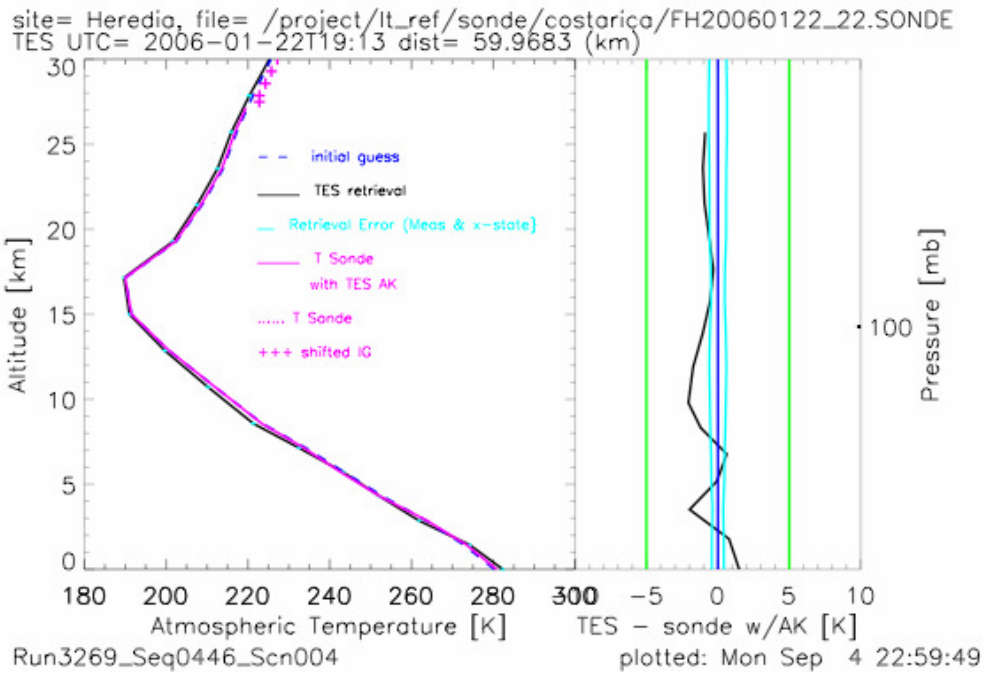

(a)

Distributed by the Atmospheric Science Data Center
http://eosweb.larc.nasa.gov

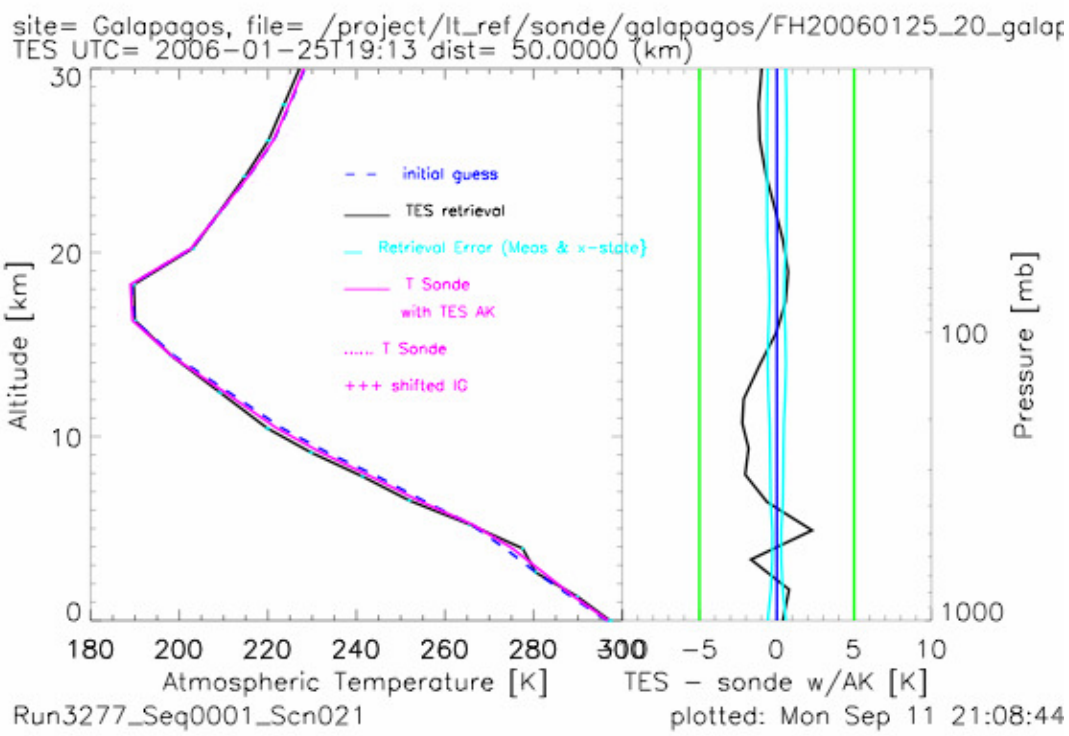

(b)

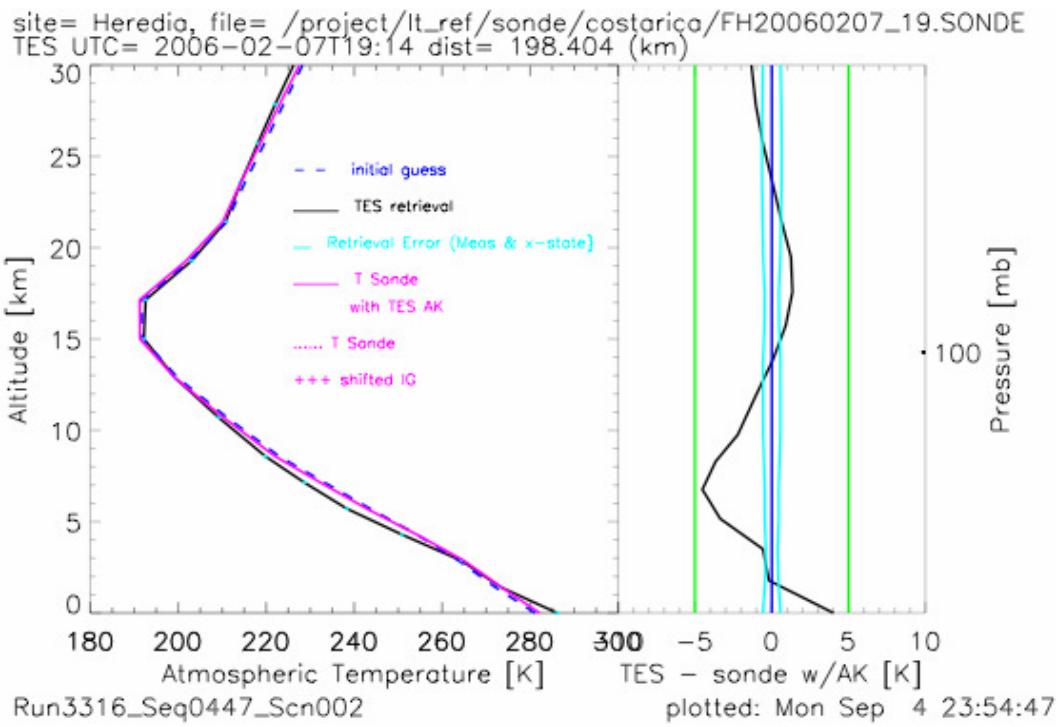

(c)

Figure 7-9 (a-c) Comparisons of TES Temperature Retrievals with Sondes launched during Ticosonde in Costa Rica and Galapagos.

Distributed by the Atmospheric Science Data Center
http://eosweb.larc.nasa.gov

7.2 TES Temperatures in Comparison with NCEP Sonde Temperatures

To help characterize TES temperature retrievals we have compared the mean difference between TES temperature profiles and NCEP sonde temperatures. The first step in the comparison is to find TES observations coincident with NCEP sonde launches. We have set a coincidence criterion that requires the TES and sonde measurements to take place within two degrees and two hours of each other. Once the relevant TES and sonde pairs have been identified, the sonde pressure grid is mapped onto the TES pressure grid, and the TES averaging kernel is applied (Section 5.1.2). Only TES profiles that pass the normal TES quality assurance criteria have been included. Additionally, a small number of profiles have also been rejected when the difference between the TES temperature and the sonde temperature at 100hPa exceeds 5K. There are relatively few cases where this is true (< 5%). In these cases, the TES initial guess temperature profile (from GMAO GEOS-4) is also very different from the reported sonde temperature profile. In other words, these sonde profiles are very different from climatology. There is no obvious geographic distribution for these cases.

For this report, we have taken sets of 4 sequential global surveys (covering approximately one week of time) with the associated matched sonde observations and calculated the mean difference as a function of pressure. For global surveys with the original 2 nadir/3 limb observation mode, this gives ~230 matched profiles. For the current 3-nadir observations mode global surveys, the coincidence criteria give ~650-750 coincident observations for a set of 4 global surveys. To search for any possible seasonal dependence, we have made mean temperature difference plots approximately quarterly for the duration of TES observations. The results are shown in Figure 7-10 and Figure 7-11. The TES temperature profiles show a consistent pattern with respect to the NCEP sonde temperature profiles in the mean. TES typically has a warm bias of 0.5-1.0 K in the 700-900 hPa pressure range, and a 1-2 K cold bias in the 100-400 hPa pressure range with respect to the sonde temperatures. In some periods TES shows a cold bias in the lower stratosphere (e.g. Jan. 2005), but this bias is not persistent and is generally < 0.5K.

Distributed by the Atmospheric Science Data Center
http://eosweb.larc.nasa.gov

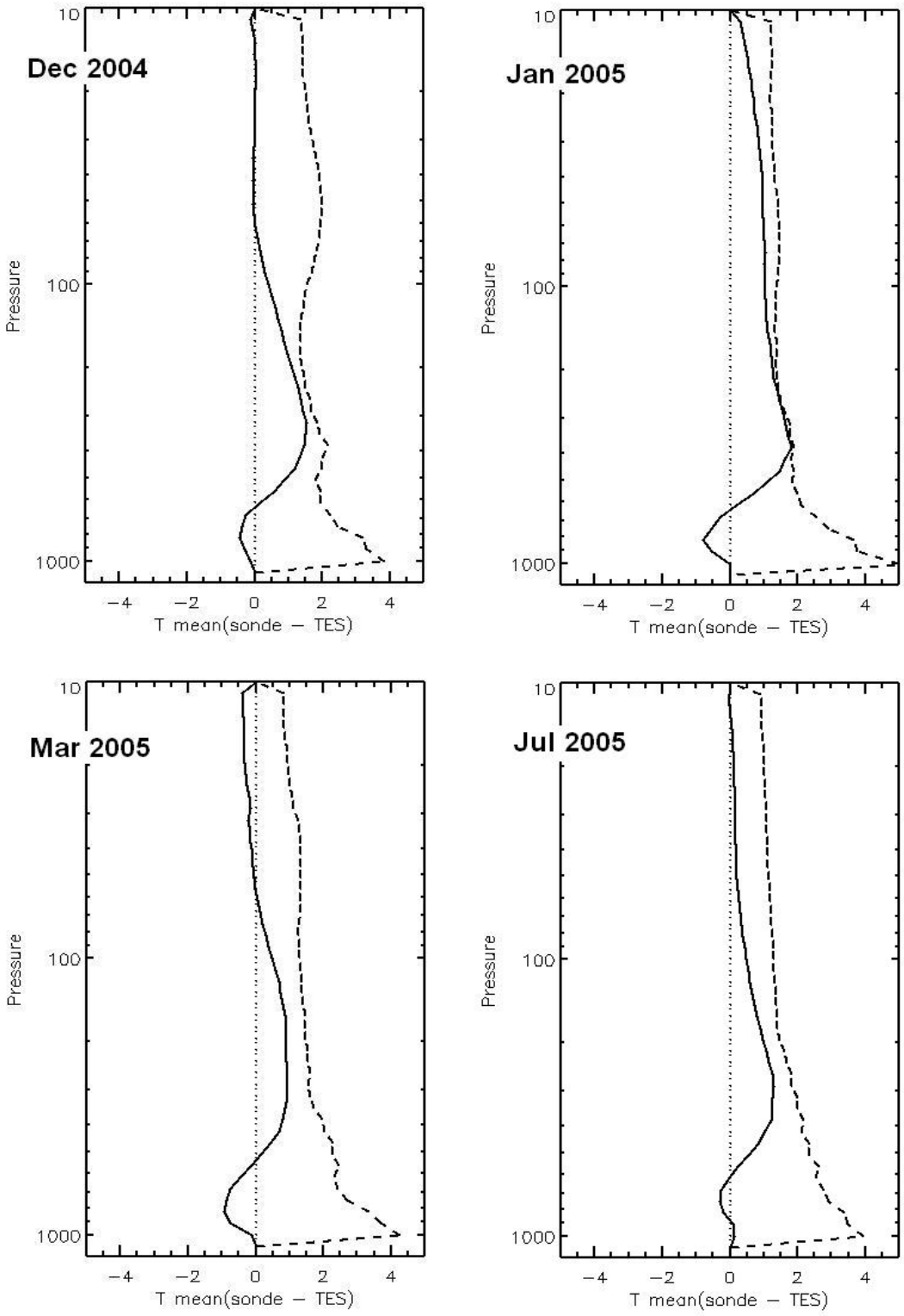

Figure 7-10 Comparison of Mean Difference between TES and NCEP Sonde Temperature Profiles for four Time Periods. The solid line is the mean temperature difference and the dashed line is the RMS of the differences. The dotted line shows zero for reference.

Distributed by the Atmospheric Science Data Center
http://eosweb.larc.nasa.gov

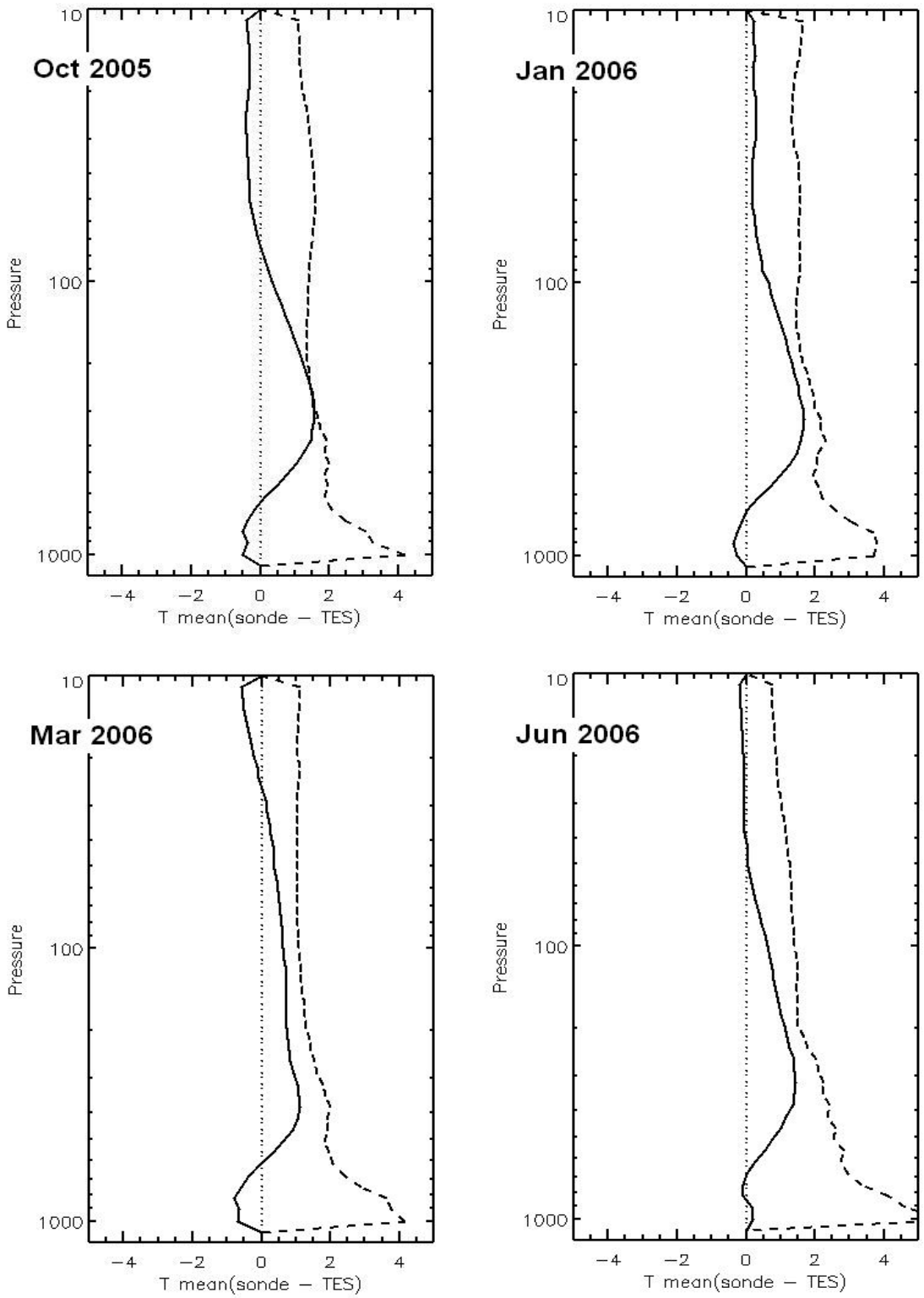

Figure 7-11 Comparison of Mean Difference between TES and NCEP Sonde Temperature Profiles for four Time Periods. The solid line is the mean temperature difference and the dashed line is the RMS of the differences. The dotted line shows zero for reference.

Distributed by the Atmospheric Science Data Center
http://eosweb.larc.nasa.gov

8. TES Sea Surface Temperature Retrievals

8.1 Introduction

Although TES is focused on tropospheric chemistry, surface temperature (skin temperature) and emissivity measurements are essential elements of the nadir observations performed. Since ocean emissivity is known accurately (Masuda, *et al.* 1988), with respect to the TES calibration requirement and detector noise, retrievals of sea surface temperatures (SST) provide a useful method for assessing TES retrievals. The large percentage of observations partially or completely obscured by clouds makes it important to TES, and potentially to other remote sensing instruments, to characterize information that can be retrieved at different cloud effective optical depths. To this end, cloud optical depths (ODs) and the degrees of freedom of signal (DOFS) of the SST measurements are examined in conjunction with SST error estimates to assess the skill of TES retrievals in the presence of clouds. Global TES SST retrievals for Nov 4-16, 2004, are compared against the Reynolds Optimally Interpolated SST (ROI SST) (information on the Reynolds OI SST can be obtained from: http://podaac-www.jpl.nasa.gov/sst/) (Smith, *et al.,* 1994).

8.2 Data

There were seven TES global surveys Nov. 4-16, 2004 inclusive. SST differences are denoted as TES – ROI.

The TES 1B2 filter that spans the spectral range between 950 cm^{-1} and 1150 cm^{-1}, which encompasses the 9.6 μm ozone band, has been used with version 2 data (release 9 retrieval software) to retrieve surface temperature, emissivity (over land), atmospheric temperature, water vapor, and ozone. This spectral band is not optimal for retrieving temperature and water in general, however for the November data analyzed the signal to noise (NESR) in the pre-selected bands covered by the 2A1 and 2B1 filters (Worden, J., *et al*. 2006) was not sufficient to allow their use.

8.3 Clouds Optical Depth and Degrees of Freedom of Signal Distributions

The TES retrieval algorithm estimates an effective cloud optical depth for all target scenes. The November retrievals provide an initial look at cloud OD distribution data and the overall performance of the TES retrieval method. A study done by (Kulawik, *et al.* 2005) has shown that retrievals with effective cloud ODs less than 0.1 give essentially the same results for atmospheric profiles as cloud free retrievals, and that the information retrieved with clouds is still significant for effective OD up to ~1.

Distributed by the Atmospheric Science Data Center
http://eosweb.larc.nasa.gov

Table 8-1 Table showing Retrievals within Cloud Optical Depth Bins

Max Optical Depth	Number of clouds	Fraction of Clouds
0 - 0.05	1482	0.303
0.05 - .1	447	0.091
.1 - .2	153	0.031
.2 - .3	135	0.028
.3 - .4	104	0.021
.4 - .5	125	0.026
-.6	144	0.029
-.7	144	0.029
-.8	122	0.025
-.9	110	0.022
-1.0	101	0.021
-1.1	92	0.019
-1.2	93	0.019
-1.3	78	0.016
-1.4	71	0.015
-1.5	69	0.014
-1.6	61	0.012
-1.7	63	0.013
-1.8	56	0.011
-1.9	60	0.012
-2.0 or greater	1180	0.241

Degrees of freedom of signal for sea surface temperature has a very different distribution, see table below. The number of retrievals drops off with increasing DOFS from 0 to 0.6 and then goes up a bit, leveling off at ~6% per 0.1 DOFS bin.

Table 8-2 Table showing Retrievals within 0.1 DOFS Bins

DOFS SST	# Retrievals	Fraction Retrievals
0.0	1214.00	0.248313
0.1	908.000	0.185723
0.2	667.000	0.136429

Distributed by the Atmospheric Science Data Center
http://eosweb.larc.nasa.gov

DOFS SST	# Retrievals	Fraction Retrievals
0.3	309.000	0.0632031
0.4	247.000	0.0505216
0.5	212.000	0.0433627
0.6	208.000	0.0425445
0.7	224.000	0.0458171
0.8	302.000	0.0617713
0.9	301.000	0.0615668
1.0	297.000	0.0607486

The SST DOFS is a critical quantity because it encompasses both the information content of the SST retrieval and the sensitivity of the retrieval. This is because, as SST is a scalar quantity, the DOFS is both the averaging kernel and the trace of the averaging kernel. The estimate for SST can be written as:

$$SST_i = SST_a + DOFS*(SST_{True} - SST_a) + \varepsilon \qquad \text{(Equation 8-1)}$$

Where SST_i is the updated (optimal) estimate, SST_a is the *a priori* sea surface temperature, SST_{True} is the true SST, and ε is the error. Because SST defines the brightness temperature of the nadir absorption spectra (due to the well defined emissivity), SST provides a self-consistent verification of the information processing system from operation of the instrument through the radiative transfer model used by TES and the accuracy of the calibration algorithm. Because SST is a surface quantity the SST DOFS also serves as a measure of how well TES overall sees to the surface through the atmosphere including below clouds which have broad spectral features. Therefore, once we determine a level of SST DOFS that meets some sensitivity requirements, we can conclude that the sounding of atmospheric constituents both above and below the cloud contains useful information retrievable from the spectra observed.

Distributed by the Atmospheric Science Data Center
http://eosweb.larc.nasa.gov

8.4 Comparison to ROI Data

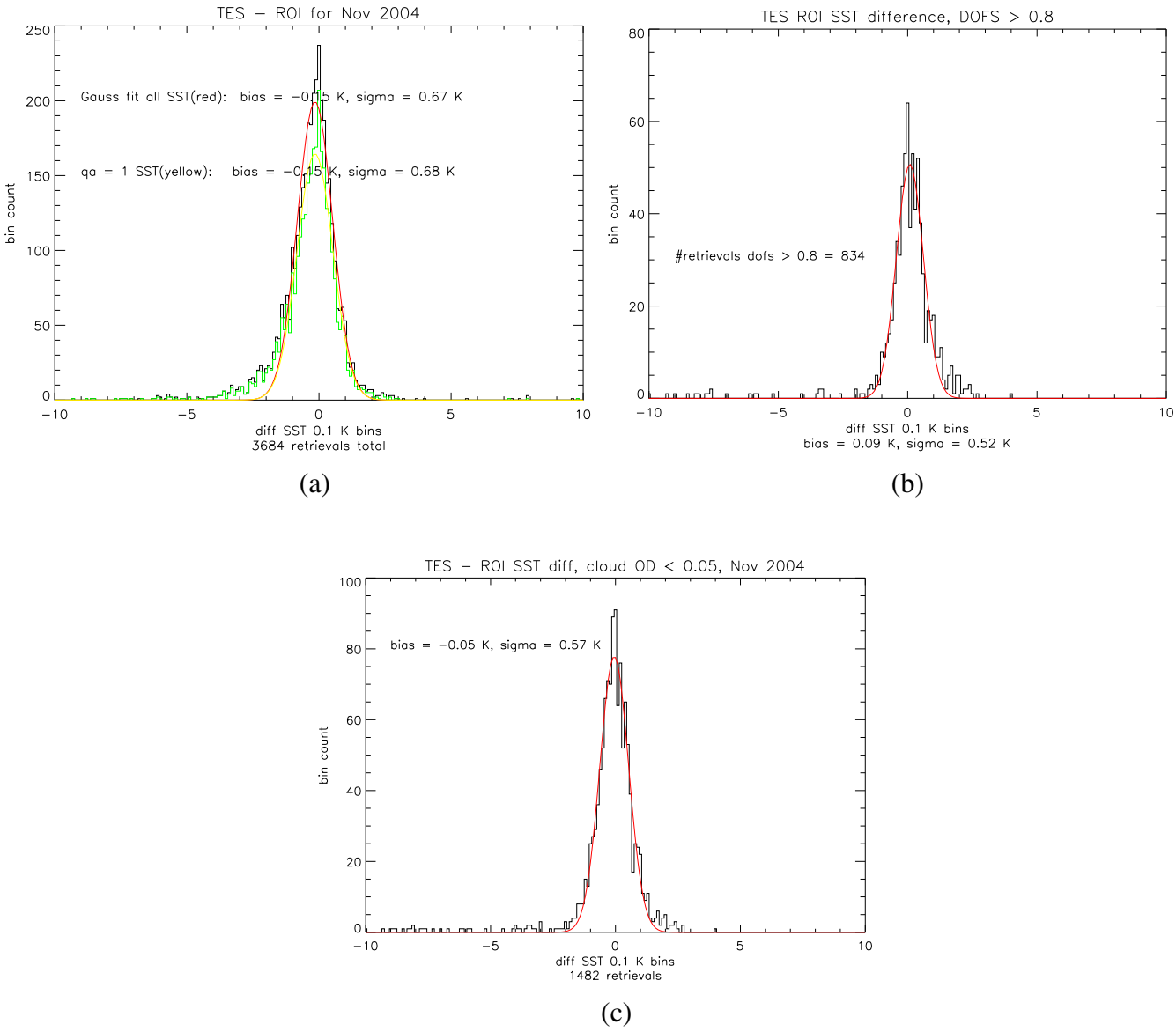

Figure 8-1 Histograms and Gaussian Fits to TES-ROI. (a) Black histogram is all Data - Fit by red Gaussian. Green Histogram is QA = 1 (good) fit by yellow Gaussian. (b) Histogram and Fit for DOFS > 0.8 (c) Histogram and Fit for Cloud OD < 0.05.

To understand the SST differences between TES and ROI we plot the histograms in Figure 8-1 which is the number of SST differences in 0.1 K bins. The distribution is strongly peaked near 0 K difference and can be fit reasonably well by a Gaussian distribution as shown in red. The key statistics TES - ROI, the RMS difference between TES and the comparison data set and the average temperature difference, or bias, are seen in Table 8-3, below.

Table 8-3 Bias, Sigma and RMS Statistics

Distributed by the Atmospheric Science Data Center
http://eosweb.larc.nasa.gov

Data	Bias (K)	Sigma (K)	RMS (K)	# Retrievals Compared
All data	-0.15	0.67	1.77	4625
Data w/QA = 1	-0.15	0.68	1.77	3684
Cloud OD < 0.05	-0.05	0.57	1.26	1482
DOFS ≥ 0.8	0.09	0.52	1.30	834

The hypothesis is that biases indicate simple systematic errors between the data sets, which can be subtracted out once they are documented, but the RMS differences contain both more complex systematic errors and uncorrelated errors due to instrument effects. Note that TES – ROI shows a slightly enhanced positive wing and a more enhanced negative wing in the histogram showing all data, Figure 8-1 (a), but for both filtering by DOFS and cloud optical depth the negative wings have been removed in Figure 8-1 (b and c).

Gaussian fits to the difference distributions have significantly smaller 1σ widths than the TES – ROI RMS widths as seen above in the table. Unsurprisingly the RMS is dominated by the outliers which the Gaussian fits have filtered out. DOFS of SST or cloud OD can be used as filters in preferentially reducing the outliers giving a physical basis for the non-normal statistics of the complete distribution.

In Figure 8-2 we see that the difference distributions do not have a significant latitudinal component between 60° S and 60° N. Therefore the temperature retrievals are not affected by latitudinal variations in calibration (due to instrument temperature drift from changing insolation), the SST itself, or variations of radiance over this range. Analysis of higher latitudes has not yet been done because the TES data sets do not flag sea ice.

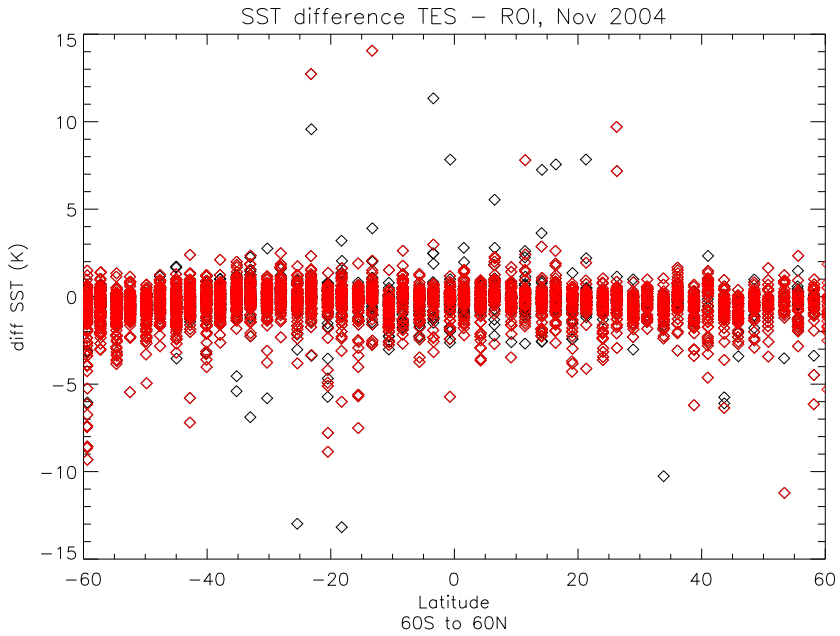

Figure 8-2 SST Differences vs. Latitude. Black shows all data, red shows data with QA = 1 (good).

Distributed by the Atmospheric Science Data Center
http://eosweb.larc.nasa.gov

8.5 Derived RMS SST Error from Comparison to AMSR-E

TES has a similar relative 1σ difference in temperature, on the order of 0.55 K for the most stringent filtering. If the 1σ width of the Gaussian is assumed to represent the RMS difference of uncorrelated measurements free of systematic errors and unaccounted for bias, then the 1σ width of the distribution, $diff_{RMS}$, is composed of the actual RMS errors of TES and ROI added in quadrature:

$$diff_{RMS} = \sqrt{TES_{RMS}^2 + ROI_{RMS}^2} \qquad \text{(Equation 8-2)}$$

Using this equation and taking the RMS error of ROI to be 0.4 - 0.5 K then the RMS error of TES is 0.23 - 0.38 K. The TES SST error is unlikely to be this small in reality. It is more likely that a high degree of correlation exists between ROI and TES. Further investigation will be required. Nonetheless it is reasonable to state that the overall RMS error of TES SST is about 0.5 K in line with the RMS error of ROI. Further, it is clear that TES does add information to the *a priori* in cases where Cloud OD < 0.05 or DOFS $\geq$ 0.8.

8.6 References

[1] Beer, R., 2006: TES on the Aura Mission: Scientific Objectives, Measurements and Analysis Overview, *IEEE Transactions on Geoscience and Remote Sensing* Special Issue on Aura, vol. 44, no. 5, May 2006.

[2] Masuda, K.T., Takashima and Y. Takayama, 1988: Emissivity of pure and sea waters for the model sea surfaces in the infrared window regions, Remote Sens. Environ, 24, 313-329.

[3] Bowman, K., et al. 2006: Tropospheric Emission Spectrometer: Retrieval Method and Error Analysis, *IEEE Transactions on Geoscience and Remote Sensing* Special Issue on Aura, vol. 44, no. 5, May 2006.

[4] Smith, T. M., R. W. Reynolds and C. F. Ropelewski, 1994: Optimal Averaging of Seasonal Sea Surface Temperatures and Associated Confidence Intervals (1860-1989). *J. Climate*, 7, 949-964.

[5] Worden, H. et al. 2006: TES L1 Algorithms: Interferogram processing, geolocation, radiometric and spectral calibration, *IEEE Transactions on Geoscience and Remote Sensing* Special Issue on Aura, vol. 44, no. 5, May 2006.

[6] Kulawik, S., et al. 2005: Implementation of Cloud Retrievals for Tropospheric Emission Spectrometer (TES) Atmospheric Retrievals – part I description and characterization of errors on trace gas retrievals, Submitted to *Journal of Geophysical Research - Atmospheres,* October 3, 2005

Distributed by the Atmospheric Science Data Center
http://eosweb.larc.nasa.gov

9. Comparison of TES Water Vapor with AIRS, Aircraft, and Sondes

A number of comparisons have been made between TES v002 water vapor and other data sources, including AIRS, aircraft, and sondes. The unique complication with water is variability over short distances. Therefore, the key to water validation is to perform statistics on large datasets to determine possible biases.

TES retrieves water vapor in the troposphere, with a sensitivity that decreases significantly at pressures less than 150 hPa, as shown below (Figure 9-1) in a plot of TES averaging kernels for water vapor. In the upper troposphere, TES has greater sensitivity to water in the tropics than at higher latitudes because the abundance of water is greater in the tropics (on a given pressure level). We will focus on comparisons with the AIRS/AMSU suite (the Atmospheric Infrared Sounder / Advanced Microwave Sounding Unit on EOS Aqua), sondes, and the tropical validation missions including the Costa Rica Aura Validation Experiment (CR-AVE) and Ticosonde.

For all of these comparisons, the TES retrievals were selected based on the recommended data quality screening. The following quality flags were applied specifically for TES water vapor retrievals:

SurfaceEmissMean_QA:	-0.1 to +0.1
KDotDL_QA:	-0.45 to +0.45
LDotDL_QA:	-0.45 to +0.45
CloudTopPressure:	90 to 1300 hPa
RadianceResidualMean:	-0.3 to +0.3
RadianceResidualRMS:	less than 1.4

TES water vapor is reported from the H_2O/HDO joint retrieval step, which comes after the O_3/H_2O/T joint retrieval step.

9.1 TES Water Vapor Comparisons with AIRS

For this validation report, water vapor profiles from nine TES v002 global surveys have been compared with AIRS v4.0 nadir retrievals. (See Table 9-1 below.)

Table 9-1 Nine TES v002 Global Surveys Compared with AIRS v4.0 Nadir Retrievals

Runid	3130	3141	3149	3172	2949	2960	2963	2967	2983
Date	10/4/05	10/12/05	10/18/05	11/9/05	7/6/05	7/12/05	7/14/05	7/16/05	7/24/05

AIRS observations are approximately 15 minutes ahead of TES observations along the same orbit track. The combined AIRS/AMSU footprint is 45 km in diameter with nearly continuous coverage along the orbit track, so AIRS nadir retrieval spatially overlap the TES 8 km by 5 km nadir retrievals. The coincidence criteria were retrievals within 0.3° latitude and longitude on the same dates and orbits. The versions of water vapor data compared were TES v002 and AIRS

Distributed by the Atmospheric Science Data Center
http://eosweb.larc.nasa.gov

v4.0, with the AIRS quality flag QA_TEMP_BOT = 0 (which applies both to data quality for both water and temperature) and the standard TES quality flags (see above). Cloud conditions for these retrievals spanned the range of TES effective optical depths from 0.01 to 10. AIRS reported water vapor is the mean mixing ratio averaged over the layer between adjacent standard pressure levels. There are 28 standard AIRS levels, and a larger number of TES levels, so TES water vapor has been integrated to match the AIRS vertical layers.

Figure 9-2 shows the bias and rms comparison between TES and AIRS with bias (green) calculated as (TES-AIRS)/TES. It is seen that TES v002 is 10 to 25% wetter than AIRS v4.0 at 150-500 hPa in the upper troposphere and 15 to 20% drier than AIRS in the lower troposphere (500-1000 hPa). This result is similar to what was found in the first TES validation report with v001 data. Figure 9-3 (a, b, and c) show the TES-AIRS comparisons for three different latitude ranges (90 S to 90 N, 60 S to 60 S, and 30 S to 30 N). Biases are very similar in all three cases, indicating that there is little apparent water bias with latitude.

9.2 TES Water Vapor Comparisons with *In situ* Measurements from sonde

During 2006, TES special observations were scheduled at the Department of Energy (DOE) Atmospheric Radiation Measurement (ARM) sites at Southern Great Plains, Oklahoma, the North Slope of Alaska, and the Tropical Western Pacific. With coincidence criteria of 2 hours and 250 km, water vapor profiles from these special observations were compared with radiosondes (both RS90 and RS92 types). As shown below in Figure 9-4, TES has a wet bias relative to ARM sondes of up to 30% at 300 hPa. There are differences between sondes and GMAO, but GMAO GEOS-4 has a known software bug that affects water vapor in the upper troposphere and lower stratosphere (S. Pawson, pers. comm.). GMAO GEOS-5 is reported to have corrected this problem, but is not available yet for comparisons.

The balloon-borne Cryogenic Frostpoint Hygrometer (CFH) was launched from Heredia, Costa Rica (9.99 N, 84.2 W), and San Cristobal, Galapagos (0.9 S, 89.62 W), as part of the Ticosonde mission in January and February 2006. On 25 January 2006, TES carried out a transect special observation (run id 3277) centered on the Galapagos Islands for a close coincidence with the launch of a combination CFH/ozonesonde. Atmospheric conditions were partly cloudy with low stratus clouds along a portion of the transect. Figure 9-5 shows that the water field measured by TES was uniform across the transect. Figure 9-6 is a comparison of the water profiles retrieved by TES and CFH on this day, showing excellent agreement.

9.3 TES Water Vapor Comparisons with *In situ* Measurements from Aircraft

During January and February 2006, the Costa Rica Aura Validation Experiment (CR-AVE) was carried out from San Jose, Costa Rica. On a series of 12 flights of the high-altitude WB-57F aircraft, both remote sensing and *in situ* instruments measured atmospheric properties in the tropical troposphere and lower stratosphere. The number of dates with close coincidences between aircraft *in situ* water profiling and TES retrievals was too small to apply statistics, but we show here two typical comparisons. On 22 January 2006, the nearest TES global survey retrieval was 43 km and 1 hour away from the aircraft measurements on takeoff. Figure 9-7 is a comparison of TES and the mean aircraft profile (averaging water measurements from several instruments on board the WB-57F aircraft: Harvard Lyman-alpha, Harvard ICOS, JPL Laser Hygrometer, NOAA, and at low altitudes ALIAS and CFH). Another comparison opportunity arose on 7 February 2006. At the end of its flight, the WB-57F aircraft spiraled down slowly

Distributed by the Atmospheric Science Data Center
http://eosweb.larc.nasa.gov

over San Jose, Costa Rica, within 43 km of the nearest TES Global Survey retrieval (9.86 N, 84.7 W). According to the pilot, the sky was exceptionally clear with some scattered cumulus clouds near the surface (especially up against the mountains, where the afternoon convection was starting to build). Figure 9-8 shows the comparison between TES and the mean aircraft *in situ* profile on 7 February 2006.

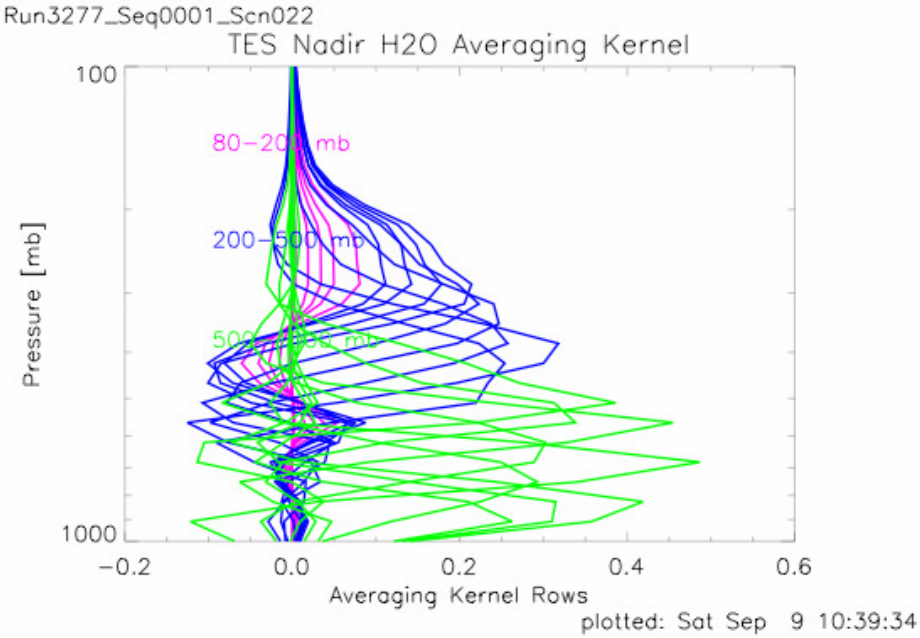

Figure 9-1 TES Nadir Water Vapor Averaging Kernel from a good Tropical Retrieval (Runid 3277, Sequence 1, Scan 022) Demonstrates Excellent Sensitivity and Vertical Resolution throughout the Troposphere, up to 150 hPa.

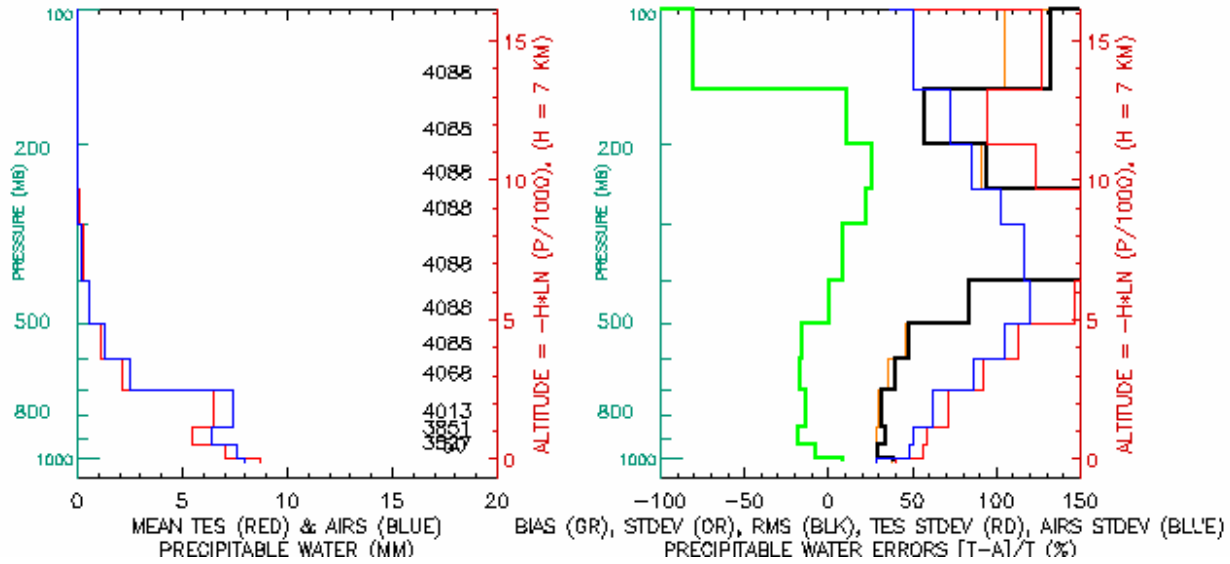

Figure 9-2 Mean Water Vapor Profiles for matched Retrievals from AIRS v4.0 and nine TES v002 Global Surveys. Left: TES Water (red), AIRS Water (blue); Right: Percent Bias (green) calculated as (TES-AIRS)/TES, and Rms Differences (black).

Distributed by the Atmospheric Science Data Center
http://eosweb.larc.nasa.gov

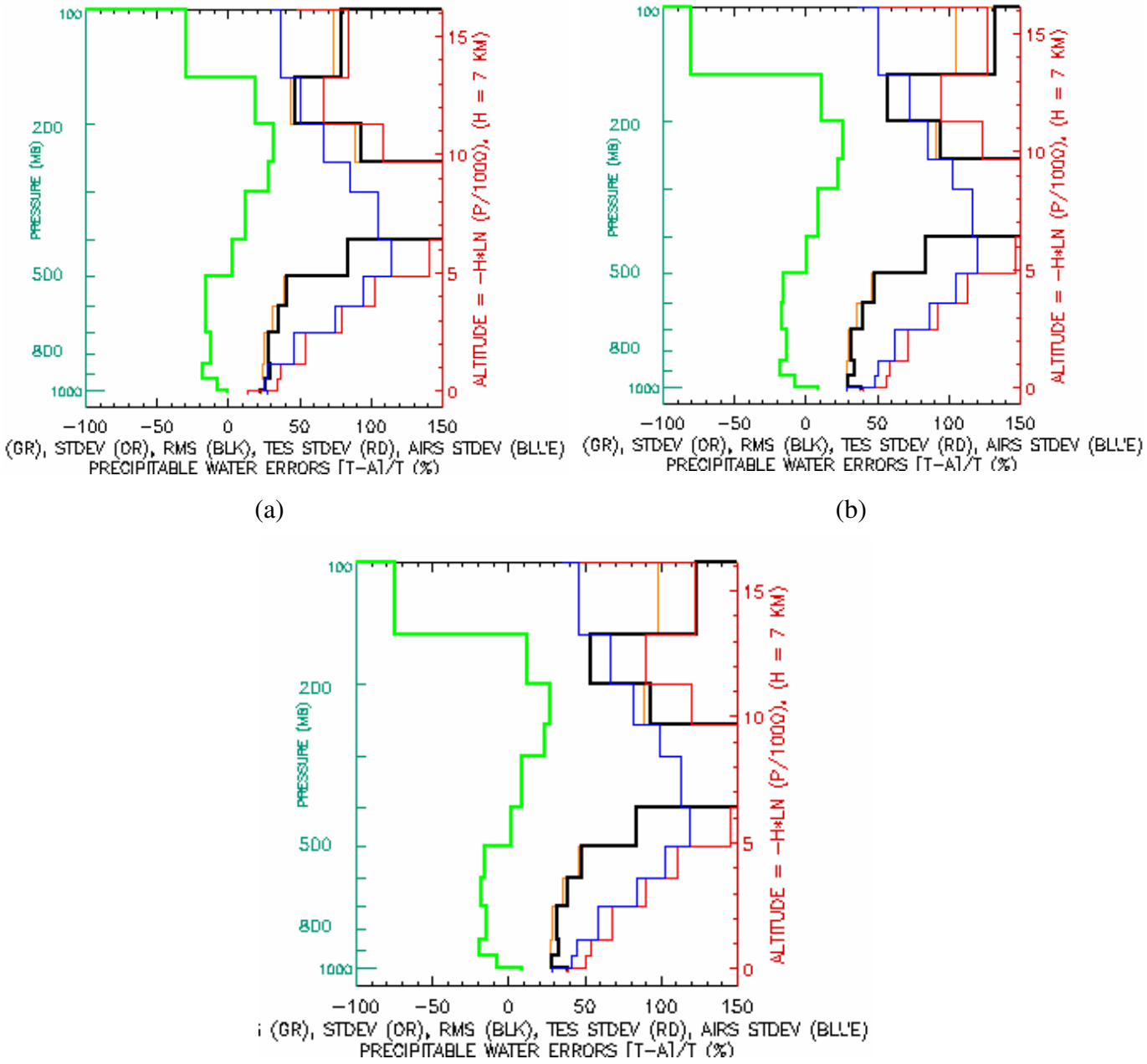

(a) (b)

(c)

Figure 9-3 **(a)** Water Comparisons for matched Retrievals from AIRS v4.0 and nine TES v002 Global Surveys: 90 S to 90 N. **(b)** Water Comparisons for matched Retrievals from AIRS v4.0 and nine TES v002 Global Surveys: 60 S to 60 N. **(c)** Water Comparisons for matched retrievals from AIRS v4.0 and nine TES v002 Global Surveys: 30 S to 30 N.

Distributed by the Atmospheric Science Data Center
http://eosweb.larc.nasa.gov

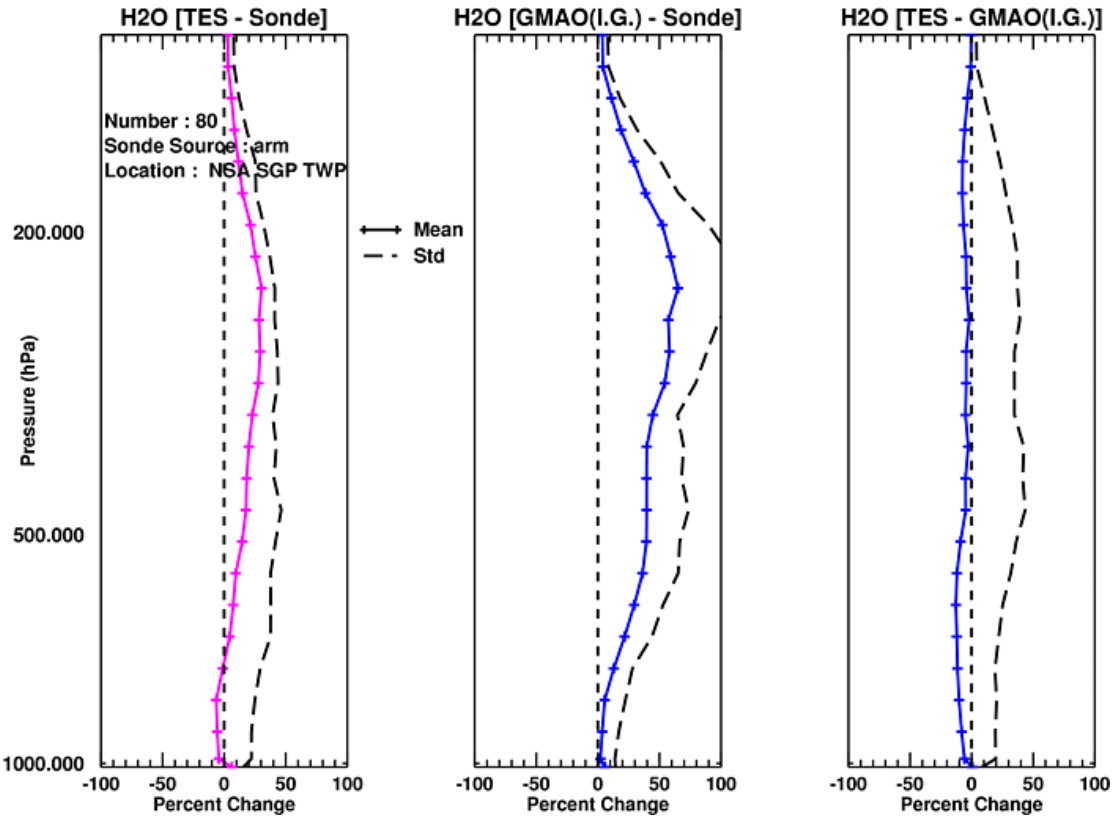

Figure 9-4 Left: Water Comparisons between TES and Sondes at all three ARM Sites, NSA, SGP, and TWP, calculated as (TES-sonde)/TES. Middle: water Comparisons between GMAO GEOS-4 and Sondes. Right: Water Comparisons between TES and GMAO GEOS-4.

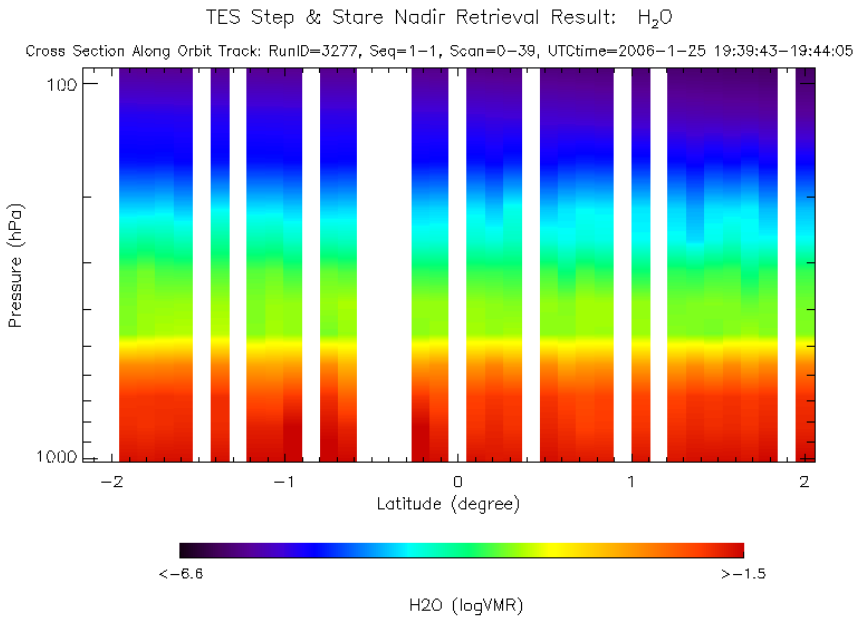

Figure 9-5 TES transect across the Galapagos Islands, RunID = 3277, 25 January 2006, shows Uniform Field of Water Vapor.

Distributed by the Atmospheric Science Data Center
http://eosweb.larc.nasa.gov

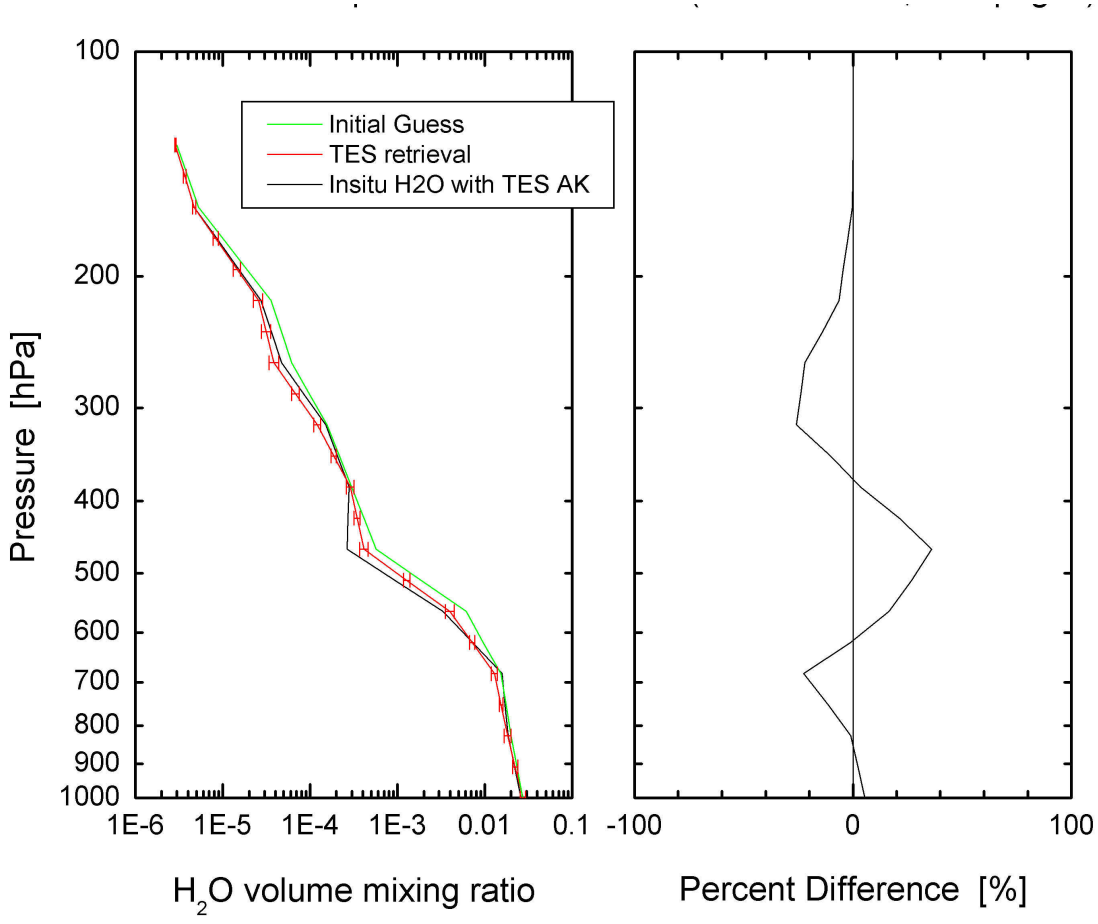

Figure 9-6 San Cristobal, Galapagos Water Vapor Profiles on 25 January 2006: TES and CFH.

Distributed by the Atmospheric Science Data Center
http://eosweb.larc.nasa.gov

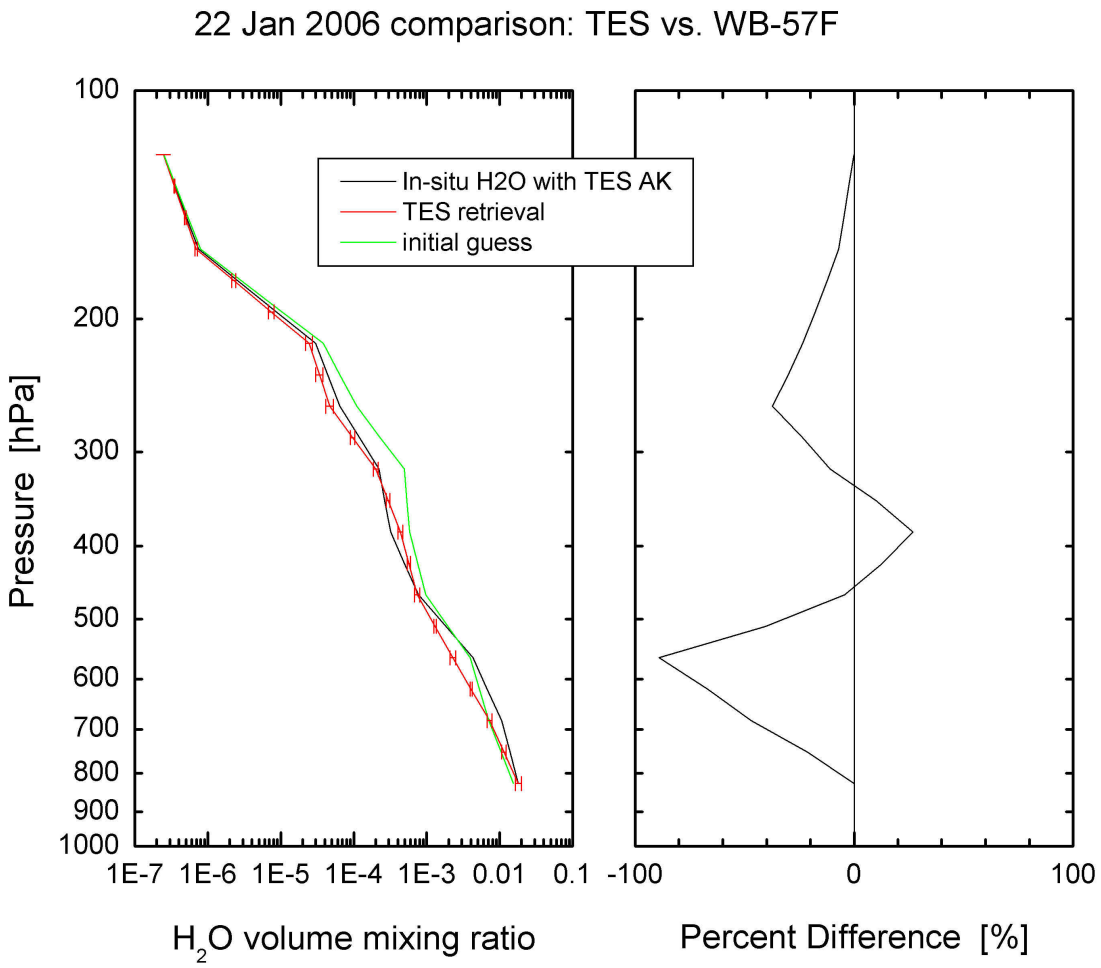

Figure 9-7 Water Vapor Profiles over Costa Rica on 22 January 2006: TES and WB-57F Aircraft (average of several *in situ* instruments).

Distributed by the Atmospheric Science Data Center
http://eosweb.larc.nasa.gov

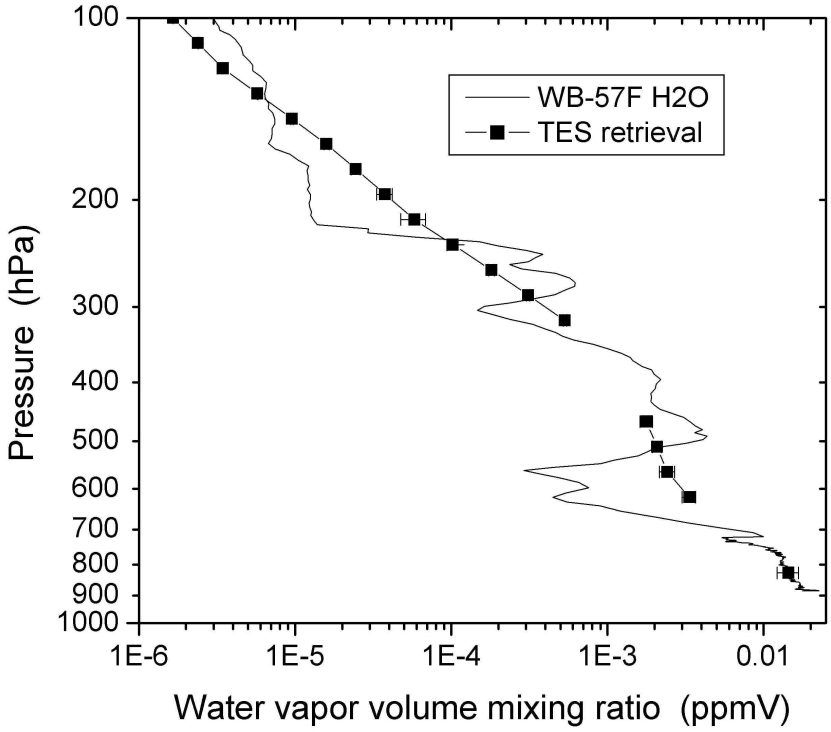

Figure 9-8 Water Vapor Profiles over Costa Rica on 7 February 2006: TES and WB-57F Aircraft (average of several *in situ* instruments).

Distributed by the Atmospheric Science Data Center
http://eosweb.larc.nasa.gov

10. Validation of TES HDO/H2O

TES is capable of measuring HDO in the troposphere from thermal infrared radiances between 1200 and 1350 cm^{-1}. Information on the simultaneous retrieval of HDO and H2O are provided in Worden et al., 2006, including a description of error characterization and spatial and vertical sensitivities. The TES measurement of HDO is made in the nadir mode and is most sensitive in the region between 450 and 850 hPa.

There are few data sets that can be used for validation of measurements of HDO in the lower troposphere. Worden et al., 2006 provides information on comparison of the HDO/H2O ratio to prior measurements and models. It has been determined that a bias of 5% may be seen in TES estimates of HDO. This bias could be largely the result of uncertainties in the HDO spectroscopic line strengths. Use of the ratio of HDO/H2O in scientific analyses lessens the effects of this potential bias in the TES data. An example of an indirect validation of TES HDO is by comparing to the aircraft instrument ALIAS. Figure 10-1 shows a comparison of measurements of HDO from both TES and ALIAS from a flight of the NASA WB-57 aircraft near Costa Rica. The two measurements show very similar distributions for HDO.

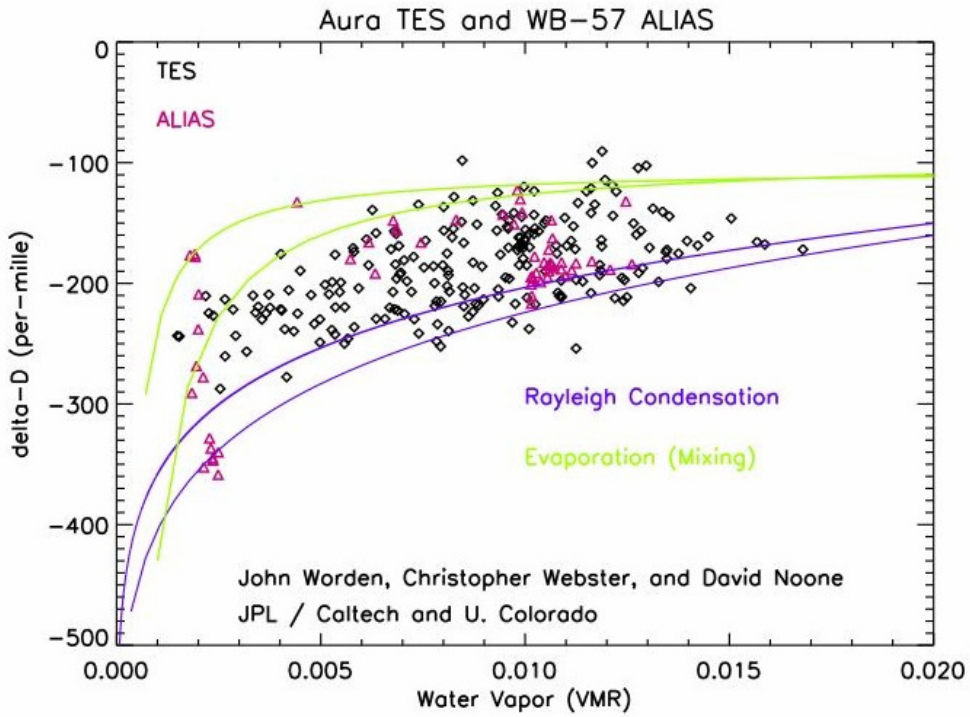

Figure 10-1 A comparison of the HDO/H2O ratio as measured by TES and the JPL ALIAS instrument on a WB-57 flight from the Costa Rica Aura Validation Experiment.

Distributed by the Atmospheric Science Data Center
http://eosweb.larc.nasa.gov

11. TES Cloud Products

TES performs a retrieval of frequency dependent effective optical depth and cloud top pressure along with the trace gas retrievals. There are a number of fields the user might be interested in:

- CloudTopPressure,
- CloudTopPressureError,
- CloudEffectiveOpticalDepth (has frequency dependence),
- CloudEffectiveOpticalDepthError (has frequency dependence), and
- AverageCloudEffOpticalDepth.

11.1 Background

TES retrieves a cloud top pressure and cloud effective optical depth for each measurement. These data have error estimates, and based on those estimates and physical principles, we can make some statements about when TES has sensitivity to cloud parameters and when it does not. Figure 11-1 and Figure 11-2 are scatter plots of the cloud top pressure and effective cloud optical depth at 975 cm^{-1}. The error estimates are plotted over the data. These show that there is small uncertainty for moderate optical depths (1-10) and higher altitude clouds (pressures from 200-800 hPa). Error estimates on both effective optical depth and cloud top pressure tend to be large for clouds with optical depths less than a few tenths. For high effective optical depth clouds (greater than 10) at pressures between 800 and 1000 hPa, error estimates for cloud top pressure grow a bit larger again.

These error estimates are consistent with our expectations for TES. Due to low thermal contrast, clouds near the surface are harder to characterize than clouds at high altitudes. Also, small effective optical depth clouds impart a small radiance change, and are harder to characterize than moderate optical depths. By the time the effective cloud optical depth becomes larger than a few, radiance is relatively insensitive to changes in optical depth, and characterization becomes more difficult.

11.2 Cloud Top Pressure

The cloud top pressure has been compared to MODIS and AIRS cloud top pressures. Only MODIS comparisons are presented in this version of the validation report. For this comparison we use the MODIS cloud top pressure that is determined from the infrared retrieval technique from the MYD06 products. TES data are paired with the nearest neighbor of the MODIS 5km by 5km data products. There is always significant overlap of the TES and MODIS footprints. We select only the MODIS data that are considered cloudy with high confidence (cloud mask value 0). Figure 11-3 shows a histogram of the cloud top pressure differences (TES minus MODIS) in hPa. Although the mean difference is less than 50 hPa, we see that there are outliers with differences greater than 300 hPa. Figure 11-3 plots the results from a set of Step and Stare runs. Global Survey runids have similar statistics.

To look into the cloud top pressure differences in a little more detail, statistics were developed after grouping data by cloud top pressure and cloud optical depth. The left hand column of Figure 11-4 shows data with effective optical depths less than 3, while the right hand column is for effective optical depths greater than 3. The upper panels show cloud top pressure less than

Distributed by the Atmospheric Science Data Center
http://eosweb.larc.nasa.gov

350 hPa, the middle panels show cloud top pressure between 350 and 700 hPa, and the lower panels show cloud top pressure greater than 700 hPa. It is seen that the histograms of cloud top pressure differences for clouds above 350 hPa are narrower. The lower optical depth clouds below 350 hPa have broad histograms although the mean differences are small. Further analysis shows that the large differences are related to the fact that the TES default initial guess for cloud top pressure is 500 hPa, while the MODIS first guess is closer to the surface pressure.

11.3 Cloud Effective Optical Depth

At present, we have limited correlative datasets for the validation of the effective cloud optical depth product from TES. For characterization purposes, we have compared MODIS visible optical depths to the TES effective cloud optical depths retrieved at 975 cm^{-1}. The average effective cloud optical depth is very well correlated to the effective cloud optical depth at 975 cm^{-1}, except at small effective optical depth, as shown in Figure 11-5.

A scatter plot of TES effective cloud optical depth at 975 cm^{-1} and MODIS cloud optical depth is presented in Figure 11-6. The expected ratio of visible to infrared optical depth is dependent on the cloud particle sizes and shapes, and is thought to be on the order of 2. Figure 11-6 shows clearly that MODIS optical depths are larger than TES effective cloud optical depths, but the scaling ranges from a factor of 10 to 1.

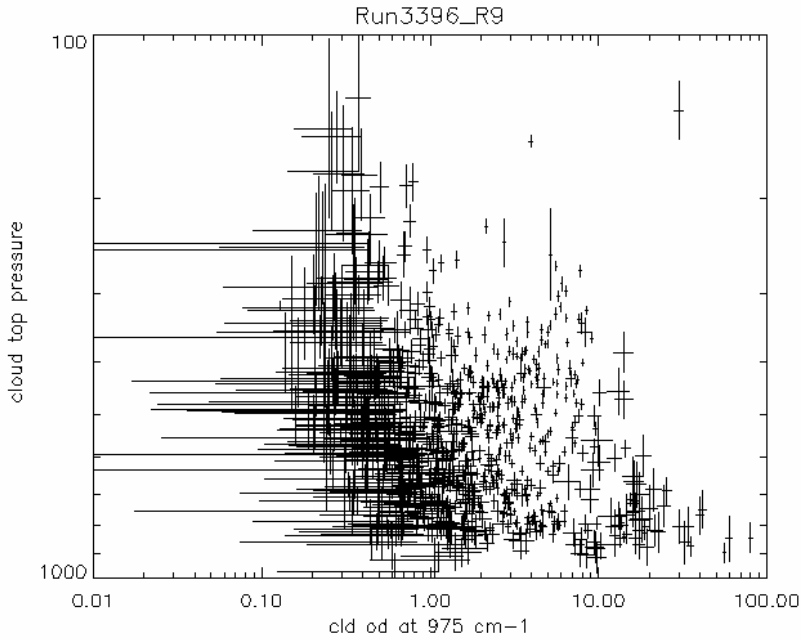

Figure 11-1 TES Retrieved Cloud Top Pressure (hPa) and Cloud Effective Optical Depth at 975 cm^{-1} with Error Estimates for Runid 3396. See tif scat_ctp_od_Run3396_R9.tif.

Distributed by the Atmospheric Science Data Center
http://eosweb.larc.nasa.gov

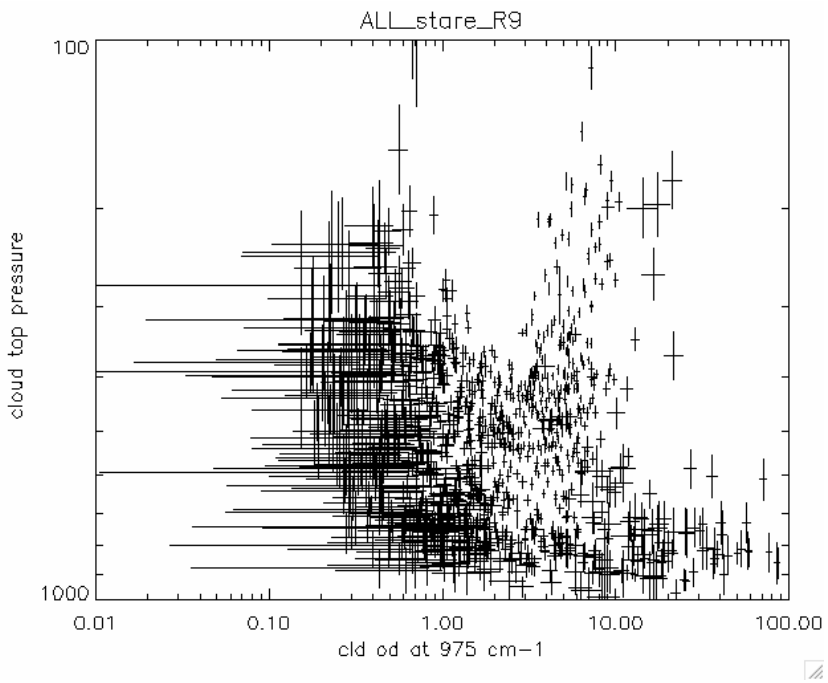

Figure 11-2 As **Figure 11-1**, but for a Collection of Step and Stare Special Observation Runids.

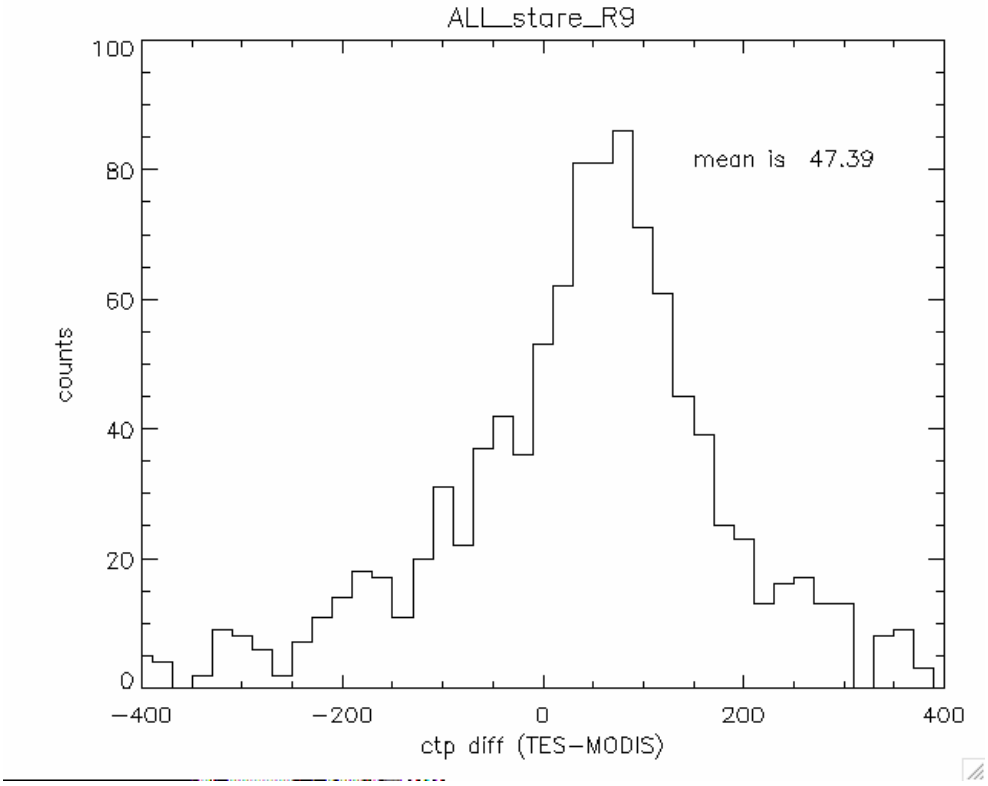

Figure 11-3 Histogram of Cloud Top Pressure Differences between MODIS and TES in hPa.

Distributed by the Atmospheric Science Data Center
http://eosweb.larc.nasa.gov

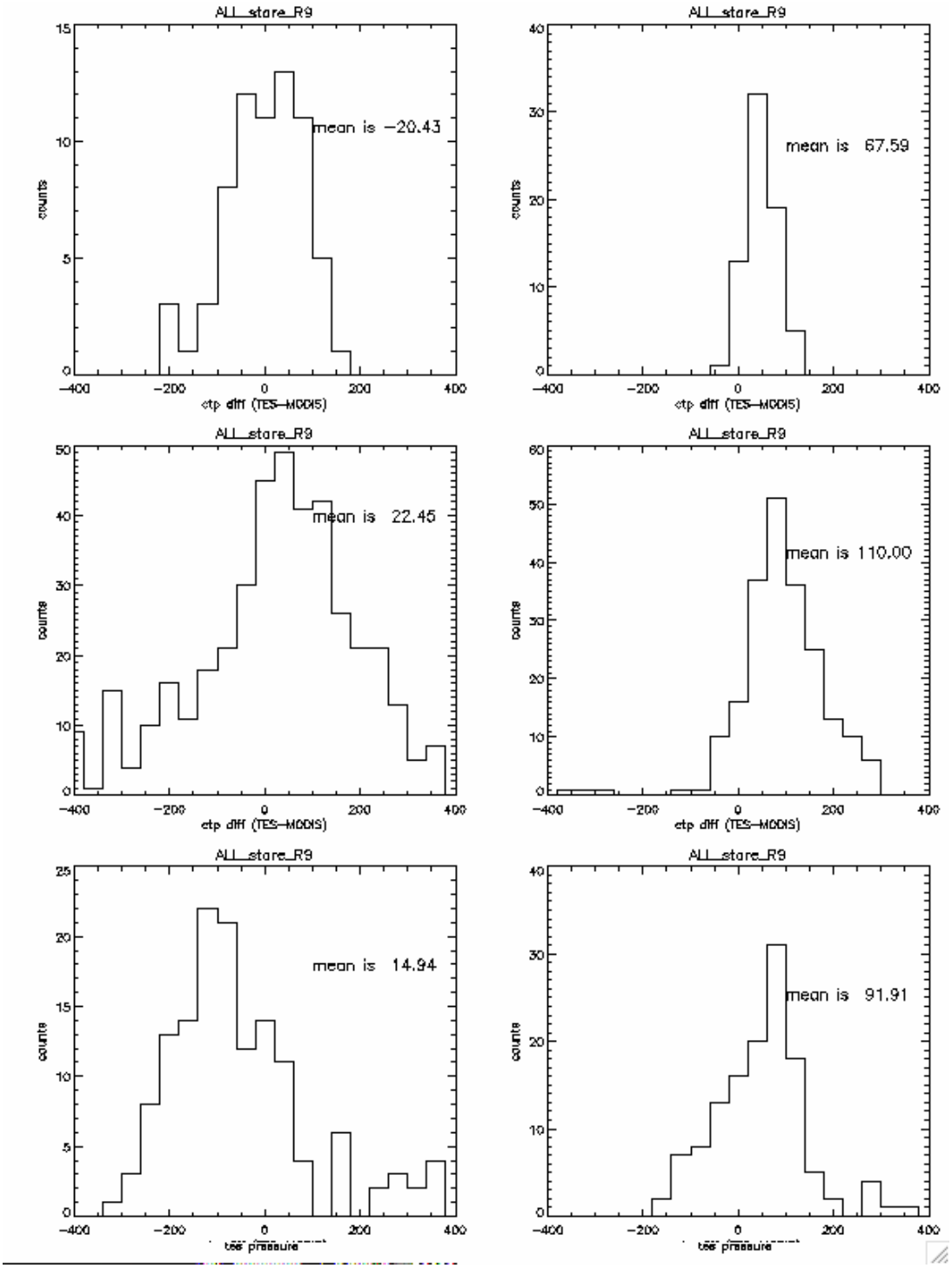

Figure 11-4 Histogram of TES-MODIS Cloud Top Pressure Differences. Left column is effective optical depth less than 3, right hand column greater than 3. Upper row is cloud top pressure less than 350 hPa, middle row is cloud top pressure between 350 and 700 hPa, and bottom row is cloud top pressure greater than 700 hPa.

Distributed by the Atmospheric Science Data Center
http://eosweb.larc.nasa.gov

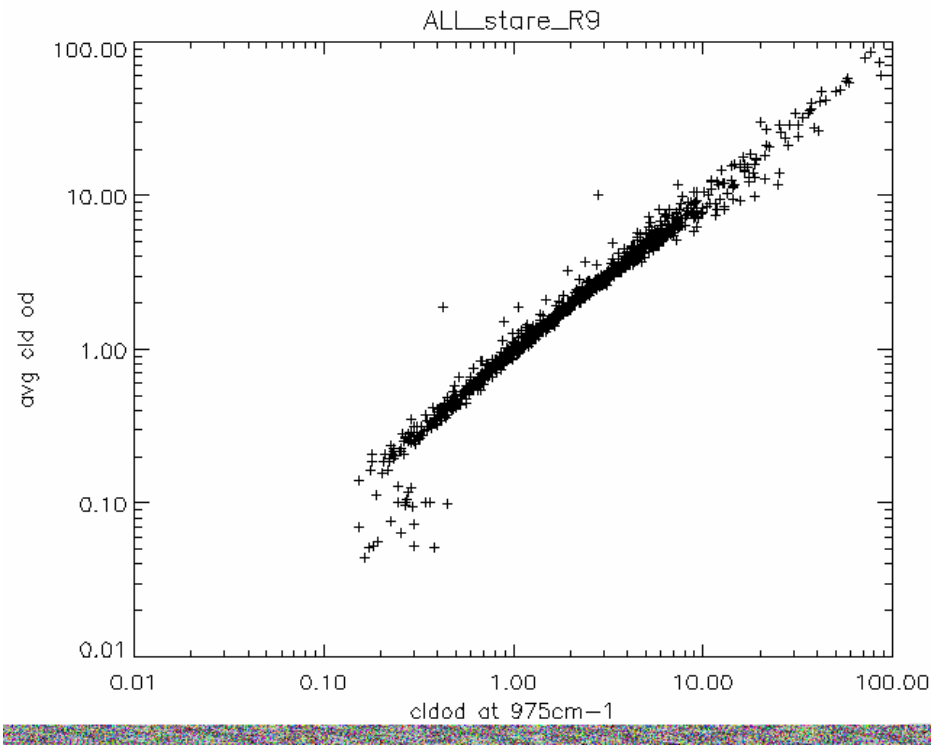

Figure 11-5 Scatter plot of Average Effective Cloud Optical Depth and Effective Cloud Optical Depth at 975 cm^{-1}.

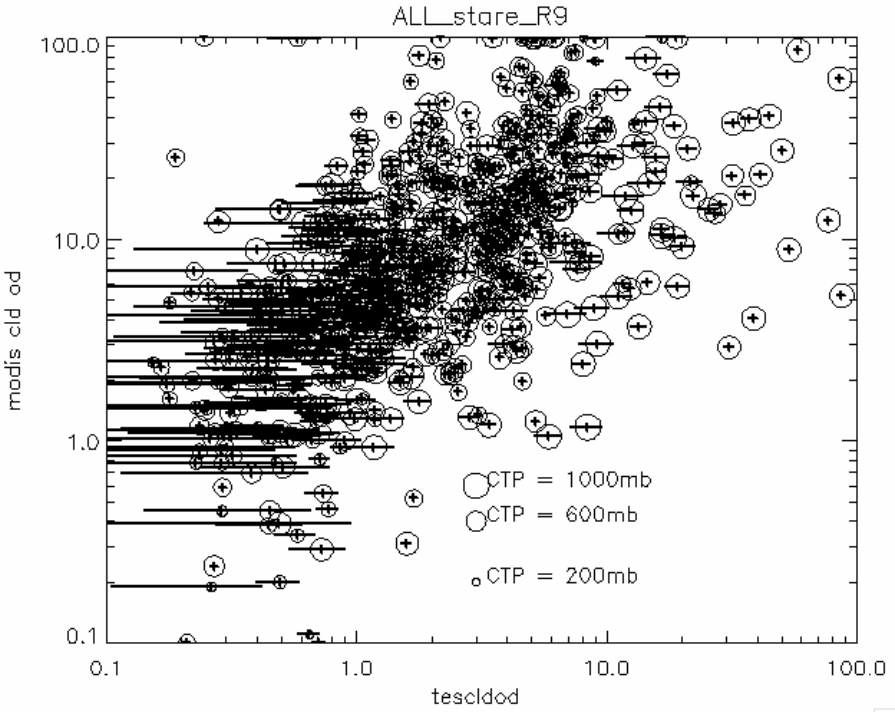

Figure 11-6 Scatterplot of MODIS Visible Cloud Optical Depth and TES Effective Cloud Optical Depth at 975 cm^{-1}.

Distributed by the Atmospheric Science Data Center
http://eosweb.larc.nasa.gov

Appendices

A. Acronyms

ACE	Atmospheric Chemistry Experiment
AIRS	Atmospheric Infrared Sounder
ALIAS	Aircraft Laser Infrared Absorption Spectrometer
AMSR	Advanced Microwave Scanning Radiometer
AMSU	Advanced Microwave Sounding Unit
ASDC	Atmospheric Science Data Center
AVE	Aura Validation Experiment
ARM	Atmospheric Radiation Measurement
ARM-SGP	Atmospheric Radiation Measurement – Southern Great Plains
CR-AVE	Costa Rica Aura Validation Experiment
DACOM	Differential-Absorption Carbon Monoxide Monitor
DIAL	Differential Absorption Lidar
DOE	Department of Energy
CFH	Cryogenic Frostpoint Hygrometer
CH_4	Methane, Natural Gas
CO	Carbon Monoxide
CO2	Carbon Dioxide
CR-AVE	Costa Rica Aura Validation Experiment
DOF	Degrees of Freedom
DOFS	Degrees of Freedom for Signal
DPS	Data Products Specification
EOS	Earth Observing System
FTS	Fourier Transform Spectrometer
GEOS	Global Earth Observing System
GMAO	Global Modeling Assimilation Office
HDF	Hierarchical Data Format
HIRDLS	High Resolution Dynamics Limb Sounder
HIS	High Resolution Interferometer Sounder

Distributed by the Atmospheric Science Data Center
http://eosweb.larc.nasa.gov

HYSPLIT	Hybrid Single-Particle Lagrangian Integrated Trajectory
IEEE	Institute of Electrical and Electronics Engineers
H2O	Dihydrogen Monoxide (Water)
HDO	Hydrogen Deuterium Monoxide (“Heavy Water”)
IG	Initial Guess
ILS	Instrument Line Shape
INTEX	International Chemical Transport Experiment
IONS	INTEX Ozonesonde Network Study
ISM	Integrated Spectral Magnitude
JPL	Jet Propulsion Laboratory
K	Kelvin
L1	Level 1
L1B	Level 1B
L2	Level 2
MISR	Multi-angle Imaging SpectroRadiometer
MLS	Microwave Limb Sounder
MMS	Meteorological Measurement System
MODIS	Moderate Resolution Imaging Spectroradiometer
MOPITT	Measurement Of Pollution In The Troposphere
MOZAIC	Measurement of OZONE on Airbus In-service Aircraft
MTP	Microwave Temperature Profiler
NASA	National Aeronautics and Space Administration
NATIVE	Nittany Atmospheric Trailer and Integrated Validation Experiment
NCEP	National Centers for Environmental Prediction
NESR	Noise Equivalent Source Radiance, Noise Equivalent Spectral Radiance
NOAA	National Oceanic & Atmospheric Administration
NH	New Hampshire
O3	Ozone
OD	Optical Depth
OMI	Ozone Monitoring Instrument
PAVE	Polar Aura Validation Experiment
PNNL	Pacific Northwest National Laboratory

Distributed by the Atmospheric Science Data Center
http://eosweb.larc.nasa.gov

PI	Principal Investigator
RMS	Root-Mean-Square
ROI	Reynolds Optimally Interpolated
Run ID	TES run identification number
SAUNA	Sodankyla Total Ozone Intercomparison
SHADOZ	Southern Hemisphere Additional Ozonesondes
SHIS	Scanning HIS
SRF	Spectral Response Function
SST	Sea Surface Temperature
STD	Standard Deviation
TBD	To Be Determined
TBR	To Be Released, To Be Reviewed, To Be Revised
TES	Tropospheric Emission Spectrometer
TOMS	Total Ozone Mapping Spectrometer
TTL	Tropical Tropopause Layer
TX	Texas
VMR	Volume Mixing Ratio
WOUDC	World Ozone and Ultraviolet Radiation Data Centre

Distributed by the Atmospheric Science Data Center
http://eosweb.larc.nasa.gov